

Low Field Microwave Absorption Studies of Normal and Superconducting States in Iron Pnictides



By

Robert Birundu Onyancha

Submitted in partial fulfilment of the requirements

For the degree

Philosophia Doctor (PhD)

In the department of physics

College of Science & Engineering Technology

University of South Africa (UNISA)

Supervisors


Prof. Vijaya Srinivasu Vallabhapurapu

Prof. Jayashree Das

December 2017

Declaration

I declare that “ **Low field microwave absorption studies of Normal and Superconducting States in Iron Pnictides**” is my own work and that all sources that have been used or quoted have been indicated and acknowledged by means of complete references.

Signature.....

Date:..... 20/12/2017

(R. B. Onyancha)

ABSTRACT

Low field microwave absorption (LFMA) or non-resonant microwave absorption (NRMA) phenomenon has turned out to be a powerful and exciting technique in characterizing superconductors and magnetic materials. The technique uses an electron spin resonance (ESR) spectrometer. Importantly, an ESR spectrometer is designed to study materials consisting of unpaired electrons (spins). Consequently, these materials show a resonance signal when the energy between two spin levels matches the radiation energy. In LFMA technique, a few magnetic materials show two absorption modes i.e. a resonance spectrum and a LFMA signal centered around zero magnetic field. Interestingly, the mechanisms of LFMA signal in these magnetic materials are yet to be fully understood.

High T_c cuprate superconductors have shown LFMA signal in the superconducting state. However, in their normal state, both the LFMA signal and the resonance signal are conspicuously not registered despite the fact that they contain paramagnetic species of Cu^{2+} . The mechanisms behind the quenching of Cu^{2+} localized moment in these materials is unresolved too. Now, with the advent of iron-based superconductors (FeSc) which were discovered in 2008, a variety of materials have been discovered with diverse properties thus providing an excellent platform to study and address some of the aforementioned debatable topics.

Therefore, this piece of work involves LFMA studies of normal and superconducting states of FeSc. We are motivated by the fact that (1) few reports have been presented on LFMA in superconducting state of these materials (2) no normal state LFMA studies have been reported thus far in any superconducting material (3) incomplete understanding of LFMA phenomenon in general (4) a possible normal state application of these materials in spintronics i.e. room temperature low field magnetic sensor and microwave absorbers.

In this study, we have observed both LFMA and resonance spectrum in the normal state of $\text{SmFeAsO}_{1-x}\text{F}_x$. The resonance spectrum which simply marks a saturation state is observed to evolve as a function of temperature and becomes 'ESR silent' in the superconducting state. More importantly, we observed a novel LFMA signal in the normal state. This signal is reported here for the first time in any superconducting material. In the superconducting state, LFMA signal is detected. Here the LFMA signal evolves as a function of temperature,

magnetic field and microwave power. Furthermore, a structure (a broad peak and narrow peak) is exhibited in all sample forms (powder and pellet) and in all doping used. This suggests that this structure is a generic feature in $\text{SmFeAsO}_{1-x}\text{F}_x$.

We have precisely differentiated the normal state LFMA signal with its counterpart in the superconducting state on three accounts namely: (1) a resonance signal is only observed in the normal state but is 'ESR silent' in superconducting state (2) the peak to peak LFMA signal intensity in the normal state increases as a function of temperature up to 180 K and then decreases onwards whereas in the superconducting state a decrease of intensity with increase in temperature is witnessed; and (3) the line width of LFMA signal in the superconducting region is ~ 100 G compared to ~ 650 G in normal state.

Key words: low field microwave absorption (LFMA), high temperature superconductors (HTSC), iron-pnictide superconductors, Josephson junctions, fluxons and normal state.

Dedication

I would like to sincerely dedicate this thesis to my family for all their unmatched contributions towards attaining this monumental milestone.

Acknowledgment

This work would have not been possible without the goodwill of esteemed individuals, group (s) and institution(s). I take this opportunity to acknowledge the following:

- First of all I wish to thank my supervisors: Prof. V. V. Srinivasu and Prof. Das Jayashree for the mentorship and guidance during the course of this noble exercise.
- I would also like to recognize the help I received from STEM (Superconductivity Technology and Emerging Materials) under the leadership of Prof. Srinivasu) group.
- Sincere thanks to Prof. Ogino and Prof. Shimoyama for the opportunity to synthesis and characterize the samples in their laboratory at the university of Tokyo.
- I wish to recognize the physics department under the chair Prof. Lekala for the moral and material support received during the course of this work.
- I am gratefull to the University of South Africa research directorate for doctoral fellowship funding through the chair of superconductivity technology.
- My utmost appreciation goes to my family for the love and financial support. May God bless you.
- Above all, to my creator, the living God, It is true indeed that your grace is sufficient.

Acronyms

HTSC	:	High temperature superconductors.
LFMA	:	Low field microwave absorption.
ESR	:	Electron spin resonance.
FeSc	:	Iron-based superconductors
NRMA	:	Non-resonant microwave absorption
SDW	:	Spin density wave
H_{c1}	:	Lower critical field
H_{c2}	:	Upper critical field
T_c	:	critical temperature
JJ	:	Josephson junctions
J_c	:	Critical current density
H	:	Pnictogen height
λ	:	Penetration depth
ξ	:	Coherence length

Table of Contents

Declaration	i
ABSTRACT	ii
Dedication	iv
Acknowledgment	v
Acronyms	vi
Thesis Structure	x
Chapter 1	1
1.1 An overview on superconductivity	2
1.1.1 Perfect Diamagnetism and Zero Resistance.....	2
1.1.2 BCS Theory.....	5
1.1.3 Ginzburg-Landau Wave Function Theory	5
1.1.4 Cuprates Superconductors	7
1.1.6 Iron-based superconductors	9
1.1.7 Emergent and debatable topics	11
1.2 Problem statement	15
1.3 Objectives	17
References	18
Chapter 2	23
Magnetic properties of type two superconductors	23
2.1 Josephson junction (JJ)	23
2.2 RF-SQUID	26
2.3 Granularity.....	28
2.4 Spin glass behavior	29
2.5 Critical state model.....	30
2.6 Two- critical state model.....	31
2.7 Flux flow and Pinning	32

2.8 Surface resistance	34
References	37
Chapter 3.....	39
Low Field Microwave Absorption (LFMA).....	39
Introduction.....	39
3.1 Experimental Set-Up.....	39
3.2 LFMA in Superconductors	41
3.3 Mechanisms of LFMA in superconductors	43
3.3.1 Portis model	43
3.3.2 Dulcic model	44
3.4 LFMA Features in HTSC.....	45
3.4.1 Quantum oscillations.....	46
3.4.2 Phase reversal ‘anomalous LFMA signal’	50
3.4.3 Anomalous hysteresis.....	51
3.6 LFMA in Magnetic materials.....	53
References	57
Chapter 4.....	61
LFMA of $\text{SmFeAsO}_{0.88}\text{F}_{0.12}$ powdered sample.....	61
I. Introduction.....	62
II. Experiment	64
III. Results and Discussion.....	64
IV. Conclusion	70
References	72
Chapter 5.....	75
NRMA of $\text{SmFeAsO}_{0.80}\text{F}_{0.20}$ material.....	75
I. Introduction.....	76
II. Experiment	78

III. Results and Discussions	78
IV. Conclusions	85
References	86
Chapter 6.....	88
Novel normal-state LFMA of SmFeAsO_{1-x}F_x	88
I. Introduction.....	89
II. Experiment	90
III. Results and Discussion.....	91
IV. Conclusions	100
References	102
Chapter 7.....	106
Summary and conclusions.....	106
LFMA in Superconducting state	106
LFMA in normal state	107
Future Investigations	108

Thesis Structure

This thesis is structured as follows:

- Chapter one provides an in-depth introduction to superconductivity which includes eventful discoveries and theories on superconductivity. An introduction to high temperature superconductivity (HTSC) is given on high T_c cuprates and FeSc. Finally an elaborate problem statement and the objectives of the study is highlighted.
- Chapter two covers a discussion on magnetic properties and features of HTSC that are related to LFMA phenomenon.
- Chapter three presents the LFMA technique. Here the experimental setup has been provided. Again, a discussion on LFMA in both superconductors (mechanisms of LFMA and features) and magnetic materials is discussed.
- Chapter four provides LFMA in powdered sample of SmFeAs(O,F) iron pnictide superconductor.
- Chapter five presents NRMA in SmFeAsO_{0.80}F_{0.20}. In this chapter, we explored NRMA signal dependence on temperature and microwave power. The results therein is compared to LFMA in SmFeAsO_{0.88}F_{0.12}.
- Chapter six provides novel normal state LFMA in SmFeAsO_{1-x}F_x. We explored LFMA studies in the normal and superconducting states of SmFeAsO_{1-x}F_x. We have explicitly distinguished the LFMA phenomenon in these two states.
- In chapter seven, a general conclusion is drawn summing up eventful findings in this work.

Chapter 1

Introduction

Superconductivity was discovered more than a century ago [1] and it depicts a dissipation-less flow of charge in a material below a characteristic temperature called critical temperature (T_c). A reduction of normal state resistivity from $10 \mu\Omega.cm$ to about $1 f\Omega.cm$ [2] in the superconducting state clearly justifies why the phenomenon is regarded as perfect conductivity ($R \approx 0$). Since then, a plethora of superconductors with diverse properties have been discovered. This has kept theoretical and experimental studies in this realm of science very active mainly for two reasons: (1) the quest to unravel the fascinating physics underpinning this phenomena; and (2) for applications purposes. Consequently, important theoretical formulations such as London equations, BCS theory, the Ginzburg-Landau theory and many more have been devised. Phenomenologically they have explained some of the fundamental occurrences in superconductivity.

In the recent past, high temperature superconductors (HTSC) such as the cuprates and iron-based superconductors (FeSc) have been discovered consequently changing the dynamics of this field. These materials are characterized by a short coherence length, the quasi two-dimensional nature, high critical fields and critical temperatures. As a matter of fact, elevated temperatures, $T_c \sim 155$ K and $T_c \sim 55$ K in cuprates and FeSc respectively have been realised. These kind of temperatures offer excellent cryo-electric device application since they can even provide enhanced stability in circumstances that require the operational temperature to be kept low. Furthermore, extremely careful preparations of high quality thin films have minimized the two-dimensional nature and extremely small coherence length which have been a hindrance towards full application of HTSC. Besides, careful manipulations of fluxons/vortices through ratchets and rectifiers have been engineered to control and remove trapped magnetic flux thus improving the device performance.

Collectively, superconductors have found applications in various quarters such as in transport (for example in Maglev trains), energy (like in electricity grids and International Thermonuclear Reactor-ITER), medical field (for diagnostics tomography with highest resolution), in microwave devices (such as filters, resonators etc.) and in fluxonics (such as

quantized magnetic flux lenses, diodes and flux pumps). These applications have dramatically revolutionized human life.

1.1 An overview on superconductivity

It is absolutely clear that since the discovery of superconductivity, significant achievements in theory and experiments have been made. Therefore, in this section, we highlight some of these attainments that include; perfect diamagnetism and zero resistance, Ginzburg Landau theory, BCS theory, high T_c cuprate superconductors and most importantly FeSc which forms the main materials under this study.

1.1.1 Perfect Diamagnetism and Zero Resistance

In 1933, Meissner and Oschenfeld noted that at temperatures below T_c , a superconductor expels the flux from its interior when exposed to a magnetic field [3]. Flux expulsion occurs regardless of whether this material is cooled with a magnetic field from normal state or it is in superconducting state when the field is introduced. This is hypothetically different from a perfect conductor in which the induced currents prevent any change of magnetic field within a conductor thus validating the fact that superconductivity is indeed a true thermodynamical state. The mapping of magnetic field with temperature exhibits a single superconducting state which is often known as **Meissner state** ($B = 0$). This is often known as perfect diamagnetism and it is only valid below critical values of both magnetic field and temperature ($H < H_c$ and $T < T_c$). At this state, the thermodynamical critical field (H_c) in relation to temperature can be expressed as

$$H_c(T) = H_c(0) \left[1 - \left(\frac{T}{T_c} \right)^2 \right]. \quad 1.1$$

When applied magnetic field exceeds H_c , the system reverts to a normal state as shown in figure 1.1. Materials such as mercury and lead exhibit only this state and are called **type I superconductors**.

Thermal properties of a superconductor are well documented in a two-fluid model devised by Gorter -Casimir in 1934 [4]. This model is built on the basic premise that by minimizing the Helmholtz free energy, conduction electrons as function of temperature can be predicted. Accordingly, at temperatures above absolute zero, a fraction of paired electrons split into normal electrons (n_n) and super electrons (n_s) due to thermal energy in the solid.

Therefore, this model postulates superconductivity as result of both paired and normal electrons with complex conductivity $\sigma_1 - j\sigma_2$.

Building on the two-fluid model, London brothers [5, 6] gave fundamental equations to explain the electromagnetic properties of a superconductor. Correspondingly, the density n of the conduction electrons at any given temperature is a summation of normal electrons (n_s) and superfluid electrons (n_n)

$$n = n_s(T) + n_n(T) \quad 1.2$$

In the normal state, $n = n_n(T > T_c)$ whereas at $T = 0$ (absolute zero) $n = n_s(0)$. Then supercurrent can be expressed in two ways as defined in equation 1.3 and 1.4. These two famous London equations provide an explicit and simple way of introducing superconductivity to Maxwell's equations thus necessitating the use of conventional solution methods. The first London equation (Equation 1.3) describes the zero resistance (perfect conductivity) where it defines the acceleration of the supercurrents caused by an electric field (E). Furthermore, equation 1.4 represents an interaction of magnetic fields with a superconductor.

$$\Lambda \frac{\partial \mathbf{J}_s}{\partial t} = \mathbf{E} \quad 1.3$$

$$\Lambda \nabla \times \mathbf{J}_s = -\mathbf{B} \quad 1.4$$

where $\Lambda = m/n_s e^2$ is the London parameter, which is related to the superconducting penetration depth. Also, $\mathbf{J}_s = n_s e v_s$ is the superconducting current density with n_s and v_s being the density of superconducting pair electrons and the velocity of superconducting electrons respectively.

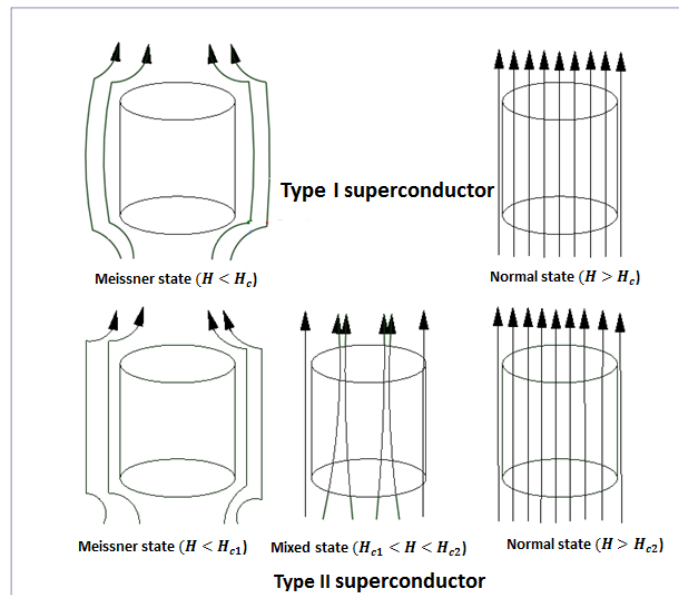


Figure 1.1: Magnetic dynamics of type I and type II superconductors below critical temperature, T_c .

According to figure 1.1, **type II superconductors** differ from **type I superconductor** mainly on one account. The type II superconductors (which include the metal alloys such as niobium-titanium, germanium-niobium and HTSC such as the cuprates and FeSc) allow the magnetic field to enter the sample. This flux penetration occurs at a characteristic field, H_{c1} , (lower critical field) which is noticeably smaller than the H_c . Here magnetic flux are quantized (fluxons/vortices) and move freely within the material. To minimize the repulsive interaction between the vortices, a triangular lattice arrangement often known as Abrikosov vortex lattice is preferred.

It is worth noting that a vortex substructure is composed of a central cylindrical normal core of radius ξ (coherence length) and surrounding region of dimension λ (penetration depth). At the axis of the normal core, the order parameter is suppressed to zero and only attains its full value at radius $\sim \xi$. The normal conducting core contains flux which is equal to flux quantum value $\Phi_0 = (hc/2e) = 2.07 \times 10^{-7} \text{ Gauss.cm}^2$.

The co-existence of superconductivity and magnetic field lines yields a **mixed state** ($H_{c1} < H < H_{c2}$). Despite the presence of magnetic fields and weak currents in this state, the superconducting nature and its coherence is preserved below H_{c2} . Fundamentally, this condition has been exploited for superconductor-based applications in strong magnetic

fields. Conversely, an application of magnetic field beyond H_{c2} , ultimately destroys superconductivity and normal state sets in.

1.1.2 BCS Theory

The BCS theory is famously named after the founders (Bardeen, Cooper and Schrieffer) [7]. The theory fundamentally explicates the combination of freely single electrons (that are close to fermi level) into Cooper pairs with charge $2e$ and mass $2m$. The interaction happens through crystal lattice and the two electrons involved in the pair formation ought to have equal and opposite momenta ($P_1 = -P_2$). The pairing can be understood as follows; consider an electron moving through a lattice which then attracts positively charged atoms of the lattice. This electron creates a distortion of the lattice thus causing an electron of opposite spin and momentum to move to a region of enhanced positive charge concentration. This scenario assumes that one electron attracts the other through the lattice vibrations and thus become correlated. Here there is a continuous and simultaneous formation and breaking of paired electrons thus the situation is assumed to be one of permanent paired electrons. This theory mimics the static model of superconductivity [8].

Unlike single electrons which are fermions and follow the the Pauli Exclusion Principle, paired electrons (Cooper pairs) are bosons which occupy a single quantum-mechanical state thus indicating that they have identical physical properties. At this state, cooper pairs exhibit a correlation at the length ξ which is of the range 100 to 1000 nm in a pure superconductor. Beyond this length, the superconducting order parameter is bound to change thus Cooper pairs are assumed to be of the size of ξ . De-pairing of Cooper pairs can happen thermally, kinetically or magnetically when, corresponding superconducting critical parameters i.e. critical temperature (T_c), critical current density (J_c) and critical field (H_c) are reached respectively. Furthermore, the BCS theory under the isotope effect shows that the $T_c \propto 1/M$ (M is mass of the isotope). According to McMillan-Rowell formula, the highest T_c of 30 K (McMillan limit) can be predicted by this model [10].

1.1.3 Ginzburg-Landau Wave Function Theory

Unlike in the BCS model where excitations are considered, the G-L theory is anchored on the fact that superconducting electrons are coherent and form a condensate. Macroscopically, the model establishes a complex wave function that is connected to number density of

superelectrons [9]. At temperatures near the superconducting transition, the free energy (F) can be expressed as

$$F = F_n + \alpha|\psi|^2 + \frac{\beta}{2}|\psi|^4 + \frac{1}{2m}|(-i\hbar\nabla - 2eA)\psi|^2 + \frac{|B|^2}{2\mu_0} \quad 1.5$$

here F_n is free energy in the normal state, α and β are phenomenological parameters, e is an electron charge, A is the magnetic vector potential, m is effective mass and $B = \nabla \times A$ is the magnetic field. On the account of minimizing the free energy in relation to the fluctuations in the order parameter and the vector potential, two celebrated G-L equations are devised as

$$\alpha\psi + \beta|\psi|^2\psi + \frac{1}{2m}(-i\hbar\nabla - 2eA)^2\psi = 0 \quad 1.6$$

$$\mathbf{J}_s = \frac{ie\hbar}{m}(\psi^*\nabla\psi - \psi\nabla\psi^*) - \frac{4e}{m}|\psi|^2\mathbf{A} \quad 1.7$$

here J_s is the superconducting current density. Equation 1.6 links an order parameter variation with applied magnetic field whereas equation 1.7 defines the superconducting current as function of the order parameter.

$$\xi = \sqrt{\frac{\hbar^2}{2m|\alpha|}} \quad 1.8$$

$$\lambda^2 = \frac{m}{4\mu_0 e^2 |\psi_0|^2} \quad 1.9$$

This theory allows prediction of two important parametric lengths namely: the coherence length (ξ) (1.8) and London penetration depth (λ) (1.9). The ξ describes the distance over which the order parameter (superelectron density) changes from a maximum value to zero. On the other hand, the λ characterizes the distance over which magnetic field is bound to change in a superconductor. It gives a description of the Meissner effect and it varies as a function of temperature as follows, $\lambda(T) = \lambda_0(1 - (T/T_c)^4)^{-0.5}$. Furthermore, G-L parameter $k \equiv \lambda/\xi$ has been used to discriminate between type I and type II superconductors. When $k < 1/\sqrt{2}$, type I superconductors are defined whereas when $k > 1/\sqrt{2}$ represents type II superconductors.

1.1.4 Cuprates Superconductors

The discovery of high T_c superconductivity in $\text{La}_{2-x}\text{Ba}_x\text{CuO}_4$ with a $T_c = 35$ K [11] remarkably marks one of the most thrilling scientific proceedings in condensed matter physics. Immediately after this discovery, a plethora of research devoted to the study of high transition temperatures was intensified, which led to the discovery of the $\text{YBa}_2\text{Cu}_3\text{O}_7$ (YBCO) superconductor with a $T_c = 90$ K [12]. This temperature is well beyond the boiling point of liquid nitrogen. In the meantime a T_c as high as 135 K in Hg-1223 has been attained [13] and on the application of pressure [14] on the same material results to a record T_c of 155 K as shown in figure 1.2 [15]. These materials are Mott insulators in the normal state and only become superconducting through doping, oxygen deficiency or an application of pressure. Furthermore, they are strongly electron correlated materials and the BCS theory fails in demystifying the nature of superconductivity. It is important to note that the BCS failure is not due to high T_c of these material since elevated temperatures can be readily accessible with reasonable material parameters [16].

The BCS failure can be explained as follows: Classical metal superconductors have a huge 'Fermi sea' of free electrons thus the condensed Cooper electrons forms a small fraction of valence electron system ($K_B T_c < E_{Fermi}$). Whereas in HTSC cuprates, doping the anti-ferromagnetic ground state leads to less charge carriers in the reservoir ($K_B T_c \sim E_{Fermi}$). Due to the complex nature of these charge carriers, strong Coulomb relations linking internal charge, spins degrees of freedom and Landau concept are not applicable. In fact the normal charges transport exhibit 'bad/strange metal behaviour with a quite high electrical resistance.

Moreover, the resistance increases linearly with increase in temperature without saturation up to melting temperature which is contrary to renowned quasi-particle behaviour in normal metal [17, 18]. The idea of expressing the superconducting wave function in BCS terms does not hold for HTSC because the macroscopic wave function keeps changing in the superconductive transition. Furthermore, occurrences of many broken symmetry in the normal state which are related to charge and spin degrees of freedom compete or cooperate with superconductivity. Thus high T_c superconductivity is more connected to magnetic dynamics and not from phononic interactions [17, 18].

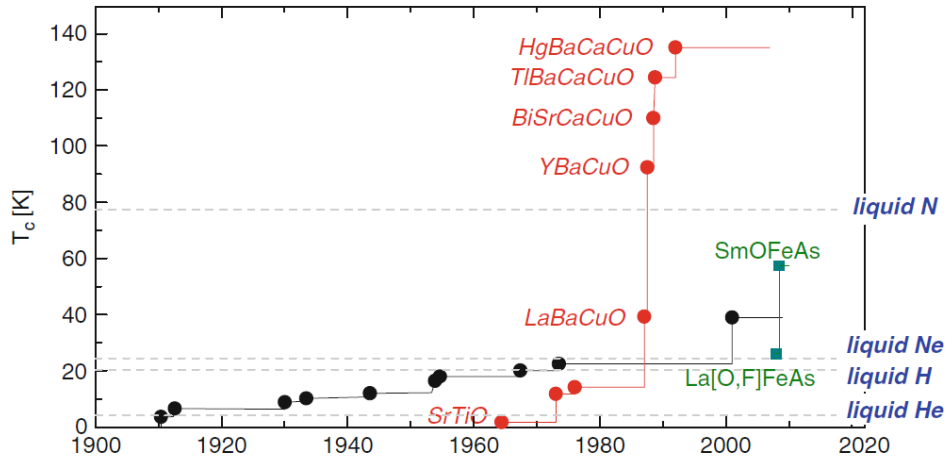


Figure 1.2: Evolution of superconductivity. Starts with discovery of superconductivity in 1911, then the discovery of HTSC in 1987 with T_c reaching 155 K (T_c above liquid nitrogen temperature) and FeSc in 2008 with T_c of 55 K [15].

Cuprate superconductors are characteristically type two superconductors with parameters $\lambda > 100 \text{ nm}$ and $\xi \sim 1 \text{ nm}$ [15, 19]. These materials are quasi-2 dimensional in nature and have small coherence length which leads to a noticeable anisotropy of superconducting properties as defined by the anisotropy factor

$$\gamma = \frac{\xi_{ab}}{\xi_c} = \frac{\lambda_c}{\lambda_{ab}} \quad 1.10$$

For instance in YBCO superconductor, the values of λ are $\lambda_{ab} = 750 \text{ nm}$ and $\lambda_c = 150 \text{ nm}$ [19] which translates to $\gamma \sim 5$. This shows that higher supercurrents are along the CuO_2 planes compared to the perpendicular direction [20, 21]. Again, the small coherence lengths of an optimally doped YBCO are $\xi_{ab} = 1.6 \text{ nm}$ and $\xi_c = 0.3 \text{ nm}$ [22]. Apart from the limitations of short ξ , in a natural way, ceramic superconductors have granular-related imperfections from cracks, secondary phase, impurities, voids, grain boundaries and oxygen deficiency.

Thus the HTSC materials are considered to be non-homogeneous systems. These imperfections which are referred to as weak links results in substantial weakening of the order parameter between superconducting grains which dramatically affects transport properties. Despite some significant material optimization techniques aimed to correct this problem, still these short-comings remain a big challenge towards full superconductor applications. Conversely, the weak link nature has been extensively exploited to good effect

as HTSC Josephson junctions (JJs) [23]. For example, JJs have been employed in complimentary logic circuits for computer related applications.

1.1.6 Iron-based superconductors

The discovery of iron-based superconductor (FeSc) materials in the year 2008 heralded an exemplary era in the field of condensed matter physics [24]. It was explicitly revealed that by doping fluorine into the oxygen site of an antiferromagnetic LaFeAsO system, superconductivity emerges with a critical temperature of 26 K [24]. As a consequence, it triggered an avalanche of research for new superconducting materials in an area that seemed unlikely before and challenged the monopoly enjoyed by cuprates as the HTSC.

Since then many materials have been discovered and accordingly grouped into 1111, 122, 111, 112, 245, 11 and perovskite type (the numbers represents the atomic ratio constituting the compound) as shown in figure 1.3 [25]. These materials are layered with building block of a square lattice of Fe^{2+} ions where pnictogen (Pn) or chalcogenide are tetrahedral coordinated as depicted in figure 1.4 [26]. The common two-dimensional Fe-As layer is similar to Cu-O layer in cuprates superconductors. The layer primarily provides charge carriers responsible for the high T_c superconductivity. In some materials, the Fe-As is sandwiched with non-superconducting buffer layers like SmO in SmFeAsO, Ca in CaFe_2As_2 and thick blocking layer ($\text{A}_4\text{X}_2\text{O}_6$) in perovskite materials along the c-axis crystallographic direction.

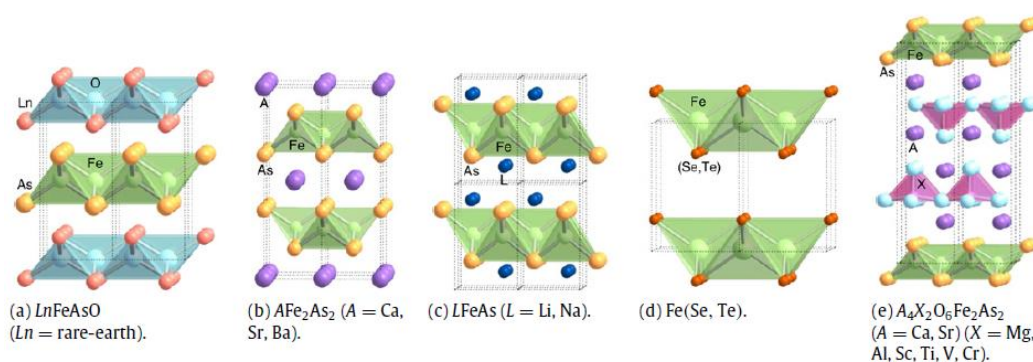


Figure 1.3: Crystal structure of FeSc representing families 1111, 122, 111, 11 and 42622 [25].

The un-doped or lightly doped FeSc materials are Pauli para metals in the normal state. At high temperatures, they undergo crystallographic transition, which precedes an antiferromagnetic phase. In general, both structural and magnetic transitions occur in a

temperature range of 130-200 K [27 -31] with an exception of $K_{0.8}Fe_{1.6}Se_2$ where structural transition and magnetic transitions occur at temperatures 578 K and 559 K respectively [32]. Notably, FeSe and LiFeAs materials do not exhibit the antiferromagnetic ordering. The emergence of superconductivity occurs when the antiferromagnetic ordering is suppressed through doping or applying pressure. An introduction of electron charge into 1111 system successfully culminated to an increase of T_c from 26 K to as high as 56 K when replacing La in LaFeAsO with rare earth metals such as Sm , Nd and Pr whose ionic radius are smaller in comparison to that of La [33 -35].

The optimum T_c in FeSc has always been associated to local lattice structure. It has been shown that T_c is very sensitive to local geometry of Pn(Ch)-Fe-Pn(Ch) angle (α) and pnictogen height (h) which is distance between the Fe-plane. The size of an angle α formed depends on the type of compound [37], applied pressure and [38] doping [37, 39]. Lee *et al* [25] proposed that optimum T_c value can be realised when the bond angle α approaches a value of $109^{\circ}5'$ and maximum h whose value is 1.38 \AA . furthermore, the h parameter and α are linked to the strength of spin fluctuation and orbital fluctuations [40].

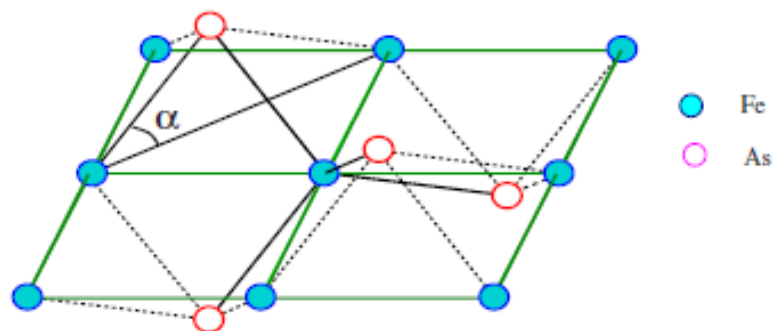


Figure 1.4: A sketch of lattice structure. The α angle formed by Fe-As bond with Fe plane changes with doping and pressure [26].

Unlike cuprates, which are single band systems with low-energy states arising from Cu^{2+} (electronic configuration is $3d^9$), FeSc are multi-band systems with common electronic band structure and the Fe-3d electrons ($3d^6$ configuration) primarily govern the fermi level. The fermi surface (for unfolded Brillouin zone) consists of two hole pockets around the Brillouin zone centre (0,0) one hole pocket at (π, π) and two electron pockets around $(\pi, 0)$ or $(0, \pi)$. The hole pockets at the Brillouin zone (0,0) and the electrons pockets near the Brillouin zone edge consists of d_{xy} and d_{yz} orbitals [26, 41].

On the other hand, hole fermi surface at (π, π) and electrons fermi surface that are away from the Brillouin zone chiefly give d_{xy} orbital [26, 41]. Importantly, although the orbitals $3z^2-r^2$ and x^2-y^2 are present in the fermi surface, their weight is relatively small [26]. Nonetheless, the presence of these multi-orbital states renders the fermiology of these materials very complex when an electron or hole charge is introduced; hence exhibiting unusual normal state or superconducting properties/features.

Like the cuprates, FeSC are type II superconductors with $\lambda > 100 \text{ nm}$ and $\xi \sim 1 \text{ nm}$ [42]. Interestingly, they are lesser anisotropic when compared to cuprates. The distance h between CuO planes in cuprates is 1 nm and $\xi_c = 0.3 \text{ nm}$ [19] whereas h between Fe-Fe layers in Ba122 is 0.6 nm and $\xi_c = 0.6 \text{ nm}$ [42]. The FeSc has B_{c2} of 50 T and 40 T for parallel and perpendicular respectively [42]. This shows that they exhibit less anisotropy thus look attractive and promising for application purposes.

1.1.7 Emergent and debatable topics

Figure 1.5 (a) shows an archetypal phase diagram of FeSc materials exhibiting structural transition, nematic order, magnetic order and superconductivity phase. This provides an exciting platform in trying to explore the close interplay between structural and magnetic dynamics of these materials on one hand, and magnetism and superconductivity on the other. Apparently, other exciting phenomena such as quantum criticality point and Bi-partite phase are revealed as well. This section presents a brief discussion of the unresolved topics as extracted from figure 1.5.

(1). Nematic phase

Nematic state is a well-recognized instability in these materials and it leads to change of lattice symmetry from tetragonal (C_4 -four fold) to an orthorhombic (C_2 -two fold) while time reversal remains unchanged [43 -47]. This normal state phase precedes the magnetic order [43, 48]. Its role in the establishment of superconductivity and its origin has elicited huge debate. Experimentally, the development of nematic order can be realised in two scenarios namely through structural distortion [44] and electronic ordering which involves spin order and charge or orbital order [43, 45]. Structural distortion is associated with phonon-driven transition where the lattice parameters a and b along the x and y directions are inequivalent [44].

The charge/orbital order results from the orbital ordering of Fe 3d electrons which prompts spin density wave. Here the occupancy number of n_{xz} and n_{yz} for orbitals d_{xz} and d_{yz} respectively becomes different [45]. On the other hand, spin ordering involves a magnetic interaction that then causes spin-nematic order. The manifestation of this is reflected on the spin susceptibility $\chi_{\text{mag}}(q)$ where it becomes different along the q_x and q_y directions of the Brillouin zone before a conventional spin density wave (SDW) state develops [43].

Symmetry dictates that the occurrence of any one of the three (lattice, spin or orbital) triggers the others and it is still unclear which one of them is the primary cause. A possibility of lattice distortion being the likely primary order is debatable given that the distortion is weak and acts as a conjugate field to a primary order as attested by resistance anisotropy measurements [46].

(2). Magnetic order

The proximity of the magnetic phase to the superconductivity phase has received attention in condensed matter physics since it is believed that magnetic fluctuations influences the binding of electrons into Cooper pairs . An important and most recent area that is thoroughly under discussion is to determine the nature of the spin ordering that defines this state. Chiefly, three scenarios have been proposed which include itinerant magnetism (weakly coupled electrons), localized magnetism (strongly coupled electrons) and a combination of both (itinerant and localized).

The itinerant scenario shows that electrons are moderately free to move from site to site in a lattice and magnetic order is a result of a stoner-type magnetic instability (this kind of magnetism is often known as spin density wave-SDW). Here spin fluctuation is achieved through fermi surface nesting between electron and hole surfaces around a wave vector $(\pi, 0)(0, \pi)$ in the unfolded Brillouin zone. The spin fluctuation is responsible for pair scattering between electron and hole pockets and it favours a sign reversing superconducting gap (s_{\pm}) [49, 50].

In the localized approach (strongly coupled), often referred to as Heisenberg anti-ferromagnetism, the electrons are strongly held to particular lattice with a very strong coulomb repulsion. Magnetic order in this case is proposed to emerge from an interaction of near neighbour and next near neighbour of local moments from Fe-3d electrons [51, 52]. On

the same context, ferro-orbital ordering is thought to be responsible for a tetragonal-orthorhombic transition. The aforementioned argument then points out that magnetic and structural transitions are driven by an ordering independent of spin degree of freedom. The localized approach is supported by an observation of magnetic moments at high temperatures above T_N and presence of spin waves throughout the Brillouin zone [53].

A unified duality magnetism nature of both components i.e. itinerant electrons and localized moments is proposed, thus leading to the referencing of these materials as ‘Hund’s metal’. In this case, the interaction between electrons is relatively strong that the mass of low energy quasiparticles are enhanced but too weak for them to be localized [54]. An inter-play between spin-orbital interaction (coupling of orbital motion and spin which has been linked to the structural, nematicity and magnetic ordering) [55, 56], and Hund’s coupling in these materials renders the determination of pairing symmetry non-trivial [56]. The interaction can induce a wide-range of uncommon physical properties that include; Anomalous Hall effect (AHE) in ferromagnetic materials [57, 58], Majorana Fermions, Spin relaxation and plays a role in coexistence of magnetism with superconductivity [59]. All these unusual magnetic-related properties and the exotic physics thereof make this class of HTSC very interesting to study.

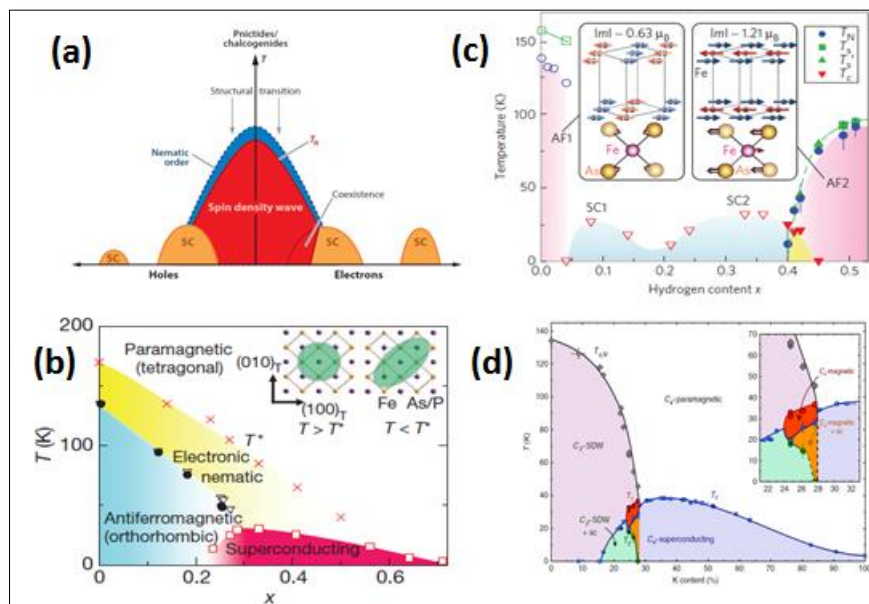


Figure 1.5: Phase diagrams of FeSc: (a) universal phase diagram [48] (b) BaFe_2As_2 [43] (c) two-dome in LaFeAsO [49] (d) the C_4 -coexistence with superconductivity in BaFe_2As_2 [64].

(3) Bi-partite phase

Another important and most recent findings made in LaFeAsO is the bipartite phase which is observed when this system is doped with larger hydrogen concentration limit ($x = 0.35$) compared to fluorine [60]. Remarkably, two superconducting domes (SC1 and SC2) are obtained which leads to an extended superconducting dome and maximum T_c of 36 K as shown in figure 1.5 (c). Suggestions have been made that the first dome ($0.05 < x < 0.18$) emanates from non-doped LaFeAsO whose $T_N = 140$ K while the second dome ($0.20 < x < 0.45$) is from LaFeAsO_{0.5}H_{0.5} with a T_N of 90 K [61].

It is believed that the two domes are because of carrier doping; in this situation, electron doping results to SC1 phase whereas hole-doping gives rise to SC2 phase with a crossover at $x = 0.20$. Another exciting observation made on this system is the merger of the two superconducting domes into one with the highest T_c of 52 K at $x = 0.20$ when pressure of 6 GPa is applied. This observation results to a deviation from the ideal values of Pn(Ch)-Fe-Pn(Ch) angle and h which have been proposed in view of attaining high T_c . On this particular case, an increase in T_c has been attributed to suppression of itinerant spin-fluctuation and simultaneous enhancement of spin fluctuation arising from localized character [62].

(4) Quantum criticality point and C₄ phase

A quantum criticality point (QCP) is realised at a point where the T_c of a phase is zero, in this case magnetic phase, at temperature $T = 0$ [63]. The QCP is a common feature in 122 and 111 families of FeSc. It is still unclear whether QCP is present and lies under the superconducting dome or it is eluded out completely [63]. In these materials, the QCP occurs near the maximum T_c when an extrapolation from magnetic phase is drawn. Its origin is still unresolved and attempts to study its interplay with superconductivity calls for suppression/destroying superconductivity by an application of magnetic fields which renders investigations complex.

Furthermore, a phase diagram of hole-doped Ba_{1-x}K_xFe₂As₂ reveals an intriguing interplay between C₄ tetragonal phase and superconductivity as shown in figure 1.5 (d) (inset is an enlarged C₄ tetragonal region showing a co-existence with superconductivity [64, 65]). It is revealed that the C₄-symmetric magnetic phase competes more with superconductivity than

C_2 orthorhombic phase [64, 65]. The C_4 phase has been linked to spin rather than orbital degrees of freedom, which then proposes an itinerant kind of magnetism in this system.

In view of the foregoing section, it is apparent that FeSc studies involve many unresolved topics which revolve around magnetism. Therefore in this piece of work, the attention will be solely directed to probing magnetic dynamics in iron-pnictides superconductors; particularly the 1111 superconductors as presented in the problem statement section. This class hold a record T_c of 56 K in SmFeAsO [36] and offers voluminous materials with diverse critical parameters (i.e. critical fields, critical temperature, and critical current).

In addition, pnictides exhibit a wide range of fascinating properties ranging from spin, and orbital degrees of freedom, lattice and charge which are fundamentally associated to the emergence of high temperature superconductivity. In the application field, they have higher isotropic critical current [66, 67] moored to good grain boundary nature as compared to cuprates, less anisotropy and high upper critical field which make them attractive in magnetic and electric power applications. Once more, the possibility of the co-existence of superconductivity with magnetism makes them appealing candidates for spintronic applications [68].

1.2 Problem statement

This study is about the low field microwave absorption (LFMA) studies in the normal and superconducting state of FeSc. To begin with, normal state (which involve magnetic order phase, nematicity phase and structural transition) study of Fe-based superconductors is of utmost importance for many reasons. It is through this state that the unconventional superconductivity emerges. Suggestions have been made that the electronic interactions in this state play a fundamental role in the realization of superconductivity. From the phase diagram, it is apparent that magnetic ordering precede the superconductivity phase. It is believed that high density magnetic fluctuations induced by a suppression of magnetic order act as a glue in binding electrons into pairs. A debate on whether this magnetic order is as a result of itinerant nature of electrons or localized moments (Heisenberg) is still unresolved. Ideally, an investigation to probe the magnetic transitions, magnetic anisotropy, spin structure and its ordering will shed light in this otherwise unsettled topic.

In superconducting state, materials are known to exhibit two prominent phenomena namely; Meissner effect and zero resistance. These properties attest to wide use of superconductors in transport sector, medical field (like in MRI), research (for example in NMR and SQUIDs), in microwave devices (such as filters, antennas and resonators) and in fluxonics (flux pumps and lenses of quantized magnetic flux) among many more. Iron pnictides superconductors are promising candidates for applications of this nature. In comparison to cuprates, they have shown superior device application properties such as high critical fields, well connected grain boundaries and isotropic current values. At high magnetic fields, this values matches, and even exceeds, those of metal-conventional superconductors. From the perspective of application, more so in microwave devices, the knowledge with regards to the response of electromagnetic radiation (microwave energy) in these materials is paramount given these devices work on the framework of taking in a signal, manipulating/processing the very signal and sending it out.

To systematically and unambiguously probe the iron pnictides superconductors both in the normal and superconducting state, LFMA known NRMA technique guarantees undisputable results. This is accomplished by the fact that the technique is non-destructive contactless and highly sensitive. Importantly, not all magnetic materials exhibit the LFMA phenomenon. In magnetic materials where this phenomenon is experienced regardless of the sample form (whether in bulk samples, thin films, powders and nanoparticles), crucial information such as magnetic anisotropy, spin ordering, domain structure and magnetic transitions are determined.

Moreover, the LFMA-related materials are considered for possible spintronic applications such as field-dependent microwave absorbers and low field magnetic sensors. The LFMA phenomenon in superconductors is proven as well and can be used to determine critical temperature, critic fields, differentiate between intrinsic and extrinsic superconductivity, detect and uniquely identifies additional phases of minute value (10^{-11} cm^3). Furthermore, the LFMA portrays fascinating features such as magnetic shielding effect, anomalous hysteresis, Wohleben effect (Paramagnetic Meissner effect), surface barrier, irreversibility line which unequivocally provides exciting physics and also informs the nature of the sample as pertains to applications purposes.

To the best of our knowledge, the LFMA study in iron pnictides both in the normal and superconducting states is scarcely reported. In fact, normal state LFMA in iron pnictides has not been reported thus far. In that regard, in an attempt to fill this gap, this work will present LFMA studies in $\text{SmFeAsO}_{1-x}\text{F}_x$ ($x = 0.05, 0.12, 0.20$) which is a member of 1111 pnictide family.

1.3 Objectives

In general, the objective of this study is to examine and understand the electromagnetic response of FeSc by use of electron spin resonance (ESR). Of particular interest will be LFMA. Therefore, the outline of the objectives is as follows;

- To study and understand the LFMA in the normal state of FeSc.
- To study LFMA in superconducting state of FeSc.
- To establish the similarity and differences between LFMA in the normal state and superconducting state and draw a correlation between the two states.
- To compare the overall microwave absorption in FeSc with cuprates and other magnetic materials which exhibit LFMA phenomenon.

References

1. Onnes, H. K. : Commun. Phys. Lab. Uni. Leiden, **120B**, 3 (1911)
2. Reed, et. al. *Materials at Low Temperatures*, Institute of Physics Publishing, Institute of Physics, London, 1998
3. Meissner, W., Ochsenfeld, R.: *Naturwissenschaften* **21** 787 (1933)
4. Gorter C. J., Casimir H. B. G.: Phys. Z. **35**, 963 (1934)
5. London F., London H.: Physica **2**, 341 (1934)
6. London F., London H.: Proc. Roy. Soc. (Lond.) **A149**, 71 (1935)
7. Bardeen J., Cooper L.N., Schrieffer J.R.: Phys. Rev. **108**, 1175-1204 (1987)
8. Werner Buckel. *Supraleitung*. VCH Verlagsgesellschaft mbH, Weinheim, 1990
9. Ginzburg V.L, Landau L.D.: Zh.Eksp. Theo. Fiz., **20**, 1064 (1950)
10. McMillan, W.L., Rowell, J.M.: Phys. Rev. Lett. **14**, 108 (1965)
11. Bednorz, J.G., Muller, K.A., Z.: Phys. B **64**, 189, (1986)
12. Wu, M. K., Ashburn, J. R., Torng, C. J., Hor, P. H., Meng, R. L., Gao, L., Huang, Z. J., Wang, Y. Q., Chu, C. W.: Phys. Rev. Lett. **58**, 908 (1987).
13. Schilling, A., Cantori, M., Guo, J. D., Ott, H. R.: Nature **363**, 56 (1993).
14. Chu, C. W., Gao, L., Chen, F., Huang, Z. J., Meng, R., Xue, Y.Y.: Nature **366**, 323 (1993).
15. Moshchalkov, V., Wordereenweber, R., Lang, W.: '*Nanoscience and Engineering in Superconductivity*' Springer-USA (2010)
16. Zeyer, R., Zwicky, G.: Z.Phys. B **78**, 175 (1990)
17. Keimer, B., Kivelson, S.A., Norman, M.R., Uchida, S., Zaanen, J.: Nature **518**, 179 (2015)
18. Roland, H., kleiner, R., Wolf, T., Zwicky, G.: ArXiv:1306.0429
19. Saxena, A. K., *High-Temperature Superconductors*, Springer-Verlag Berlin-Heidelberg (2010, 2012)
20. Grasso, G., Flükiger, R.: Supercond. Sci. Technol. **10** 223 (1997)
21. Sato, J., Ohata, K., Okada, M., Tanaka, K., Kitaguchi, H., Kumakura, H., Kiyoshi, T., Wada, H., Togano, K.: Physica C **357-360** (2001) 1111; Okada, M.: Supercond. Sci. Technol. **13**, 29 (2000)

22. Plakida, N. P.: *High-Temperature Superconductivity*, Springer-Verlag Berlin-Heidelberg (1995)
23. Gross, R., Alff, L., Beck, A., Froehlich, O. M., Koelle, D., Marx, A.: *IEEE Trans. Appl. Supercond.* **7**, 2929 (1997)
24. Kamihara, Y., Watabane, T., Hirano, M., Hosono, H.: *J. Am. Chem. Soc.* **130**, 3296 (2008)
25. Lee, C.H., Kihou, K., Iyo, A., Kito, H., Shirage, P.M.: *Solid state commun.* **152**, 644-648 (2012)
26. Calderon, M.J., Valenzuela, B., Bascones, E.: *Phys. Rev. B* **80**, 094531(2009)
27. Nomura, T., Kim, S.W., Kamihara, Y., Hirano, M., Sushko, P.V., Kato, K., Takata, M., Shluger, A.L., Hosono, H.: *Supercond. Sci. Technol.* **21**, 125028 (2008)
28. Cruz, C., Huang, Q., Lynn, J.W., Li, J., Ratcliff, W., Zarestky, J.L., Mook, H.A., Chen, G.F., Luo, J.L., Wang, N.L., Dai, P.: *Nature (London)* **453**, 899 (2008)
29. Margadonna, S., Takabayashi, Y., McDonald, M. T., Brunelli, M., Wu, G., Liu, R.H., Chen, X.H., Prassides, K.: *Phys. Rev. B* **79**, 014503(2009)
30. Kamihara, Y., nomura, T., Hirano, M., Kim, J.E., Kato, K., Takata, M., Kobayashi, Y., Kitao, S., Higashitaniguchi, S., Yoda, Y., Seto, M., Hosono, H.: *New J. Phys.* **12**, 033005 (2010)
31. Hess, C., Kondrat, A., Narduzzo, A., hamann-Borrero, J.E., Klingeler, R., Werner, J., Behr, G., Buchner, B.: *Europhys. Lett.* **87**, 17005 (2009)
32. Wei, B. Zhen, H. Q., Fu, C. G., Green, M. A., Ming, W. D., Bao, H.J., Ming, Q.Y.: *Chinese Phys. Lett.* **28**, 086104 (2011)
33. Rotundu, C.R., Keane, D.T., Freelon, B., Wilson, S.D., Valdivia, P.N., Courchesne, B.C., Birgeneau, R.J.: *Phys. Rev. B* **80**, 144517 (2009)
34. Kanagaraj, M., Arumugam, S., Kumar, R.S., Selvan, N.R.T., Muthu, S.E., Thakur, G.S., Yoshino, H., Murata, K., Ganguli, A.K., Zhao, Y.: *Appl. Phys. Lett.* **100**, 052601(2012)
35. Wang, C., Li, L., Chi, S., Zhu, Z., Ren, Z., Li, Y., Wang, Y., Lin, X., Luo, Y., Jiang, S., Xu, X., Cao, G., Xu, Z.A.: *EPL* **83**, 67006(2008)

36. Ren, Z.A., Lu, W., Yang, J., Yi, W., Shen, X.L., Li, Z.S., Chen, G.C., Dong, X.L., Sun, L.L., Zhou, F., Zhao, Z.X.: *Chin. Phys. Lett.* **25** (2008) 2215
37. Nomura, T., Inoue, Y., Matsuishi, S., Hirano, M., Kim, J. E., Kato, K., Takata, M., Hosono, H.: *Supercond. Sci. Technol.* **22**, 055016 (2009)
38. Kimber, S.A.J., Kreyssig, A., Zhang, Y.Z., Jeschke, H.O., Valentí, R., Yokaichiya, F., Colombier, E., Yan, J., Hansen, T.C., Chatterji, T., McQueeney, R.J., Canfield, P.C., Goldman, A.I., Argyriou, D. N.: *Nature Mater.* **8**, 471(2009)
39. Zhao, J., Huang, Q., de la Cruz, C., Li, S., Lynn, J. W., Chen, Y., Green, M. A., Chen, G. F., Li, G., Li, Z., Luo, J. L., Wang, N. L., Dai, P.: *Nature Mater.* **7**, 953 (2008)
40. Kuroki, K., Usui, H., Onari, S., Arita, R., Aoki, H.: *Phys. Rev. B.* **79**, 224511(2009)
41. Hosono, H., Kuroki, K.: *Physica C* **514**, 399-422(2015)
42. Putti, M., Pallecchi, I., Bellingeri, E., Cimberle, M. R., Tropeano, M., Ferdeghini, C., Palenzona, A., Tarantini, C., Yamamoto, A., Jiang, J., Jaroszynski, J., Kametani, F., Abaimov, D., Polyanskii, A., Weiss, J.D., Hellstrom, E.E., Gurevich, A., Larbalestier, D. C., Jin, R., Sales, B. C., Sefat, A. S., McGuire, M. A., Mandrus, D., Cheng, P., Jia, Y., Wen, H. H., Lee, S., Eom, C. B.: *Supercond. Sci. Technol.* **23**, 034003 (2010)
43. Kasahara, S., Shi, H. J., Hashimoto, K., Tonegawa, S., Mizukami, Y., Shibauchi, T., Sugimoto, K., Fukuda, T., Terashima, T., Nevidomskyy, A. H., Matsuda, Y.: *nature* **486**, 382(2012)
44. Kim, M. G., Fernandes, R. M., Kreyssig, A., Kim, J. W., Thaler, A., Bud'ko, S. L., Canfield, P. C., McQueeney, R. J., Schmalian, J., Goldman, A. I.: *Phys. Rev. B* **83**, 134522 (2011)
45. Yia, M., Luc, D., Chua, J.H., Analytisa, J.G., Sorinia, A. P., Kempera, A. F., Moritza, B., Mod, S. K., Moorea, R.G., Hashimotoa, M., Leea, W.S., Hussaind, Z., Devereauxa, T. P., Fishera, I.R., Shena, Z.X.: *PNAS* **108**, 6878-6883 (2011)
46. Chu, J.H., Kuo, H.H., Analytis, J. G., Fisher, I. R.: *Science* **337**, 710 (2012)
47. Baek, S.H., Efremov, D.V., Ok, J.M. Kim, J.S., Brink, J., Büchner, B.: *Nat. Mater.* **14**, 210 (2015)

48. Chubukov, A.: Annu. Rev. Condens. Matter Phys..**3**, 57-92(2012)
49. Kuroki, K., Onari, S., Arita, R., Usui, H., Tanaka, Y., Kontani, H., Aoki, H.: Phys. Rev. Lett. **101**, 087004 (2008)
50. Mazin, I.I., Singh, D.J., Johannes, M.D., Du, M.H.: Phys. Rev. Lett. **101**, 057003 (2008)
51. Ma, F., Lu, Z.Y. : Phys. Rev. B **78**, 224517(2008)
52. Si, Q., Abrahams, E.: PRL **101**, 076401(2008)
53. Dai, P., Hu, J., Dagotto, E.: Nat. phys. **8**, 709 (2012)
54. Yin, Z. P., Haule, K., Kotliar, G.: Nat. Phys. **10**, 845(2014)
55. Borisenko, S.V., Evtushinsky, D.V., Liu, Z.H., Morozov, I., Kappenberger, R., Wurmehl, S., Büchner, B., Yaresko, A.N., Kim, T.K., Hoesch, M., Wolf, T., Zhigadlo, N.D. : Nat. Phys. **12**, 311(2016)
56. Borisenko, S., Evtushinsky, D., Liu, Z., Morozov, I., Kappenberger, R., Wurmeh, S., Buchner, B., Yaresko, A., Kim, T., Hoesch, M., Wolf, T., Zhigadlo, N.: Phys. Status Solidi B **254**, 1600550(2017)
57. Sacramento, P.D, Araujo, M.A.N., Viera, V.R, Dugaev, V.K, Barnas, J.: Phys. Rev. B **85**, 014518(2012)
58. Nagaosa, N., Sinova, J., Onoda, S., MacDonald, A.H., Ong, N. P.: Rev. Mod. Phys., **82**, 1539 (2010)
59. Lo, S.T., Lin, S.W., Wang, Y.T., Lin, S.D., Liang, C.T.: SCI. REP. **4**,5438 (2014)
60. Iimura, S., Matsuishi, S., Sato, H., Hanna, T., Muraba, Y., Kim, S.W., Kim, J.E., Takata, M., Hosono, H.: Nature Commun. **3**, 943 (2012)
61. Hiraishi, M., Iimura, S., Kojima, K.M., Yamaura, J., Hiraka, H., Ikeda, K., Miao, P., Ishikawa, Y., Torii, S., Miyazaki, M., Yamauchi, I., Koda, A., Ishii, K., Yoshida, M., Mizuki, J., Kadono, R., Kumai, R., Kamiyama, T., Otomo, T., Murakami, Y., Matsuishi, S., Hosono, H.: Nature Physics **10**, 300(2014)
62. Kobayashi, K., Yamaura, J., Iimura, S., Maki, S., Sagayama, H., Kumai, R., Murakami, Y., Takahashi, H., Matsuishi, S., Hosono, H.: Sci. Reports **6**,39646 (2016)
63. Abrahams, E., Si, Q.: J. phys. Condens. Matter **23**, 223201(2011)

64. Böhmer, A.E., Hardy, F., Wang, L., Wolf, T., Schweiss, P., Meingast, C.: Nat. Commun. **6**, 7911 (2015)
65. Mallett, P. P., Marsik, P., Rizi, M.Y., Wolf, T., Böhmer, A. E., Hardy, F., Meingast, C., Munzar, D., Bernhard, C.: PRL **115**, 027003 (2015)
66. Moll, P.J.W., Puzniak, R., Balakirev, F., Rogacki, K., Karpinski, J., Zhigadlo, N. D., Batlogg, B.: Nat. Mater. **9**, 628 (2010)
67. Gurevich, A.: Rep. Prog. Phys. **74**, 124501 (2011)
68. Patel, U., Hua, J., Yu, S. H., Avci, S., Xiao, Z. L., Claus, H., Schlueter, J., Vlasko-Vlasov, V. V., Welp, U., Kwok, W. K.: Appl. Phys. Lett. **94**, 082508 (2009)

Chapter 2

Magnetic properties of type two superconductors

In this chapter, magnetic properties of type II superconductors are reviewed. More particularly, fundamental realms of magnetic dynamics which have a close relation to LFMA phenomenon are selectively discussed. These include, Josephson junction, rf-SQUIDs, granularity, critical state (Bean model, Kim Anderson), two-level critical state, spin glass effect, flux flow, pinning and surface resistance.

2.1 Josephson junction (JJ)

Superconducting condensate as a macroscopic quantum state is defined by wave function in equation 2.1. Here $\rho(r)$ and θ are the probability density of superconducting electrons and wave function connected to flow of supercurrent respectively [1].

$$\varphi(r) = \sqrt{\rho(r)}e^{i\theta(r)} \quad 2.1$$

In case two superconductors are separated by a very thin tunnelling barrier of length of the order ξ , their superconducting wave functions will overlap and the barrier will exhibit a coherent phase thus a supercurrent will quantum-mechanically flow from one superconductor to another via the tunnelling barrier without voltage drop. Here the thin barrier acts as a weak coupling/link thus forming a JJ as shown in figure 2.1. The whole phenomenon is called the Josephson effect. Apart from tunnelling barrier [superconductor-insulator-superconductor (SIS)], a JJ can be realised through; metal separation often known as proximity junction [superconductor-metal-superconductor (SNS)], through point contact, and micro-bridge (constriction) which is designed to allow a flowing current to exceed I_c only at the constriction.

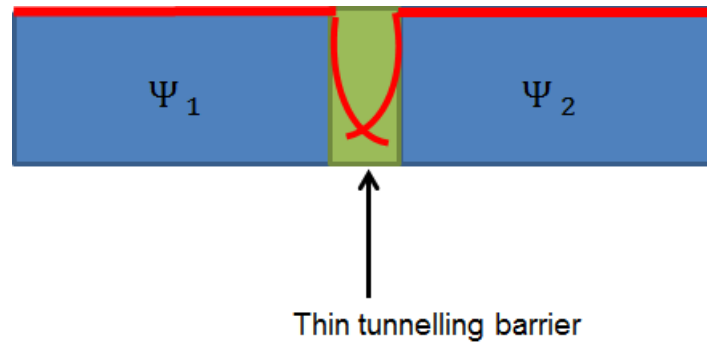


Figure 2.1: schematic diagram of a Josephson junction

Consequently, the current and voltage across the junction can be expressed by equations 2.2 and 2.3 respectively.

$$I_s = I_c \sin \theta \quad 2.2$$

$$V = \frac{\Phi_0}{2\pi} \frac{d\theta}{dt} \quad 2.3$$

Here, $\theta = \theta_1 - \theta_2$ is the superconducting phase difference of two superconductors forming a junction, and $I_c > 0$ is the critical current parameter of JJ. When $I_s = 0$ (no external current applied), $\theta = 0$ and it corresponds to the minimum of energy (ground state) whereas the solution $\theta = \pi$ corresponds to the energy maximum and is unstable. These two equations define DC Josephson effect which shows that even without an application of voltage across the junction, an electric current can flow and its magnitude is proportional to θ . Conversely, when finite voltage is applied, an AC Josephson effect is established and the current oscillates as

$$I(t) = I_c \sin(2eVt / \hbar) \quad 2.4$$

In granular/ceramic superconductors, JJs are ubiquitous where they are formed in a natural way between the superconducting grains. The supercurrent is governed by Josephson coupling energy as devised in equation 2.5. This energy is a function of both temperature (T) and magnetic field (H). At very low temperatures $T \ll T_c$ the superconducting grains are strongly coupled together with a strong Josephson coupling energy and weak links have large supercurrent similar to bulk superconductivity. However, at $T \sim T_c$, the Josephson coupling energy weakens due to an increase in thermal energy which then amounts to a reduction in supercurrent.

$$E_j(T) = \frac{\hbar I_c}{2e} = \frac{h}{8e^2 R_n} \Delta(T) \tanh\left(\frac{\Delta(T)}{2K_B T}\right) \quad 2.5$$

where I_c is the critical current between grains forming a junction, R_n is resistance of the junction when in the normal state and $\Delta(T)$ is the BCS energy gap.

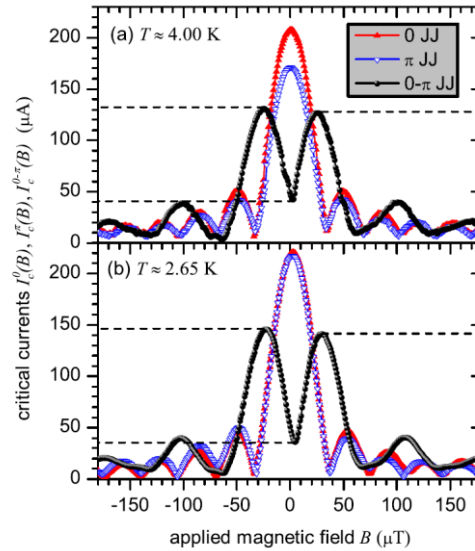


Figure 2.2: Critical currents of 0 JJ (red), π JJ (blue), and 0- π JJ (black) measured at (a) 4.2 K and (b) 26.5 K [2]

Depending on the type of separation between grains, the JJ critical current as function of magnetic field can be a maximum or minimum at zero field as shown in figure 2.2. This often leads to the appearance of interesting features such as phase reversal and the Wolleben (paramagnetic Meissner) effect in LFMA studies.

Furthermore, the formation of 0, π and 0- π JJs can be used in SIFS technology in complimentary logic circuits, in RSFO with active π junctions and in π qubits [2]. Again, low ξ in the c-axis between CuO-CuO layers lead to the formation of intrinsic Josephson junction (ijj) effect within the unit cell [3]. The ijj utilizes the Josephson effect where direct current voltage is naturally converted into a high frequency electric current. It can be used in applications where it can act as a source of sub terahertz and terahertz frequencies [3].

2.2 RF-SQUID

An RF superconducting quantum interference device (SQUID) is one of the most celebrated devices fabricated by exploiting the properties of Josephson junction effect and is capable of measuring small magnetic flux variations. It involves a configuration comprised of a superconducting loop interrupted by a single Josephson junction as shown in figure 2.3. The dynamic and static characteristic of this system has been studied [4] and its single-valued wave function is defined as

$$\oint P \cdot dl = kh \quad 2.6$$

here k is an integer and $P = m * v + \frac{e^*}{c} A$ is the canonical momentum of a cooper pair. The total flux enclosed in this kind of loop (Φ) is the summation of the self-induced flux ($\Phi_i = LI$) and external applied flux (Φ_x) and can be expressed as;

$$\Phi_x = \Phi + Li_c \sin\{(2e / \hbar)(\Phi - k\Phi_0)\} \quad 2.7$$

$$Li = -Li_c \sin\{(2e / \hbar)(Li + \Phi_x - k\Phi_0)\} \quad 2.8$$

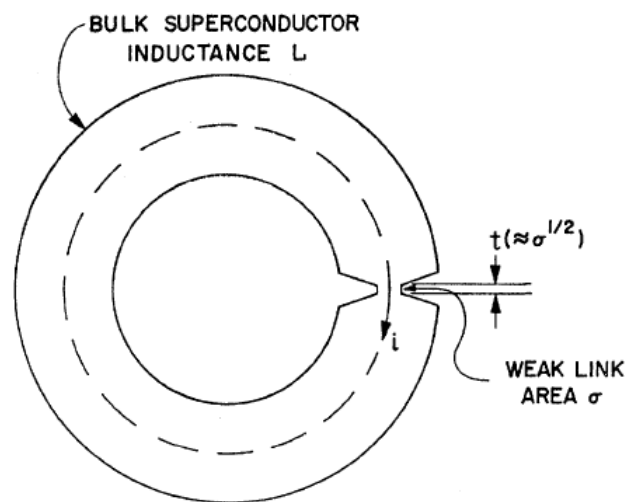


Figure 2.3: Superconducting ring with inductance L , the length of weak link t with a cross section σ [4].

Then the Gibbs energy of this loop is expressed as

$$G = \frac{1}{2} Li_0^2 G = \frac{1}{2} Li_0^2 \sin^2 \left[\frac{2\pi}{\Phi_0} (\Phi - k\Phi_0) \right] - \frac{i_0 \Phi_0}{2\pi} \cos \left[\frac{2\pi}{\Phi_0} (\Phi - k\Phi_0) \right] + G_0 \quad 2.9$$

The first term denotes the magnetic field and the second term defines the junction coupling energy. The variations of the total current i and the Gibbs free energy G versus the applied external magnetic flux Φ_x in the $i_0 > \Phi/2\pi$, $i_0 = \Phi/2\pi$, and $i_0 < \Phi/2\pi$ is shown in the figure 2.4. In the case where $i_0 < \Phi/2\pi$, the curves are single-valued whereas for $i_0 > \Phi/2\pi$, the curves are multi-valued. A variation of external flux as a function of time results to transitions between adjacent fluxoids states as the junction reverts to the normal state (i.e $i = i_0$). These transitions happen precisely at the values of $\Phi_x = k\Phi_0 \pm (\Phi_0/4 + Li_0)$. As a result, an emf, $\varepsilon = -\delta\tau\Phi$, is expected to be induced in the closed circuit and a change in flux can be calculated using 2.7 while the time interval is taken to be the induction decay time of the loop $\tau = L/R_n$, (here R_n normal resistance of the junction).

The emf results to microwave power absorption that can be related to spectral lines (quantum oscillations) observed in low field microwave absorption measurements (equally spaced spectral lines are discussed in the next chapter). Furthermore, modelling powdered sample of YBCO as system consisting of weakly connected superconducting rings (RF-SQUIDS) has been invoked to discuss the anomalous DC field dependence of LFMA [5]. Here the anomaly is deconstructed on the basis of microwave absorption loss emanating from rf induced supercurrents that drive damped fluxons which are pinned in non-hysteretic JJs.

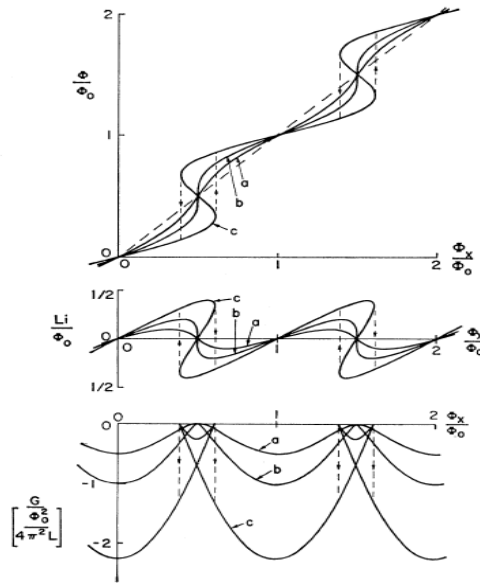


Figure 2.4: Magnetic flux (Φ) circulating current (I) and free energy (G) of an RF SQUID as functions of the external magnetic field Φ_x . The curves correspond to (a) $i_c = \Phi_0/\pi L$, (b) $i_c = \Phi_0/2\pi L$, and (c) $i_c = \Phi_0/4\pi L$ [4]

2.3 Granularity

HTSC are granular in nature caused by the ever-present weak links resulting from imperfections, grain misalignment and short coherence length [6]. This is attested to by a two-stage transition from a normal state to a long-range and coherent superconductivity state exhibited by experiments such as resistivity, magnetic susceptibility, and specific heat measurements [7-13]. To that effect, superconducting grains which are usually of the order of micron in size are separated by non-superconducting matrix. This happens in all sample material forms i.e. thin films, single crystals and polycrystalline. As a matter of fact, weak links in the form of JJs can be formed within a unit cell owing to adequate low inter-layer coupling [3]. These weak bonds result in a depression of the order parameter and they dictate the electromagnetic properties of any granular superconductor.

Due to granularity, magnetic field lines are allowed to enter a system at low fields smaller than the lower critical fields ($H_{c1} = \Phi_0/(4\pi\lambda^2)\ln\lambda/\xi$). The material remains superconducting on condition that the applied field is less than the upper critical fields ($H_{c2} = \Phi_0/(2\pi\xi^2)$). Despite the presence of magnetic field lines (fluxons) in this regime, coherence of superconductivity state is preserved which is main attribute of these materials for strong magnetic field applications. This quantized fields, (fluxons), get pinned inside

grains or within the weak links translating to what is known as intra-pinning and inter-pinning respectively.

Damped motion of fluxons is fundamentally one of the important mechanism which leads to microwave loss in granular superconductors and has been proposed to be the main mechanism that leads to LFMA signal. Once more, in LFMA studies, fluxons are related to fascinating features such as anomalous magnetization/hysteresis and spin-glass behaviour which are truly a manifestation of granularity. The implication of granularity on material application is huge. For instance weak coupling results in a reduced overall critical current density of a material and fluxon motion leads to flux flow resistivity.

2.4 Spin glass behavior

As discussed in section 2.3, due to defects such as cracks, voids, oxygen deficiency and grain boundaries, HTSC are comprised of an ensemble of clusters of superconducting grains which are weakly linked into closed loops via the Josephson effect. The weak bond can be either due to proximity effect or Josephson tunnelling. The weak link supports screening super-currents in response to an externally applied DC field. These grains whose dimensions are comparable to penetration depth are coupled by the pair-tunnelling Hamiltonian defined as[14]

$$\kappa = \sum_{\langle ij \rangle} J_{ij} \cos(\phi_i - \phi_j - A_{ij}) \quad 2.10$$

with supercurrent from grain i to grain j

$$I_{ij} = \frac{2eJ_{ij}}{h} \sin(\phi_i - \phi_j - A_{ij}) \quad 2.11$$

Here J_{ij} is the energy of JJ between grains i and j ; ϕ_i is the phase in i and A_{ij} is the phase factor expressed as

$$A_{ij} = \frac{2\pi}{\Phi_0} \int_i^j \vec{A} \cdot d\vec{l} \quad 2.12$$

It has been shown that the fluxons enter such an array of the field interval $\Delta H = \Phi_0/S$ (here S is the area of the clusters at 2π phase slips). As magnetic field is varied, phase slips will occur at $\Phi = (n + 1/2)\Phi_0$ (here n is an integer), when the system hops from one energy state to another. Each phase slips will generate a voltage between neighbouring grains in accordance with the JJ

$$V(t) = \frac{\hbar}{4\pi e} \delta_t \gamma \quad 2.13$$

This results to an energy dissipation through the normal resistance of the coupling junction.

The time averaged power absorption experienced is formulated as

$$P = \frac{1}{R_n} \langle V^2(t) \rangle \quad 2.14$$

where R_n is the normal state Josephson junction resistance. The spin glass behaviour has been associated to microwave absorption lines which are characteristically narrow, well spaced and anisotropic. The lines have been attributed to damped motion of fluxons into regular array of twin planes in a sample [15].

2.5 Critical state model

This section briefly highlights various critical state models namely: the Beans' model, Kim-Anderson model, linear model and the power law.

The **Beans' model** is devised by considering the slab of hard superconductor from a macroscopic point of view. It is built on the basic premise that when a magnetic field is applied, a macroscopic supercurrent circulates in the sample. Here the model considers two possible states for current density: the current density is either zero for areas that never experience magnetic field and maximum (either positive or negative) in areas with magnetic field. Now the critical state is arrived at if the critical current density J_c flows everywhere in the sample [16,17]. For a slab of thickness D the magnetization relations are given as;

$$-4\pi M = H - H^2 / 2H^* \quad \text{for } H \leq H^* \quad 2.15$$

$$-4\pi M = H^* / 2 \quad \text{for } H \geq H^* \quad 2.16$$

where $H^* \equiv \pi J_c D / 5$ represents the field value at which the flux density reaches the centre of the slab. This model is sample size dependent given that the total current density is proportional to the sample size.

Kim Anderson model's is a generalization of Bean's critical model where the concept of critical states is considered. In this regard, every macroscopic region of a sample carries a critical current density determined by local magnetic field at that region. Experimentally, the model was devised on tubular sample. In that regard, an application of an external magnetic field along the tube axis leads to induced currents in the sample which opposes any change.

On further increasing of the externally applied field, the induced currents penetrate further into the the sample hence attaining a critical state. In this model, the J_c is assumed to take the relation 2.17 [18].

$$J_c = \frac{k}{B_0 + |B_i|} \quad 2.17$$

where k shows the capacity of a sample to carry current, and is thermodynamic critical field of a material. This relation yields a parabolic variation of B_i inside the sample.

The Kim Anderson model is universal and it can result to other fundamental critical state models on assumption of some factors. For instance, in case $B_0 > B_i$, equation 2.17 will yield $J_c(B_i) = A - C|B_i|$ which is the **linear model**; here A and C are positive constants. Moreover, assuming that k and B_0 are infinite in which k/B_0 is a constant, leads to a Bean's model. The **power law** model is arrived at if $B_0 = 0$ thus simplifying equation 2.17 to $J_c(B_i) = k/|B_i|$ in which the power of B_i is -1 [19].

2.6 Two- critical state model

The critical state model discussed in section 2.5 falls short in elucidating most of the magnetic features in HTSC materials. One notable feature is the anomalous hysteresis where the sample reaches a minimum before coming to zero for a reverse field sweep than in forward field scan. Contrary, in conventional superconductors the hysteresis curve in the reverse field is higher than in the forward scan and attains a minimum only at negative values of the field as shown in figure 2.5.

It is important to note that single critical state models demystifies magnetic process of macroscopically homogeneous samples where the flux density in the entire sample is controlled by a single critical current density. This means that all the fluxons present have same magnitude of contribution towards microwave loss (hysteresis). On the contrary, in the ceramic/granular superconductors, two critical current density are present; an intra-granular current density in the grains and an inter-granular current density in weak links of JJ-type.

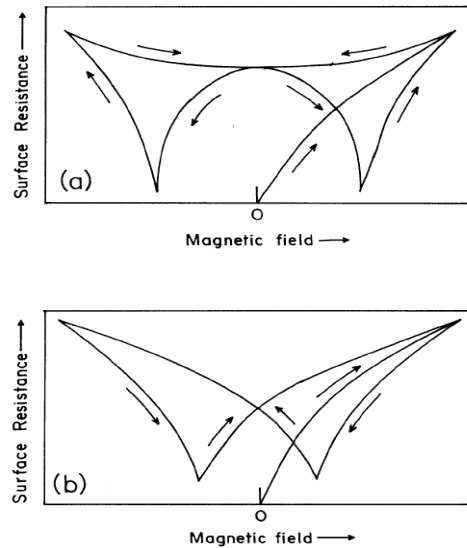


Figure 2.5: An illustration of surface resistance hysteresis based on models: (a) the single critical state and (b) the two-level critical state [20].

The two-level model by Ji *et al* [21] seems to describe main hysteresis features in HTSC. This model is built on the assumption that flux gradient in a macroscopic level is governed by an average of flux density from grains. This gradient is determined by J_c whose value is 100 A cm^{-2} (inter-granular). Whereas, on the local level, the gradient is determined by J_c whose value is $\sim 10^4\text{--}10^5 \text{ cm}^{-2}$ (intra-granular).

Consequently, two types of fluxons are considered in this model. First, is the fluxons that pass through the inter-granular or weakly superconducting regions. They are free to move and are often known as grain boundary fluxons. The other are strongly pinned/trapped fluxons inside the grains. This model reproduces most of the essential surface resistance features exhibited HTSC.

2.7 Flux flow and Pinning

As of now, it is clear that fluxons in a superconductor dictates magnetic dynamics. The fluxons enter the superconductor through weak-links whenever the externally applied field exceeds the lower critical field of the JJ as shown in figure 2.6. If the fluxon is subjected to a driving force such as the Lorentz force (from applied current, force due to temperature gradient or magnetic field), it will start to move. This fluxon motion is only subjected to a drag or friction/viscous force ($-\eta v$) which acts in the opposite direction. Due to the fact that these materials are granular, some flux lines get pinned by sample imperfections.

At equilibrium (critical point), where the pinning force is equal to Lorentz force ($F_p = F_L = J \times B$), the field lines are completely pinned (where $J = n_s e v_s$ with n_s as the density of superconducting electrons and v_s as superfluid velocity). The pinning force F_p is dependent on both temperature and local magnetic induction B . However, with an increase of current, the Lorentz force surpasses the potential pinning force. At this state, the velocity of the fluxon is defined as $\Phi_0 J / \eta = v$. A steady state of motion of fluxons results in an electric field defined as

$$E = Bv = \frac{B}{\eta} \Phi_0 J = \rho_{ff} J \quad 2.18$$

The term $\rho_{ff} = \frac{B}{\eta} \Phi_0$ is referred as the flux resistivity which can as well be formulated as

$$\rho_{ff} = \rho_n \frac{B}{B_{c2}} = \frac{n \Phi_0}{c^2 \eta} \quad 2.19$$

where ρ_n is the normal-state resistivity, B_{c2} is the upper critical field, n is the fluxons density and η is the coefficient of fluxon viscosity. Following the Barden-Stephen model [22], η can roughly be expressed as

$$\eta \approx \frac{\Phi_0 H_{c2}}{\rho_n c^2} \quad 2.20$$

Accordingly, the flux resistivity can be represented approximately to be;

$$\rho_{ff} \approx \rho_n \frac{B}{H_{c2}} \quad 2.21$$

The Flux resistivity leads to both power dissipation ($J \cdot E$) and an increased transport entropy (noise) from the normal core. Furthermore, it modifies critical superconducting properties of a material thus becoming an obstacle in superconductor-related applications.

Importantly, pinning through artificial engineered defects has been introduced as a remedy. These is achieved through use of magnetic particles, secondary phase, defects through columnar and ion irradiation, and compositionally modulated super lattice [23- 28]. The structured form of pinning give control over fluxon/vortex pattern- dynamics and further enhance dissipation-less current that a superconducting material can maximally sustain. The introduced pinning centers energetically favour a normal core to reside within them. The superconducting condensation energy at the pinning site is the maximum pinning energy which can be expressed as

$$U_{cp} = (H_c^2/8\pi)\pi\xi^2 = [\Phi_0/8\pi\lambda(T)]^2 \quad 2.22$$

Here all symbols have their usual meaning. As $T \rightarrow T_c$, λ increases $\lambda^2(0)/\lambda^2(T) \sim (1 - T/T_c)$ leading to drop in pinning energy [23].

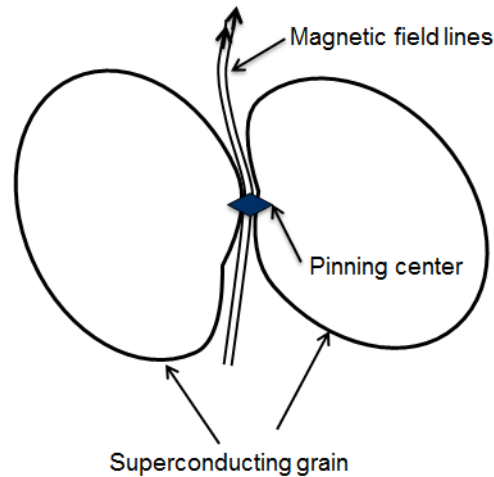


Figure 2.6: Magnetic fields lines (fluxons) thread through weak links formed between superconducting grains.

On the other hand, despite the fact that fluxons act as the hindrance to a full realization of superconductor-related applications, their presence has been exploited in the field of fluxonics. Here fluxons are manipulated and controlled analogous to electronics where electrons are manipulated. Manipulation involves vortex channelling and vortex ratchets which control the net motion of the vortices. This idea has minimized the noise by removal of trapped magnetic flux thus resulting in improved performance of superconductor-based devices such as lenses of quantized magnetic flux and diodes [29].

2.8 Surface resistance

Surface impedance Z_s is a vital quantity which can generally be used to probe the mechanisms of electronic conduction of a superconductor. With intrinsic surface resistance R_s and intrinsic surface reactance X_s , surface is expressed as;

$$Z_s = R_s + iX_s = \sqrt{\frac{j\omega\mu_0}{\sigma_s}} \quad 2.23$$

where σ_s is the complex conductivity, ω is the angular frequency of the radiation, and μ_0 is permeability of free-space. The surface resistance (R_s) defines the dissipated energy which is fundamentally important in providing information on properties of (1) the superconducting

ground state and the low-lying excitation and (2) superconductor-based devices performance. Conversely, the surface reactance (X_s) represents the energy stored in the conductor.

For an archetypal HTSC system and in microwave regime, resistance and reactance can be expressed based on two-fluid model as 2.24 and 2.25 respectively [30].

$$R_s = \frac{1}{2} \omega^2 \mu_0 \sigma_n \chi_n \lambda_L^2 \quad 2.24$$

$$X_s = \omega \mu_0 \lambda_L \quad 2.25$$

where σ_n , λ_L and χ_n are is the temperature dependent London penetration depth, conductivity in the normal state and the fraction of the normal fluid respectively. From equation 2.24, it can be seen that R_s is chiefly contributed by the normal fluid. The X_s is proportional to λ_L (can be used to determine penetration depth as defined in 2.26 and 2.27) [31].

$$X_n(T) = 1 - (\lambda_0^2 / \lambda_L^2) \quad 2.26$$

$$\lambda_L = \lambda_0 / \left(1 - (T / T_c)^4\right)^{1/2} \quad 2.27$$

where λ_0 is the penetration depth at $T = 0$ K.

Figure 2.7 shows at a glance the microwave surface resistance versus frequency of *Cu* and *YBCO*. It is clear that the surface resistance of *YBCO* is three orders less than that of *Cu*. This automatically signifies smaller microwave loss in *YBCO* compared to *Cu* in the mobile communication regime. Negligible or zero resistance is one of the fundamental properties exploited in superconductor-related applications thus superconductors offer a substantial advantage in microwave applications. The negligible losses afforded by superconductors is exploited in improving the quality factors $Q = f_0 / \Delta f$ (where f_0 and Δf are the centre frequency and resonance respectively) of filters and resonators. Equally, it results in miniaturization of the available devices [29].

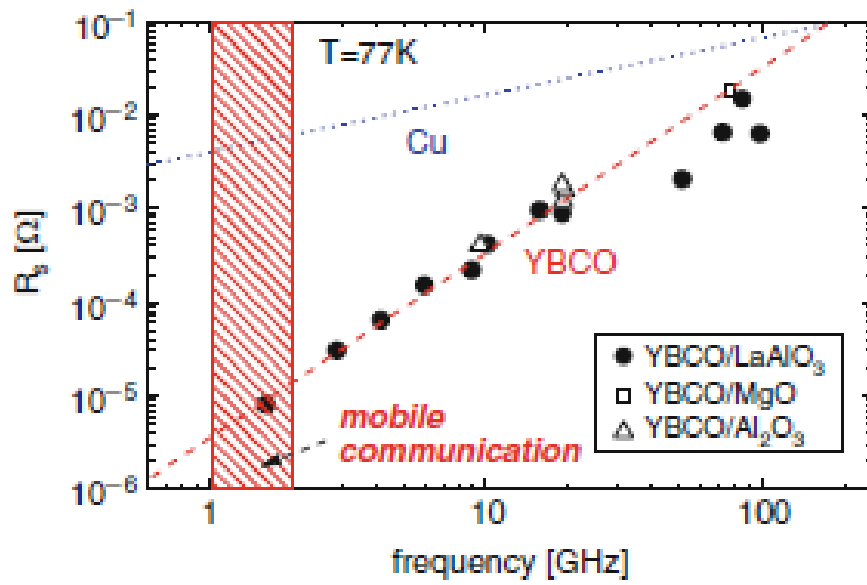


Figure 2.7: Microwave surface resistance of YBCO films and Cu at $T=77\text{ K}$ [29].

References

1. Barone, Paterno: Physics and Applications of the Josephson Effect, (John Wiley & Sons, Inc., New York) 1982
2. Weides, M., Kemmler, M., Kohlstedt, H., Waser, R., Koelle, D., Kleiner, R., Goldobin, E.: PRL **97**, 247001 (2006)
3. Welp, U., Kadowaki, K., Kleiner, R., nature **7**, 702 (2013)
4. Silver, A.H., Zimmerman, J.E.: Phys. Rev. **157**, 317 (1967)
5. Srinivasu, V.V., Bhat, S.V., Kumar, N.: solid state commun. **4**, 375-378 (1994)
6. Deutscher, G., Muller, K.A.: Phys. Rev. Lett. **59**, 1745 (1987)
7. Singh, S. J., Shimoyama, J. I., Yamamoto, A., Ogino, H., Kishio, K., Supercon.Sci. **26**, 065006 (2013)
8. Fang, L., et al Nat. Commun. **4**, 2655 (2013)
9. Lida. K., et al Nat. **3**, 2139 (2013)
10. Gerber, T., Grenet, M., Cyrot, J., Beille.:Phys. Rev. Lett. **65**, (1990) 3201
11. Pureur, P., Costa. R.M., Rodrigues, P., Schaf, J., Kunzler, J.V.: Phys. Rev. B **47**, 11420 (1993)
12. Janod, E., Junot, A., Graf, T., Wang, K.Q., Triscone, G., Muller, J.: Physica C **216**, 129 (1993).
13. Loram, J.W., Cooper, J.R., Mirza, K.A.: Supercond. Sci. Technol. **4**, S391 (1991).
14. Ebner, D., Stroud.: phys. Rev. **B 31**, 165 (1985)
15. Blazey, K.W., Portis, A.M., Muller, K.A., Bednorz, J.G., Holtzberg, F.: Physica C **153-155**, (1988) 56-58
16. Bean, C.P.: Phys. Rev. Lett. **8**, (1962) 250
17. Bean, C.P.: Rev. Mod. Phys. **36**, 31 (1964)
18. Kim, Y.B., Hempstead, C.F., Strnad, A.R.: Phys.Rev. **129**, 52 (1963)
19. Yamamoto, K., Mazaki, H., Yasuoka, H.: Phys. Rev. B. **47**, 915 (1993)
20. Raychaudhuri, P.: Supercond. Sci. Technol. **9**, 447-452 (1996)
21. Ji, L., Rzchowski, M.S., Anand, N., Tinkham, M.: Phys. Rev. B **47**, 470 (1993)
22. Tinkham, M.: Introduction to Superconductivity, (McGraw Hill, New York) 1975
23. Jan, D. B., Coulter, J. Y., Hawley, M. E., Bulaevskii, L. N., Maley, M. P., Jia, Q. X.: Appl. Phys. Lett. **82**, 5(2003)

24. Dou, S. X., Soltanian, S., Horvat, J., Wang, X. L., Zhou, S. H., Lonescu, M. Liu, H. K.:
Appl. Phys. Lett. **81**, 3419 (2002)
25. Panarina, N. Y., Talanov, Y. I., Shaposhnikova, T. S., Beysengulov, N. R. Vavilova, E.
Phys. Rev. B **81**, 224509 (2010)
26. Lee, S., et al nature **12** 392 (2013)
27. Talanov, Y., et al Supercond. Sci. Technol. **26**, 045015 (2013)
28. Fang, L., et al Nature Commun. **4**, 2655 (2013)
29. V. Moshchalkov, R. Worderenweber, W. Lang, 'Nanoscience and Engineering in
Superconductivity' (Springer-USA, 2010)
30. Wu, C. J., Chen. Y. L.: Prog. Electromagn. Res. **111**, 433 (2011)
31. Aly, A. H. Sabra, W. Physica C **495**, 126 (2013)

Chapter 3

Low Field Microwave Absorption (LFMA)

Introduction

Since the discovery of HTSC, significant research work has been reported highlighting fascinating properties and exotic features of these materials using electron spin resonance (ESR) spectrometer. Here we demonstrate that the ESR spectrometer still remains a powerful tool in characterizing superconductors. Importantly, given that superconducting materials are not ordinarily paramagnetic systems, the signal observed in HTSC is distinctively different from resonance absorption mode (saturation state). It is well known that the resonance signal originates from magnetic transition which occurs when the energy difference between two energy levels of a system is equal to the radiation energy [1].

On the contrary, the signal recorded in HTSC is centered around zero DC magnetic field and often known as LFMA or NRMA or MMMA. This chapter provides a discussion on the experimental set up. Furthermore, a review on LFMA phenomenon both in superconductors and in magnetic materials is presented.

3.1 Experimental Set-Up

The main measurements discussed in this work were recorded in a Bruker EMX electron spin resonance (ESR) spectrometer (block diagram in figure 3.1). In general, the ESR machine works as follows: a Klystron (monochromatic microwave source) generates microwave energy and feeds a critically coupled cavity through a rectangular hollow wave-guide. The reflected microwave power from the cavity is directed to the detector (microwave diode), and consequently converted into an electric current. This yields a signal that is proportional to the value of microwave power reflected by the sample. Radiations (microwaves) that get reflected from the diode are uniquely directed to a wedge and accordingly converted to heat.

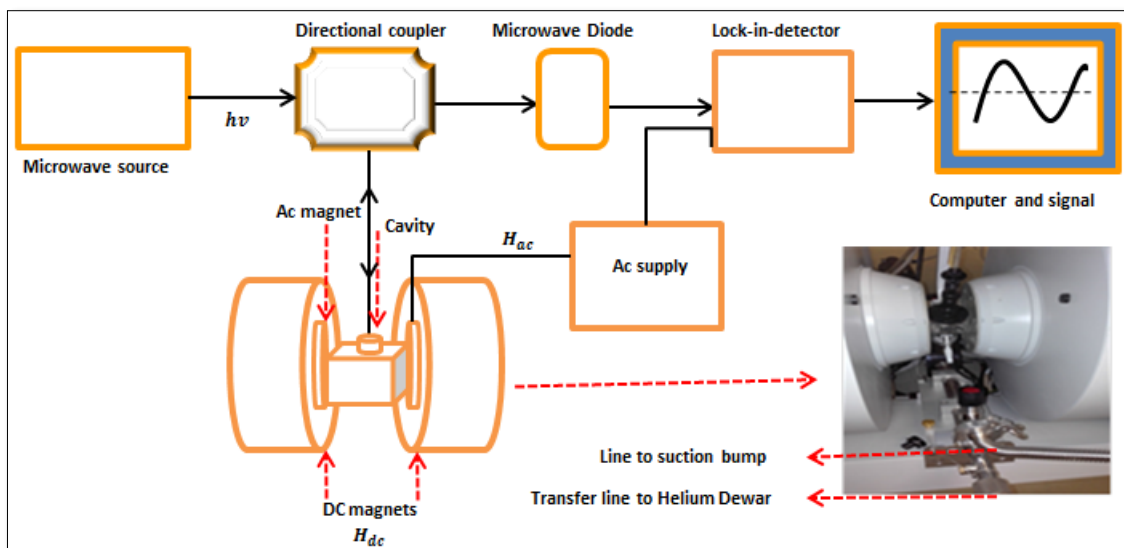


Figure 3.1: a block diagram of an electron spin resonance spectrometer.

It is imperative to state that the detector operates at a constant current and this is made possible through extra microwave power supplied by reference arm. Then the phase shifter ensures that reference arm, microwaves signal and reflected microwaves signal are in phase when they combine at the diode. The signal is once more fed into a lock-in detector which uniquely averages signals thus optimizing the amplitude and phase while quashing statistical noise. Therefore any sample that absorbs microwaves can cause an ESR signal which is then displayed on the computer as microwave power derivative signal. This signal is a result of a combination of three different fields namely: static DC magnetic field from the DC magnets, a collinear low frequency AC field with 100 KHz frequency superimposed on static DC magnetic field and a transverse microwave fields.

$$H(t) = H_0 + H_m \cos \omega_m t + H_{mw} \cos \omega_{mw} t \quad 3.1$$

Here H_0 is the DC magnetic field, H_m is the AC field amplitude and H_{mw} is the field amplitude of microwave radiation. The AC field is often known as a modulation field whose sole role is to introduce modulation (variations) in the the DC magnetic field.

In this work, a cryostat (Oxford Instruments ESR 900 helium continuous flow cryostat) was used. By using a suction pump, the cryostat was evacuated to avoid condensation. Consequently, the liquid helium in a dewar was drawn by an evacuated chamber transfer line where it was evaporated to cold gas and fed to cavity. The temperature control unit was used to ensure desired temperature measurements were made accurately.

Furthermore, prior to any measurement in the superconducting state, a zero field cooling (ZFC) procedure was performed where the sample was cooled at zero magnetic field to the required temperature. Measurements were taken in two field sweep ranges; low field sweep (-250 G through zero to +250 G) and high field sweep (-500 G through zero to + 9500 G).

Samples were synthesized by solid state reaction route using pure SmAs, Fe, Fe₂O₃ and FeF₂. The starting reagents were mixed and pressed into pellets under a pressure of 40 MPa and then sintered at 900^o C for 45 h in evacuated quartz ampoules. Prior to LFMA measurements, fundamental studies such as microstructural analysis (SEM, TEM), resistivity DC magnetization and VSM were performed. Microstructural analysis helps to uniquely analyse the grain-grain connections, reveal voids (defects) and determine the grain sizes.

Essentially, resistivity, DC magnetization and VSM provides information on transition temperatures and reveal inter-granular and intra-granular superconductivity thus provides a guide in setting out parameters upon which LFMA measurements can be carried out. The LFMA measurements were carried out at X-band regime (9.4 GHz) with modulation frequency of 100 kHz and on temperature range of 4-300 K.

3.2 LFMA in Superconductors

LFMA is an exhilarating phenomenon which has developed into a dominant and unambiguous technique in characterizing superconducting materials. It involves an observation of very intense, broad and non-resonant signal around zero magnetic fields. The technique is explicit, highly sensitive and non-destructive (contactless). In superconductors, the phenomenon was first reported in granular thin film of conventional superconductor [2] and later supported by Kim et al and Muller et al in the studies of conventional *Pb* and *Sn* thin films respectively [3, 4]. Thoughtfully, it was revealed that the phenomenon could only be exhibited in materials with JJs whose thickness is more than ξ [3, 4].

Despite these early studies, the LFMA phenomenon in superconductors was rarely known until 1987 when it was observed in high T_c ceramic YBCO [5,6] and later followed by other research groups [7-13]. Since then, LFMA studies have been broadly carried out in a variety of superconductors such as alkali fullerenes [14], borocarbides and oxyfluorides [15, 16], granular conventional superconductors both type I and type II [17, 18] MgB₂ [19] and in FeSc [20, 21].

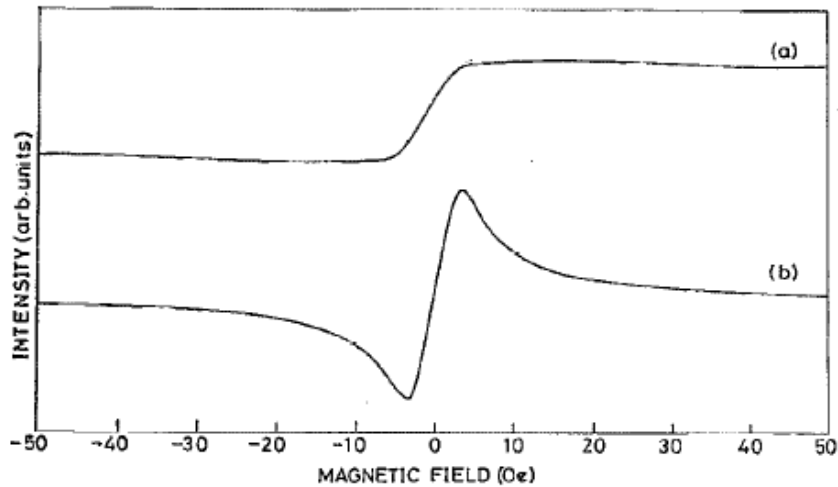


Figure 3.2: Non-resonant microwave absorption (NRMA) of 123 sample (a) pellet (b) Thin film [22].

It is clear that HTSC materials are two dimensionally layered in nature, have short coherence length and high operating critical temperatures. These characteristics contribute to inter-grain and intra-grain mesoscopic defect structures. As a result of these defects, field-dependent LFMA features such as anomalous hysteresis [23], Wolleben effect [24,25], surface barrier effect [26], shielding effect [27] spin glass effect [28] two peaks [29] and phase reversal [30,31] are observed. Interestingly, these features are related to superconducting parameters like penetration depth, irreversibility field, critical current density and critical fields which as a result gives comprehensive information necessary for material application. Furthermore, in a unique way, LFMA phenomenon can precisely discriminate different types of fluxons (inter-granular and intra-granular fluxons).

It has been established that LFMA signal depends on temperature, magnetic field, microwave power and sample form [22]. For instance, the LFMA line shapes and features reported in single crystals are unequivocally complex compared to those in polycrystalline sample. Conversely, this signal is independent of microwave frequency. Attempts to carry out LFMA measurements at Q-band (35 GHz) [32] and K-band (24 GHz) [33] have revealed that there is no clear field position dependence on frequency. Consequently affirming that LFMA signal is essentially a non-resonant phenomenon.

Furthermore LFMA signal is anti-symmetric around zero field and is often opposite in respect to resonance (ESR) spectrum i.e. It shows a minimum microwave absorption at zero field and absorption increases with an increase of magnetic field. This kind of absorption is called ‘normal absorption’. However, a different scenario usually referred as ‘anomalous absorption’ emerges when the absorption signal is a maximum at zero DC field and then decreases with an increase in field.

3.3 Mechanisms of LFMA in superconductors

Due to a variety of LFMA line shapes and complex LFMA features, there is no single model that can exhaustively explain the LFMA signal. Various research groups have presented models that specifically explain specific data. The following section presents two of the most celebrated models which arguably capture most of the LFMA features.

3.3.1 Portis model

The Portis’ model demonstrates that the amplitude of LFMA signal is linearly related to surface area thus implicating that this phenomenon emanates from the surface resistance. It involves ‘shaking’ of fluxons inherent in Josephson-like junctions in a superconducting material by microwave field. It is important to state that this process occurs in JJ of twin boundary nature and not in bulk superconductor. Due to relatively low viscosity in JJ in comparison to the bulk, fluxon velocities in the former are orders of magnitude smaller than the latter. Now when these the highly mobile fluxons are driven by surface microwave currents, they result to dissipation which is exhibited as LFMA signal in the granular HTSC [11].

The nucleation of fluxons requires that the externally applied DC magnetic field must exceed the lower critical field H_{c1j} and the junction should be large enough to allow for flux quantization. At the junction, microwave field variation induces current which leads to an oscillation of fluxons as

$$M \frac{d^2x}{dt^2} + \eta \frac{dx}{dt} + kx = \frac{1}{c} j_i \Phi_0 \quad 3.2$$

Here M and k are the mass unit distance and restoring force respectively. The η is the viscosity given by

$$\eta = \frac{\Phi_0 H_{c2}}{\rho_n c^2} \quad 3.3$$

The resistance and reactance accrued for this motion can be given by equations 3.4 and 3.5 respectively.

$$R = X_0 [(-1 + (1 - 4f^2 B/B_0^2)^2)/2]^{0.5} \quad 3.4$$

$$X = X_0 [(1 + (1 - 4f^2 B/B_0^2)^2)/2]^{0.5} \quad 3.5$$

where B_0 is the effective field beyond which flux-flow loss dominates, X_0 is the impedance at zero magnetic field, λ is the penetration field, ω is the microwave frequency, μ is the magnetic permeability, η is the viscosity coefficient, f represents the fraction of reely or weakly pinned fluxions and B is the applied field.

According to this model, the microwave loss is a minimum at zero applied field and increases with an increase of DC field. However, some materials show a maximum microwave loss at zero magnetic field and a decrease with an increase of applied field.

3.3.2 Dulcic model

This model is based on microwave absorption arising from Josephson junction on the sample surface when it is subjected to external DC magnetic field variation. As aforementioned, granular/ceramic HTSC constitute non-superconducting matrix which separates superconducting grains (bulk). In a superconducting state, both the bulk and weak links contributes to shielding effect emanating from Meissner screening current and Josephson screening current respectively [12].

In an event the magnetic field is altered from zero, flux penetrates the sample through the weak links of JJ-type; reducing the shielding effect provided by Josephson currents, by reduction factor $F(H) = [\sin(\pi H/H_0)/(\pi H/H_0)]$ hence an increase in microwave absorption sets in (H_0 is the magnetic field value for which the junction contains only one quantum of a flux Φ_0 , and is given as

$$H_0 = \Phi_0/L(2\lambda + t) \quad 3.6$$

where Φ_0 , λ , L , t , is the flux quantum, the penetration depth, the junction length and the junction thickness. Furthermore, whenever there is a reduction of the critical currents, the

junction can decouple even for significantly small currents. Consequently, this leads to flux jumps in loops arising from the weak links. The phase slips causes voltage $(V(t) - (h/2e)d\theta/dt)$ across the junctions and an average number of such as function of the applied field gives the normal microwave loss.

The transport current of this kind of a junction is the summation of boundary current I_0 induced by DC magnetic field and microwave current $I_{mw}\cos(\omega_m t)$ [12]

$$\frac{ch}{4\pi e} \frac{d^2\varphi}{dt^2} + \frac{1}{R} \frac{h}{4\pi e} \frac{d\varphi}{dt} + I_c \sin\varphi = I_0 + I_{mw}\cos(\omega_m t) \quad 3.7$$

On ignoring the capacitive contributions, the absorbed power in the junction is defined as

$$P = P_n \frac{1}{1+\eta} \quad 3.8$$

Here η is the junction parameter defined as

$$\eta = \frac{I_c^2 (\cos\varphi)^2}{\left(\frac{h}{8\pi e} \omega_{mw}\right)^2} \quad 3.9$$

Then the LFMA derivative signal intensity representing this junction is devised as

$$S_m = \frac{((1/2)I_m^2 \omega R)^2}{\left(\frac{h}{4\pi e R} \omega_{mw}\right)} \times \frac{I_c}{(1+\eta)^{3/2}} \times \left(-\frac{dI_c}{dt} H_m + I_m \sin\varphi\right) \cos(\omega_m t) \quad 3.10$$

where R is the junction resistance, η is the junction parameter, ω_m is the modulation frequency, ω_{mw} is the microwave frequency and phase difference.

The first term of the equation describes the reversible (non-hysteretic) phenomenon which in essence is independent of the direction of the DC field sweep whereas the second term characterizes an hysteretic (irreversible) response.

3.4 LFMA Features in HTSC

LFMA related features in superconductors are many and fascinating. They include: oxygen deficiency in YBCO, second and third peaks, magnetic shielding effect, paramagnetic effect, quantum oscillations, anomalous hysteresis and surface barrier. This section divulges on a few of these features which are fundamentally relevant to the subsequent chapters of this thesis.

3.4.1 Quantum oscillations

In single crystals of HTSC such as YBCO, $\text{Nd}_{2-x}\text{Ce}_x\text{CuO}_4$ and $\text{Tl}_2\text{Ba}_2\text{CaCu}_2\text{O}_{8+y}$ [28 34-36], discrete, narrow and equally spaced spectral lines (shown in figure 3.3) are observed. These lines are highly dependent on field modulation, usually observed at relatively few mOe of field modulation. Conversely, at large field modulation, the LFMA signal is registered which strictly implies that LFMA is basically a superposition of quantum oscillations [28]. Yet again, they are dependent on temperature, field modulation and microwave power [34-36]. At high magnetic field scan, they exhibit hysteresis where some forward scan lines are destroyed on a reverse field [36]. To account for this feature, we briefly highlight the explanations put forth by Blazey model, Vichery model and Xia model [28, 34, 35, 37-39].

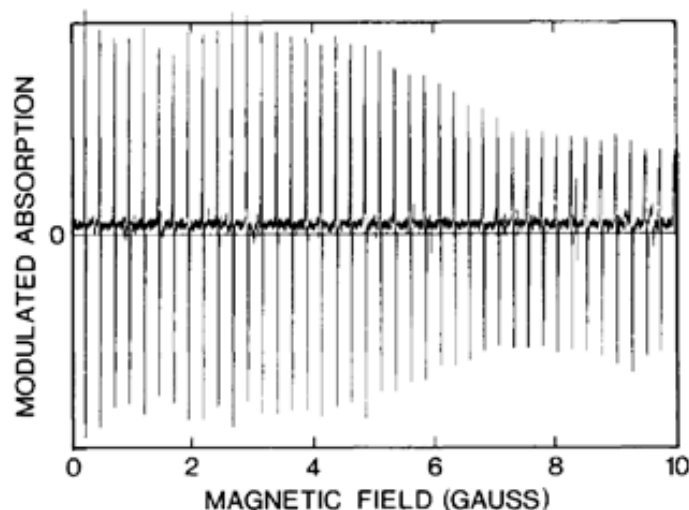


Figure 3.3: Microwave absorption spectrum of YBCO single crystal at 4.4 K [28].

1. Blazey model

This model depicts that spectral lines are as a result of nucleation and annihilation of fluxons in Josephson junctions [28,35]. According to his model, the field position of P^{th} spectral line from zero is defined as

$$H \cos \theta = +(P + 1/2)\Delta H \quad 3.11$$

where θ is an angle between applied quasi-static field and the $\langle 110 \rangle$ direction. The $\Delta H = \Phi_0/S$ is the minimum inter-line field with S being a magnetic cross-section area. For

nucleation to occur, microwave induced currents should at least be equal to junction critical current. Imperatively, the critical current for fluxon nucleation is proportional to the fluxon energy density [28,35]

$$\varepsilon_1 = (1/4\pi)\Phi_0 H_{c1} \quad 3.12$$

The total energy density for a single fluxon nucleation induced by magnetic energy can be assumed to be

$$\varepsilon_j = \varepsilon_{1j} + u_m \quad 3.13$$

u_m is obtained from a magnetic system with the energy density expression (u_n) and n fluxons.

$$u_n/u_0 = 4(H_0/\Delta H - n)^2 \quad 3.14$$

here $u_0 = (1/32)\pi\Delta H$ is equal to the energy of the lowest level crossing. At $H_0 = (n+1/2)\Delta H$ the energy u_n of a state with n fluxons is equal to the energy u_{n+1} fluxons and there is no magnetic energy associated with the nucleation of a fluxon threshold [28,35]. Transition from p to the $p+1$ state occurs whenever the field up (forward) sweeps through the intersection between the microwave power level and the p -fluxons level. This transition corresponds to further nucleation of fluxon.

A similar transition from the $p+1$ fluxons state to the p fluxons state should occur when the field down (reverse) sweeps through the intersection between the microwave power level and down the $p+1$ fluxons level. This corresponds to annihilation of a fluxon. So it was expected that alternate nucleation and annihilation of fluxons should occur in a nucleation cycle and the corresponding microwave absorption signal is a series of equally spaced spectral lines.

Microwave power dependence of quantum oscillations was exhibited in YBCO material in which the shape and number of lines evolved with the change in microwave power [28,35]. With an increase of microwave power at fixed temperature, the lines broaden into absorption bands that can be defined as

$$2\delta H / \Delta H = (P / P_0)^{1/2} - (P_c / P_0)^{1/2} \quad 3.15$$

where $2\delta H$ is the band, $P_c(T)$ is the threshold microwave power and P_0 characterizes the temperature-independent rate at which $2\delta H / \Delta H$ increases above threshold. Close to a temperature T near T_c , the P_0 varies as $(1 - T / T_c)^{3/2}$ [28,35].

2. Vichery Model

Vichery et al [37,38] have assumed that the superconducting loop constitutes N identical Josephson junctions and the model describes the presence of these spectral lines and their dependence on microwave power. In a magnetic field, the energy of p^{th} state can be defined as

$$E_p(\Phi) = -N \frac{\Phi_0 I_c}{2\pi} \cos\left(\frac{2\pi}{N} \left(p - \frac{\Phi}{\Phi_0}\right)\right) + \frac{1}{2} LI_c \sin^2\left(\frac{2\pi}{N} \left(p - \frac{\Phi}{\Phi_0}\right)\right) + K \quad 3.16$$

where $\Phi = \Phi_{\text{ext}} + LI$, Φ_0 is the flux quantum, L is the inductance l and I_c are connected by the relation $I = I_c \sin \Delta\phi$ and K is a constant.

The likely transition between p and $p+1$ state occur at

$$\Phi_{\text{ext}} = p\Phi_0 \pm (N\Phi_0 / 4 + LI_c) \quad 3.17$$

This transition occurs when $I = \pm I_c$ which experiences overlapping of p and $p+1$ energy states. Now, the overlap between two successive states in terms of magnetic field is defined by parameter Ω

$$\Omega = 2LI_0 + N\Phi_0 / 2\Phi_0 \quad 3.18$$

With the magnetic field given assumed to be the sum of static field H_0 and microwave field $H_w \sin \omega t$. For $2H_w < \Omega / S$, there is no appearance of periodic transitions in successive states regardless of the value of H_0 . However, when $2H_w > \Omega / S$ spectral transitions are observed which then implies that there is microwave power threshold at which this lines can occur. A sequence of some sharp periodic peaks appears for some values of H_0 . The Fourier component of ε in phase with microwave field gives microwave power absorption as

$$P = \omega \frac{\Phi_0}{2\pi L} \left(2LI_c + N \frac{\Phi_0}{2} - \Phi_0 \right) \quad 3.19$$

The derivative of equation 3.19 as a function of DC magnetic field accounts for LFMA spectral lines.

3. Xia and Stroud Model

This model is built on the assumption that superconducting grains form weakly coupled loops [39]. The supercurrent between two superconducting grains i and j can be expressed as

$$I_{ij} = I_c \sin\left(\frac{2\pi}{N}[1 + f(t)]\right) \quad 3.20$$

here $I_c = 2eJ / \hbar$ is the junction critical current, l is an integer, and $f(t) = f_0 - f_1 \cos(\omega t)$ is the total flux through the loop. Evidently, $f_0 = SH_0 / \Phi_0$ and $f_1 = SH_1 / \Phi_0$ (S is the loop area). When magnetic field is applied to this system, phase slips will occur at $\Phi = (n + 1/2)\Phi_0$ as a result of a flux change with time in the loop. Then voltage slips produces a voltage difference $V(t) - (h/2e)d\theta/dt$ in accordance to Josephson relations thus leading to energy absorption through normal resistance of junction. The absorbed power averaged over time can be expressed as

$$P = \frac{1}{R_n} \langle V^2(t) \rangle \quad 3.21$$

The power signal (spectrum) is uneven resulting from an abrupt change in the supercurrents brought about by flux slips. This model has been used to elucidate the LFMA line shape [40]. Here an assumption is made that the LFMA signal is a superposition of quantum oscillations when using Boltzmann distribution function.

$$f = \exp\left(-\frac{\Phi l}{k_B T}\right) \quad 3.22$$

where l is the current in the loops and $\Phi = BA$ is the flux through the loop of an area A .

3.4.2 Phase reversal ‘anomalous LFMA signal’

Phase reversal involves a changeover from say the ‘normal’ minimum microwave absorption at zero DC field to maximum microwave absorption at exactly the same field. The feature has been exhibited in cuprates and FeSc materials. It is dependent upon sample form [24, 25, 41, 42], temperature [31] and microwave power [30, 43, 44]. In a powder YBCO superconductor, LFMA signal evolves as a function of rf powers and shows a minimum zero field microwave absorption at lower rf powers which crosses over to a maximum absorption at higher rf power levels as depicted in figure 3.4 (a).

Similar LFMA phase reversal dependence on microwave power has been reported in $\text{SmFeAsO}_{1-x}\text{F}_x$ [43]. Collectively, the anomaly has been analysed on the basis of non-linear response of fairly weak coupled superconducting rings ubiquitously distributed in a sample. The presence of both hysteretic and non-hysteretic JJ in a system results to a distinctively different kind of response to microwave power [30].

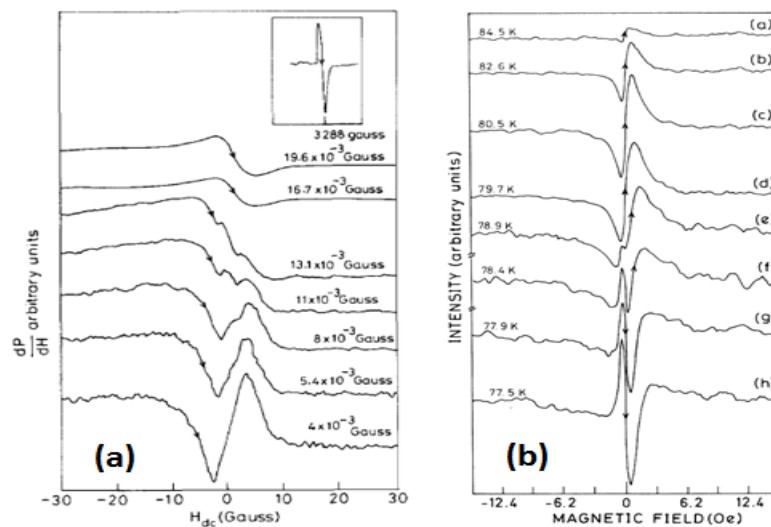


Figure 3.4: LFMA derivative signal dependence on (a) rf fields [30] (b) Temperature [31]

Furthermore, temperature dependence LFMA phase reversal shown in figure 3.4 (b) has been demystified on the framework of an effective medium theory. Here, the sample is assumed to be consisting of a volume fraction (x) of superconducting islands embedded in non-superconducting metallic regions [31]. The volume fraction x is a function of temperature (T) and applied magnetic field (H) thus it monotonically decreases as function of these parameters. So close to T_c , where the phase reversal is witnessed, the model alludes

that x is dramatically reduced. The microwave loss mechanism at this temperature is attributed to conductivity of normal fractions thus giving a phase reversal in a natural way.

The knowledge of phase reversal has been used to good effect in unearthing **Paramagnetic Meissner effect** (PME) which is commonly known as **Wohleben effect**. The effect is an abnormal paramagnetic response to weak magnetic fields exhibited by some HTSC (see figure 3.5). Methodical studies reveal that the effect is due to presence of π junctions [24, 25 42] and it is an extrinsic feature related to mesoscopic structures that favour formation of spontaneous orbital currents in the ground state [24, 25]. For PME to be observed, π junction critical current should be of the order 10^5 - 10^6 Acm⁻² and this effect is independent of the size of grains as revealed in BSCCO sample [24, 25]. This large critical current for π junctions can only be associated to the intra-grain junctions rather than inter-grain junctions. Finally, the effect is strongest for powders whose c-axis is aligned parallel to magnetic field and sample annealing has no effect.

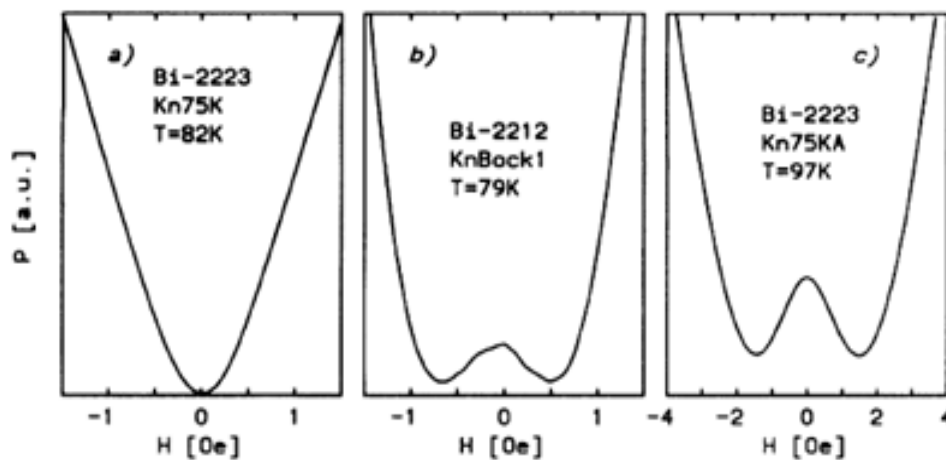


Figure 3.5: Microwave absorption phase reversal (Paramagnetic Meissner effect) of powdered Bi-HTSC [42].

3.4.3 Anomalous hysteresis

Direct magnetizations and LFMA measurements have been used extensively to study the magnetization process in HTSC. Direct magnetizations studies have revealed a normal hysteresis in which magnetic curve for increasing field lies below decreasing magnetic curve as shown in figure 3.6 (b) . On the contrary, LFMA studies show an anomalous hysteresis where the decreasing magnetic curve lies above the increasing field (figure 3.6 (a)). The

anomaly is a generic feature in both unconventional superconductors (like MgB_2 , La-Sr-Ca-Cu-O and in YBCO) [35,45,46] and in conventional superconductors (such as Nb_3Sn granules, Al granular thin films and in GaAs layers) [47, 48]. Interestingly, under similar conditions, the DC magnetizations in YBCO and BCSSO reveal normal hysteresis [49] whereas LFMA studies show anomalous behaviour [50, 51].

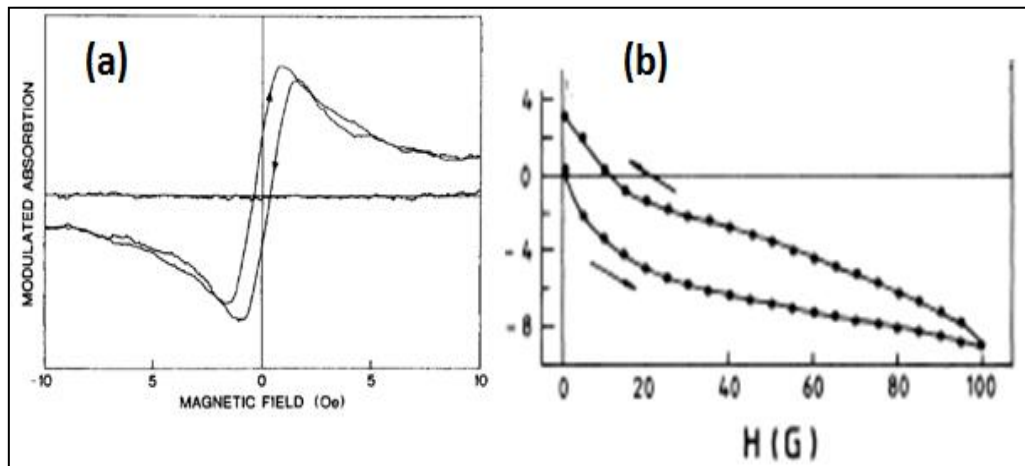


Figure 3.6: A Comparison between (a) LFMA hysteresis [35] and (b) Magnetization hysteresis [52] in YBCO superconductor.

An argument based on thermally/Lorentz force induced fluxons (energy stabilized Josephson junction fluxons-ESJ) has been proposed as the main cause of this anomaly [53]. The ESJ fluxons increases the number of freely and mobile fluxons which can only be detected by extra sensitivity of the LFMA technique and not any DC magnetization methods. In that regard, a combination effect of the three fields ($H_{DC}+H_{mw}+H_m$) in LFMA technique provides extra energy required to decouple the weak links thus fluxons enter the system at lower temperatures and lower magnetic field. Another possibility is based on a combination of Portis and Dulcic models [10,11] in which Tripathy et al [54] argues that the anomaly is a result of different responses to magnetic field emerging from diverse weak links. The simulation based on the combination of the two models precisely matched the experimental data.

Likewise, a two critical state model which is a modification of Bean's critical state model has been used to invoked the anomalous hysteresis [23]. In addition to intra-granular fluxons

(pancake fluxons), this model includes the role of inter-granular fluxons. The model alludes that the inter-granular fluxons have higher mobility and higher number density. Furthermore, the intra-granular critical current density J_{cg} is of many orders larger compared to inter-granular current. In a macroscopic level, the flux gradient is determined by the inter-granular current density.

On the other hand, the intra-granular current density dictates the flux gradient on the local level within single grains. The model further alludes of the existence of two types of fluxons; free/ weakly moving fluxons or grain boundary fluxons and grain pinned/trapped fluxons. According to this model, the electromagnetic loss is as a result of the freely or weakly pinned fluxons [23].

3.6 LFMA in Magnetic materials

In contrast to superconductors, ESR derivative signal in magnetic materials exhibits two absorption modes i.e. at low field near zero magnetic field and at high magnetic fields as shown in figure 3.7 [55]. The high field absorption spectrum is the resonance signal (full saturated state) and it satisfies Larmor condition ($\omega = \gamma H_{res}$). The resonance signal is associated to absorption of microwave radiation when the frequency of magnetic spin precession of a material matches microwave frequency. Chiefly, it is characterized by two parameters; the linewidth (ΔH_{pp}) and the resonance field (H_{res}).

Our focus is on LFMA spectrum (unsaturated state) exhibited at low fields. Like in superconductors, LFMA signal in magnetic materials is either inverted (opposite) or is in phase with the resonance signal. The spectrum occurs at fields far from the resonance spectrum thus affirming that this phenomenon is non-resonant. Magnetic materials that exhibit this phenomenon can be used in spintronics applications like in low field magnetic sensors, spin valves and magnetic tunnelling junctions.

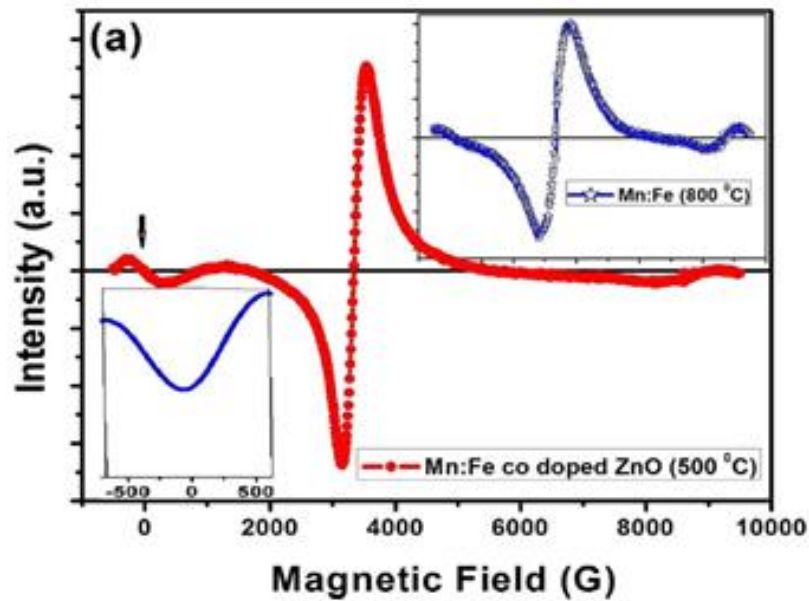


Figure 3.7: Derivative of microwave absorption exhibiting LFMA signal and resonance signal for Mn:Fe sample adapted from [55].

Conversely, the mechanism behind this phenomenon in magnetic materials is yet to be fully understood and varied interpretations have been proposed. For instance, in the case of magnets and ferrites, the signal has been ascribed to an onset of the ordered phase therefore offering an elusive mechanism to monitor magnetic (spin) ordering in these systems [56, 57]. Again, in soft magnetic materials and semiconductors, this phenomenon has been attributed to low field spin magnetization processes and magneto-resistive effects respectively [58-59]. In silicate glass, it has been argued that LFMA phenomenon is a result of magneto-induced microwave conductivity [60]. Finally, in small band gap insulators, this phenomenon has been attributed to non-resonant spin rotation in a partially saturated sample that emanates from the magnetization process of the ordered state [61].

A correlation between magneto-impedance (which is a result of change of skin depth due to change of transversal permeability induced by external magnetic field) and LFMA has been established. Experimentally, it has been shown that the maximum point of a magneto-impedance signal coincides with the minimum and maximum regions of the LFMA signal [62, 63]. According to Montiel et al [64], the two phenomena have a common origin i.e. they are as a result of absorption of electromagnetic radiation by spin systems that are modified by domain configuration and are strongly dependent on the anisotropy field.

Similar observations have been made on transition metal (TM) co-doped with ZnO [55]. Here there is a clear match of the magneto-impedance with LFMA data at room temperature but the correlation collapses at low temperatures as shown in figure 3.8. In this case, the mechanism that leads to LFMA signal has been argued based on a possible role of Anomalous Hall effect (AHE) and Ordinary Hall effect (OHE) that follows magnetization and applied field respectively [55].

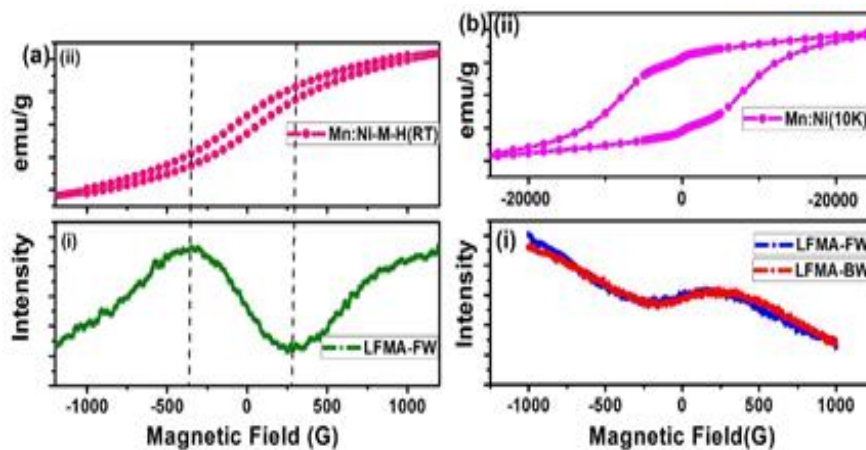


Figure 3.8: A correlation of magneto-impedance data with LFMA at room temperature and collapse (mismatch) at 10 K [58].

Like in superconductors, the LFMA signal in magnetic materials exhibits features worth mentioning. For example a sign reversal has been witnessed in Ni-Zn ferrites and accordingly associated to the occurrence of the triangular or canted Yafet-Kittel spin arrangement [65]. This occurrence has been used to establish the magnetic dynamics of nickel. A Curie transition at $T \sim 630$ K has been established by the use of magnetic anisotropy and demagnetization field extracted from LFMA signal [64].

LFMA hysteresis is another feature observed when the field is cycled. The hysteresis has been associated with non-uniform surface magnetization processes far from the saturation state, which strongly depend on the magnetic order [66]. Precisely, this kind of an absorption easily gets modified by an externally applied field thus changing susceptibility. Therefore, whenever magnetic field is cycled it results in change of domain configurations and the hysteresis occurs [66].

The presence or absence of hysteresis in LFMA signal has been used to distinctively identify and provide credible information with regards to microwave absorbing centers in magnetic

materials. For instance, a linear and non-hysteretic absorption signifies a dielectric loss in magneto-electric materials [67 -70].

References

1. Shaltiel, D., Krug Von Nidda, H-A., Shipiro, B.Y., Bogoslavsky, B., Rosenstein, B., Shapiro, I., Tamegai, T.: *Physica C* **470**, 1937-1942(2010)
2. Indovina, P.L., Onoti, P., Tabet, E.: *Solid State Commun.* **8**, 1721 (1970)
3. Kim, Y.W., deGraaf, A.M., Chen, J.T., Friedmanand E.J., Kim, S.H.:*Phys. .Rev.B* **6**,887(1972)
4. Muller, K.A., Pomerantz ,M., Knoedler, C.M.: *Phys.Rev.Lett.***45**,832 (1980)
5. Bhat, S.V., Panguly, P., Rao, C.N.R.: *Pramana J. Phys.* **28** L425 (1987)
6. Bhat, S.V., Ganguly, P., Ramakrishnan, T.V., Rao, C.N.R.:*Pramana J. Phys* **20**, L559 (1987)
7. Stankowski, J., Kahol, P.K., Dalal, N.S., Moodera, J.S.: *Phys. Rev. B* **36**, 7126 (1987)
8. Dunny, R., Hautala, J., Ducharme, S., Lee, B., Symko, O.G., Taylor, P.C., Zheng, D.J., Xu, J.A.: *Phys. Rev. B* **36**, 2361(1987)
9. Blazey, K.W., Muller, K.A., Bednorz, J.G., Berlinger, W., Amoretti, G., Buluggiu, E., Vera, A., Maticotta, F.C.: *Phys. Rev.B* **36**, 7241 (1987)
10. Dulcic, A., Rakvin, B., Pozek, M.: *Europhys. Lett.* **10**, 593–598 (1989)
11. Portis, A.M., Blazey, K.W., Muller, K.A., Bednorz, J.G.: *Europhys. Lett.* **5**, 467 (1988)
12. Srinivasu, V.V., Bhat, S.V., Muralidhar, G.K., Mohan Rao, G., Mohan, S.: *Pramana* **40**, 119 (1993)
13. Stalder, M., Stefanicki, G.,Warden, M., Portis, A.M.,Waldner, F.: *Physica C* **153–155**, 659–660 (1988)
14. Roberts, J., Petit, P., Yildirim, T., Fischer, J.E.: *Phys. Rev B* **157**, 1226 (1998-II)
15. Kadam, R.M., Sastry, M.D., Hassain, Z., Mazumdar, C., Nagarajan, R., Gupta, L.C.,Godart,C.andVijayaraghvan,R.: *Physica C* **232**,359 (1994)
16. Kadam, R.M., Wani, B.N., Sastry M.D., Rao, URK.: *Physica C*, **246**,262 (1995)
17. Suss, J.T., Berlinger, W., Portis, A.M., Muller, K.A., Jeanneret B., Martinoli, P.: *Solid State commun.* **71**,929(1989)
18. Kheifets, A.S. and Veinger, A.I.: *Physica C* **165**, 491 (1990)
19. Saharangi , S., Bhat, S.V.:<http://arxiv.org/fH/cond-Mat/papers/0511701.pdf>
20. Panarina, N.Y., Talanov, Y.I., Shaposhnikova, T.S., Beysengulov, N.R., Vavilova, E.: *Phys. Rev. B* **81**, 224509 (2010)

21. Talanov, Y., Beisengulov, N., Kornilov, G., Shaposhnikova, T., Vavilova, E., Nacke, C., Panarina, S., Hess, C., Kataev, V., Buchner, B.: *Supercond. Sci. Technol.* **26**, 045015 (2013)
22. Srinivasu, V.V., Thomas, B., Hegde, M.S., Bhat, S.V.: *J. Appl. Phys.* **75**, 4131 (1994)
23. Ji, L., Rzechowski, M.S., Anand, N., Tinkham, M.: *Phys. Rev. B* **47**, 470 (1993)
24. Knauf, N., Fischer, J., Schmidt, P., Roden, B., Borowski, R., Buchner, B., Micklitz, H., Freimuth, A., Kataev, V., Khomskii, D.I.: *Europhys. Lett.* **35**, 541 (1996)
25. Knauf, N., Fischer, J., Schmidt, P., Roden, B., Borowski, R., Buchner, B., Micklitz, H., Freimuth, A., Khomskii, D.I., Kataev, V.: *Physica C* **299**, 125 (1998)
26. Rastogi, A., Srinivasu, V.V., Hedge, M.S., Bhat, S.V.: *Physica C* **234**, 229-231 (1994)
27. Srinivasu, V.V., Pinto, R., Sastry, M.D.: *Applied superconductivity* **4**, 195-201 (1996)
28. Blazey, K.W., Portis, A.M., Muller, K.A., Bednorz, J.G., Holtzberg, F.: *Physica C* **153-155**, 56-58 (1988)
29. Srinivasu, V.V.: *J. Supercond. Nov. Magn.* **23**, 305 (2010)
30. Srinivasu, V.V., Bhat, S.V., Kumar, N.: *Solid state Commun.* **4**, 375-378 (1994)
31. Bhat, S.V., Srinivasu, V.V., Kumar, N.: *Phys. Rev. B* **44**, 10121 (1991)
32. Tyagi, S., Gould, A., Bhagat, S.M., Manheimer, M.A.: *Physica C* **1569**, 162-164 (1989)
33. Pakulis, E.J., Osada, T.: *Phys. Rev. B* **37**, 5940 (1988)
34. Blazey, K.W.: *Phy. Scr. T* **29**, 92 (1989)
35. Blazey, K.W., Hohler, A.: *Solid state Commun.* **72**, 1199 (1989)
36. Poppl, A., Kevan, L., Kimura, H., Schwartz, R.N.: *Phys. Rev. B* **46**, 8559 (1992)
37. Vichery, H., Beuneu, F., Lejay, P.: *Physics C*, **159**, 823 (1989)
38. Vichery, H., Albenque, F.R., Beuneu, F., Lejay, P.: *Physica C* **1583**, 162-164 (1989)
39. Xia, T. K., Stroud, D.: *Phys. Rev. B* **39**, 4792 (1989)
40. Owens, F.J.: *Physica C*, **171**, 25 (1990)
41. Kusmartsev, F.V.: *Phys. Rev. Lett.* **69**, 2268 (1992)
42. Braunish, W., Knauf, N., Kataev, V., Neuhausen, S., Grutz, A., Kock, A., Roden, B., Khomskii, D., Wohlleben, D.: *Phys. Rev. Lett.* **68**, 1908 (1992)
43. Onyancha, R.B., Shimoyama, J., Singh, S.J., Hayashi, K., Ogino, H., Srinivasu, V.V.: *Physica C: Supercond. Appl.* **533**, 49-52 (2017)

44. Onyancha, R.B., Shimoyama, J., Singh, S.J., Ogino, H., Srinivasu, V.V.: J Supercond Nov. Magn. **30**, 1097 (2017)
45. Sarangi, S., Bhat, S.V.: <http://arxiv.org/ftp/condmat/papers/0511701.pdf>, pp. 1–45
46. Khachatryan, K., Weber, E.R., Tejedor, P., Stacy, A.M.: Phys. Rev. B **36**, 8309 (1987)
47. Mahel, M., Benacka, S.: Solid State Commun. **83** 615 (1992)
48. Baranowski, J.M., Weber, Z.L., Yau, W.F., Weber, E.R.: Phys. Rev. Lett. **66**, 3079 (1991)
49. Pradhan, A.K., Roy, S.B., Chaddah, P., Chen, C., Wanklyn, B.M.: Phys. Rev. B **52**, 6215 (1995).
50. Dulic, A., Crepeau, R.H., Freed, J.H., Schneemeyer, L.F., Waszczak, J.V.: Phys. Rev. B **42**, 2155 (1990)
51. Pakulis, E.J., Chandershekar, G.V.: Phys. Rev. B **39** 808(1989)
52. Pradhan, A.K., Roy, S.B., Chaddah, P., Chen, C., Wanklyn, B.M.: Phys. Rev. B **52**, 6215 (1995)
53. Padam, G. K., Arora, N.K., Ekbot, S.N.: Mat. Chem and Phys. **123**, 752-755 (2010)
54. Tripathy, M.R., Srivastava, G.P., IEEE Trans. Magn. **35** (1999) 4079
55. Tebogo, M., Srinivasu, V. V., Das, J., Solid State Commun. **243**, 60–64 (2016)
56. Srinivasu, V.V., Lofland, S.E., Bhagat, S.M., Ghosh, K., Tyagi, S.D.: J. Physics Letters **86**, 106 (1999)
57. Veinger, A., Zabrodiskii, T., Tisnek: J. Alloys and Compounds **369** (2004) 751
58. Montiel, H., Alvarez, G., Betancourt, I., Zamarano, R., Valenzuela, R.: Appl. Phys. Lett. **86**, 072503 (2005)
59. Alvarez, G., Zamorano, R.: J. Alloys and Compounds **369**, 231(2004)
60. R. Rakhimov, H. Ries, D. Jones, L. Glebov, Appl. Phys. Lett. **76**, 751 (2000)
61. Gavi, H., Ngom, B.D., Beye, A.C., Strydom, A.M., Srinivasu, V.V., Chaker, M., Manyala, N.: J. Magn. Mater. **324**, 1172 (2012)
62. Montiel, H., Alvarez, G., Betancourt, I., Zamarano, R., Valenzuela, R.: Appl. Phys. Lett. **86**, 072503 (2005)
63. Alvarez, G., Montiel, H., Cos, D., Zamorano, R., Arribas, A. G., Barandiaran, J.M., Valenzuela, R. : J. Non-crystalline solids 353, 902-904 (2007)
64. H. Montiel, G. Alvarez, doi.org/10.5772/55962

65. Valenzuela, R., Ammar, S., Nowak, S., Vazquez, G.: J. Supercond. Nov. Magn **25**, 2389-2393 (2012)
66. Montiel, H., Alvarez, G., Betancourt, I., Valenzuela, R., Zamorano, R.: Superficies Vacio 19 (3) (2006) 27-29
67. Alvarez, G., Font, R., Portelles, J., Zamorano, R., Valenzuela, R.: J. Phys. Chem. Solids **68**, 1436 (2007).
68. Alvarez, G., Montiel, H., Barron, J.F., Gutierrez, M.P., Zamorano, R.: J. Magn. Magn. Mater. **322**, 348 (2010).
69. Alvarez, G., Cruz, M.P., Durán, A.C., Montiel, H., Zamorano, R.: Solid State Commun. **150**, 1597 (2010).
70. Alvarez, G., Peña, J.A., Castellanos, M.A., Montiel, H., Zamorano, R.: Rev. Mex. Fis. S **58** (2), 24 (2012).

Chapter 4

LFMA of $\text{SmFeAsO}_{0.88}\text{F}_{0.12}$ powdered sample

This section was published as “R. B. Onyancha^{a*}, J. Shimoyama^b, S. J. Singh^c, H. Ogino^{d,e} and V. V. Srinivasu^a. *Temperature dependence low field microwave absorption in a powder sample of SmFeAs(O,F) iron pnictide superconductor. J Supercond Nov Magn (2017) 30:1097–1102*”

Temperature dependence low field microwave absorption in a powder sample of SmFeAs(O,F) iron pnictide superconductor.

I. Introduction

Low field microwave absorption (LFMA) technique employed in electron spin resonance (ESR) spectrometer is a very factual and exhilarating tool in the study of superconducting materials due to its relevance in microwave device applications (such as antennae, transmission lines, strip-line resonators, filters, and high-Q cavities) and partly for fundamentally understanding the physics in these materials. It can essentially depict vital information of superconductors such as critical current density, critical field, shielding effect, hysteresis and vortex dynamics [2-6]. Granularity in ceramic high T_c superconductors from cracks, voids, grain boundary and vacancy forms weak links in a material and plays an enormous role in electromagnetic response of sample. They significantly affect the pair potential when the size is in the order parameter range or more ($\xi \sim 1.2 \text{ nm}$) [7]. Then in a natural way Josephson junctions are formed in which the non-superconducting layer between the superconducting grains acts as a barrier.

Josephson junctions in the form of inter-particle micro-shorts in powders inter-grain in crystals and intra-grain in twinned systems portrays remarkably different features in LFMA line shape signal [8]. Depending on the layer (barrier) separating the two superconducting grains, the phase of a Josephson junction critical current density ($I_c = I_0 \sin \varphi$) gets altered. Consequently, it affects the Fraunhofer pattern of the critical current as a function of applied magnetic field ($I_c = I_c(0) [\sin(H/H_0)(H/H_0)]$) which significantly changes the LFMA line shape signal [9]. Worthy mentioning is the LFMA 'phase reversal' where a maximum microwave absorption at zero field instead of a minimum zero field microwave absorption has been witnessed and attributed to the presence of π junctions [10, 11].

It has been established that the field dependence of surface resistance of HTSC materials is peculiar to the conventional type II superconductor [12]. In fact, the surface resistance curve in the conventional type II superconductor for the positive decreasing field is higher than that of the increasing field and reaches to minimum only at negative field values whereas in zero field cooled (ZFC) HTSC material, the decreasing field is lower than in the increasing field and the minimum occurs at fields slightly higher than zero field. This results to an anomalous

kind of hysteresis in HTSC and it is a clear manifestation of granularity. To elucidate this phenomenon, Ji *et al* [6] proposed a two-level critical state in ceramic HTSC material whereby two distinct critical current densities exist i.e. a large intra-grain critical current and a much weaker inter-grain current. However, on a situation where the inter-grain current is of order of intra-grain current, the two critical state system mimics homogeneous system and behaving as a one critical state with a normal hysteresis.

The discovery of iron pnictide superconductors recently has opened a new opportunity to the unconventional superconductivity. This family provides exclusively novel and diverse materials to explore exotic physics in high T_c superconductivity. Again, as given their relatively high T_c , high critical fields, high critical currents, and less anisotropy [13-17], these materials are comparable, if not superior, to high T_c cuprates in device application. Since the advent of these materials, a lot of work has been reported and reviewed presented [18-20]. To advocate for an application of these materials in microwave device fabrication, methodical high-frequency studies is paramount to ascertain surface impedance-related information. Therefore, here we report a comprehensive study of temperature dependence LFMA in $\text{SmFeAsO}_{0.88}\text{F}_{0.12}$ of parent compound SmFeAsO [21] (here after represented as Sm1111) with powder sample of average particle size of $\sim 3\mu\text{m}$ in the superconducting region (0 – 40 K). Powdered samples provide weak particle contacts resulting to the formation of inter-particle micro-shorts.

In general, LFMA studies in powdered sample of iron pnictides have received relatively no attention despite the fact that they provide a rich platform in exploring the marvellous weak links-related information. For that reason, in an attempt to unravel some fundamental LFMA characteristic in Sm1111, we have carried out an electromagnetic response measurement on powder sample of this particular material. We have observed a structure with two peaks (broad peak and narrow peak) which are identical to the one reported on a pellet of the same sample [1]. This plainly indicates that the structure is not necessarily confined to pellet sample only. Also, the LFMA intensity is found to evolve as function of temperature. This temperature dependence of the LFMA intensity is interpreted on the framework of effective medium model in which coupling and decoupling of Josephson junction is considered. By cycling the field, a temperature-dependent anomalous hysteresis is noted.

II. Experiment

The $\text{SmFeAsO}_{0.88}\text{F}_{0.12}$ polycrystalline samples were synthesized by solid state reaction technique. Thus far, the samples have been thoroughly characterized [1, 22-24]. A small piece of the pellet sample was then ground by using an agate mortar and pestle to obtain the powder. The particle size was determined by TEM and granularity revealed from SEM monograph. The ESR measurements were recorded using a Bruker EXM spectrometer operating in the X-band at 9.4 GHz frequency. The spectrometer was equipped with liquid helium flow from the Dewar to access low temperatures. More importantly, the ESR records the power P absorbed by the sample from the transverse magnetic microwave field as the static magnetic field H is scanned. Then to minimize the signal to noise ratio, a lock-in technique with field modulation is employed and a derivative signal (dP/dH) is recorded. The DC magnetic field in the range $-250 \leq H_{DC} \leq 250$ G was applied for low field sweep and $-500 \leq H_{DC} \leq 9000$ G for high field scan measurements.

III. Results and Discussion

Figure 4.1 (a) shows a TEM monograph of powdered SmFeAs (O,F) sample. From the figure, the particle size can be estimated as $\sim 3 \mu\text{m}$. Besides, Figure 4.1 (b) represents a SEM image which portrays clear inter-particle micro- contacts. It then points out that the sample is highly granular. The inter-particle micro-shorts and other weak links between superconducting grains form a network of Josephson junctions. Profoundly, the weak links renders the intrinsic properties of high T_c materials complicated.

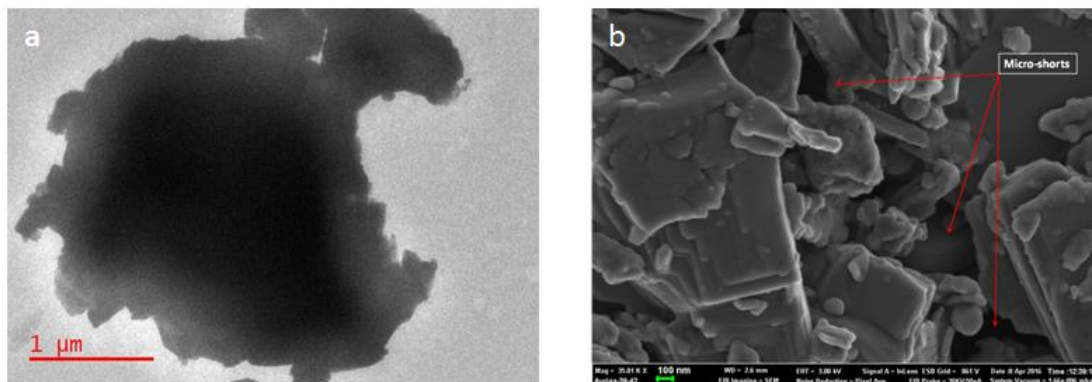


Figure 4.1: (a) is TEM and (b) is SEM monographs of a powdered sample of Sm1111 iron pnictide superconductor.

To investigate the effect of temperature on LFMA in this sample, field modulation amplitude of 5 G and microwave power of 0.710 mW were employed. The field was swept continuously from -250 through 0 to + 250 G on temperature range 10 K- 40 K as shown in figure 4.2. The LFMA line shapes have a typical intense derivative signal centered around zero field. Also, an observation of a structure similar to what is reported in pellet sample [1] where a broad peak and narrow peak changes as a function of temperature is exhibited. Furthermore, the line shape signals evolve as a function of temperature as depicted in the inset of figure 4.2 (plot of signal intensity vs temperature).

Figure 4.3 represents a LFMA signal swept at high magnetic field (-500G through 0 to + 9000 G). The inset (a) shows resonance signal carried out at room temperature to act as phase reference. It is evident that LFMA has an opposite signal to the reference resonance signal which implies a minimum at zero field. Whereas, the inset (b) represents a LFMA signal at 40 K to indicate an existence of LFMA at this temperature. However, the signal at this temperature is faint and is consistent with reported work on pellet sample. Importantly, the structure (broad peak and narrow) observed at low field sweep is absent in high field sweep. Instead, a rather sharp peak is observed. This might be as a result of different sweeping rates. The sweep rates used are; 250 G/ min for low field sweep and 4750 G/ min at high field sweep which indicates that there can be ‘smearing off’ of some regions in high field sweep line shape.

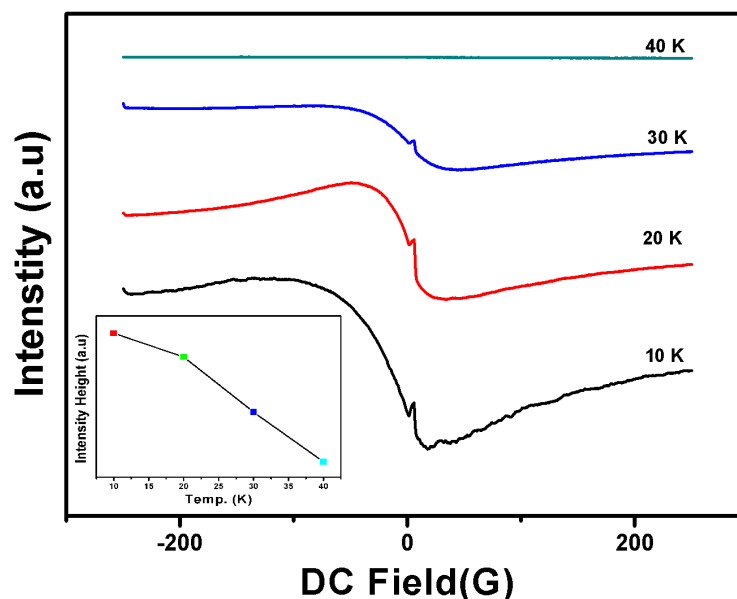


Figure 4.2: LFMA of ZFC Sm1111 at various temperature values (10 -40 K) on microwave power 0.710mW. The inset is a plot of signal intensity height vs temperature.

An appearance of an intense LFMA signal around zero field is a common feature in high T_c cuprates superconductors [25-31] and in iron pnictides superconductors [1, 24, 32]. Briefly, part of the regions of LFMA line shape can be explained by invoking the model of microwave losses resulting from Josephson junctions ubiquitously present in ceramic superconductors where the LFMA signal intensity is proportional to surface current, modulation currents and microwave currents induced by the magnetic field sweep, modulation field and microwave fields respectively [33]. Then the signal intensity can be expressed as

$$S_m = \frac{(\frac{1}{2}I_{mw}^2 R)^{1/2}}{(\frac{1}{R2e}\omega_{mw})} \frac{I_c}{(1+\eta)^{3/2}} \times \left(-\frac{dI_c}{dH} H_m + I_m \sin\varphi_0\right) \cos(\omega_m t) \quad 4.1$$

where R , I_c , φ_0 and η are the junction resistance, the junction critical current, the phase difference across the junction and the junction parameter respectively. The junction parameter $\eta = \eta_0 F^2(H)$ is temperature dependent given $\eta_0 \propto I_c^2(0, T)$. The H_m is the amplitude of modulation field, ω_m is the modulation frequency and ω_{mw} is the microwave frequency with I_m and I_{mw} being currents induced by ω_m and ω_{mw} respectively. The model points out that I_c is a function of both magnetic field and temperature. An increase of an applied DC magnetic field then reduces the Meissner shielding effect of the junction which results to the penetration of magnetic field instigating dissipation. Furthermore, when Josephson junctions are large enough $d > \lambda_L$ the vortices nucleate in these junctions and dissipation is through viscous motion of vortices driven by microwave current [34]. Here the loss is proportional to the number of freely and loosely pinned vortices. In fact the two models were called upon to elucidate the presence of the structure (broad peak and narrow peak) in pellet sample [1, 24].

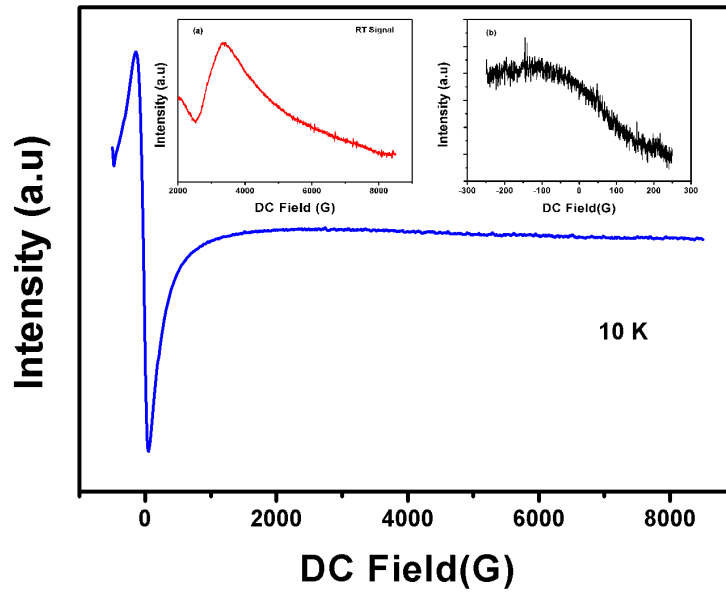


Figure 4.3: LFMA of ZFC Sm1111 at high magnetic field sweep (-500 to 9000 G) at microwave power and temperature of 15 K. The insert (a) is the LFMA at 40 K at low field sweep to indicate that absorption is present up to 42 K similar to pellet in [1]. The inset (b) is resonance field at room temperature used here as a reference signal phase.

It is of essence to mention that the pellets have grain boundaries and intra-grain weak links. However, on grinding them the grain boundaries are reduced and instead inter-particle weak links together with intra-grain weak links prevail and dictates the transport and magnetic dynamics in powders. In view of this, we can argue that the structure of broad peak and narrow peak occurs in powder given that the grain boundaries in the pellet sample are replaced by inter-particle micro-shorts (detach between particles) which contribute to narrow peak and intra-grain responsible for the presence of broad peak.

A. Temperature dependent signal intensity

In attempting to understand the evolution of signal intensity with temperature, we treat the sample as consisting of both superconducting and non-superconducting regions with superconducting grain size greater than coherence length. So, close to the onset transition temperature, the superconducting grains are weakly coupled and the order parameter phase keeps fluctuating. Here an intra-granular current generated within superconducting grains provides shielding effect. On decreasing the temperature more grains and regions within grains became superconducting. This increases superconducting domains and bulk superconductivity sets in when thermal energy ($K_B T$) is exceedingly smaller than Josephson coupling energy ($(1/2\pi)J_c \theta_0$).

At lower temperatures, grains get coupled and inter-granular currents starts to contribute. So both inter-granular and intra-granular currents exist and cause LFMA when they interact with microwaves. In fact, at low temperatures inter-granular coupling is very strong and provides Meissner shielding effect. This explains high signal intensity at low temperatures. In view of this, Bhat et al [35] indicates that at given T and H , a signal intensity of a system with a superconducting volume fraction x can be expressed as

$$V/V_0 = \alpha/(1 - 3x) + \frac{1}{x}(1 - 3x)/(1 - \frac{3}{2}x)^2 \quad 4.2$$

where $V_0 = I_0/(k^2\omega C_p)$, $\alpha = 4\pi a^2\omega\mu_0\sigma_N$, α is the conductivity, a is sample dimension, ω is the frequency, μ_0 is permeability and C_p is the capacitance.

Based on Bhat et al model, the trend of LFMA intensity can be argued as follows; as the temperature is increased, there is a gradual decrease of critical current as a result of weakening of Josephson coupling energy. This then necessitates fluxons penetration into the sample. As a consequence, the superconducting volume fraction x steadily decreases. Therefore, the signal intensity reduces with increase in temperature as depicted in the inset of figure 4.2.

B. Anomalous hysteresis

In figure 4.4 we represent the LFMA signal obtained by sweeping the magnetic field from – 500 G through 0 to + 5000 G and back to – 500 G for temperatures 10 K, 15 K, 20 K, and 30 K. Partly, it can be observed that the LFMA signal is lower during the backward sweeping (decreasing field) of the magnetic field than in the forward (increasing field) and it reaches a minimum well before the sweep field reaches the zero field. This constitutes the hysteresis of a material which is a manifestation of magnetization processes and the area is occupied by magnetic vortices in superconductors hence exhibiting the lossy (dissipative) region.

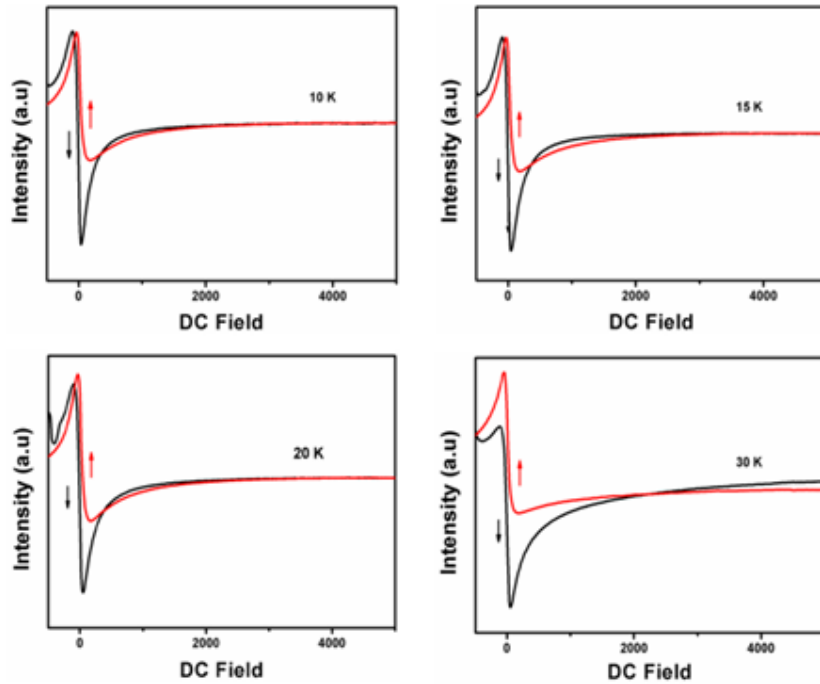


Figure 4.4: The LFMA measured on ZFC Sm1111 powder sample at temperatures 10, 15, 20 and 30 K. the arrows indicate the change of direction of external DC magnetic field field.

This anomaly has been observed in magnetization measurements [12, 36, 37] and LFMA studies [6] of high T_c cuprates. In our work, the phenomenon is observed at all the temperature measured. It therefore vehemently points to a two-component system which vindicates the assumptions made above of treating our sample as a system consisting of superconducting grains and inter-particle and other weak links.

This phenomenon can be understood on the basis of approximately treating a sample as a two-level superconducting system [6]. The superconducting crystallite (grains) with strong superconductivity and Josephson type weak bonds formed between the grains. Unlike in the conventional critical state model where a macroscopy single J_c governs the gradient of the flux everywhere in a homogeneous superconducting sample, a two-level system portrays two distinct current densities which include, a large J_g inside grains and a weaker one in the inter-grain weak bonds. Yet again, it is presumable that two types of pinning do exist namely; (1) grain pinned fluxons which are strongly pinned inside the grains and (2) weakly pinned grain boundary fluxons (they are fairly free since inter-granular bonds have relatively weak pinning centers).

The gradient of the flux density inside the grains is much larger than in inter-grain. On a macroscopic scale, the flux density averaged over many grains should have a gradient

determined by the intergranular critical current density. Owing to the weakly pinning strength, the electromagnetic energy dissipation in this system is mainly dominated by the flux density in the inter-granular regions. Prominently, an application of external magnetic field significantly affects the inter-granular fluxons dynamics in this kind of systems.

This is in fact attested in figure 4.4 and can be explicitly discussed as follows; with forward sweeping of DC magnetic field, fluxons are trapped both inside grains and on inter-granular region. However, on backward sweep (reversing the field), some of the trapped fluxons are no longer supported by DC magnetic field. As a result they form closed loops around the inter-granular sites. The collective local current density then drives a reverse flux into the grains through weakest junctions [6, 36]. Consequently, the averaged field in the inter-granular region becomes instantaneously less compared to field during forward sweep. As a result the microwave absorption absorbed during the downward sweep is correspondingly less than during forward sweep hence revealing the anomaly as shown in figure 4.4.

An alternative explanation is that, if we presume the sample to form a Josephson type-network of weak bonds (where the superconducting grains are weakly connected by non-superconducting matrix), the resistive/ dissipative part is predominantly determined by the inter-grain weak links. Then the LFMA intensity of this kind of a system can be represented by Eq. (1). Here the first term of this equation is independent of magnetic field and represents the reversible part. On the other hand, in the 2nd term, the sign changes ($\varphi_0 \rightarrow -\varphi_0$) when the field is reversed hence representing the irreversible term. The critical current of the junction given as $I_c(\theta, T) = I_c(0, T)F(\theta)$ is a function of magnetic field (H) given as $F(\theta) = [\sin(\pi\theta/\pi\theta_0)/(\pi\theta/\pi\theta_0)]$ (the $F(\theta)$ is the junction reduction parameter) [33]. It can be noted that when the DC magnetic field is increased, the I_c decreases. There occurs a variation of inter-granular fluxons density when the field is swept in the forward and backward manner since the phase is changed ($\varphi_0 \rightarrow -\varphi_0$). Therefore this variation in fluxons results to anomalous hysteresis behaviour.

IV. Conclusion

In conclusion, we have carried out LFMA studies in powder sample of Sm1111 material. It has been noted that LFMA signal evolves as a function of temperature. The line shape has a structure (a broad peak and narrow peak). This structure is similar to what is reported in

pellet sample of the same material. The variation of signal intensity with temperature has been noted and elucidated on the framework of effective medium theory. Again, an anomalous hysteresis which depicts the granular nature of high T_c superconductors was observed and explicated on the context of two-level critical state model.

References

1. Onyancha, R.B., Shimoyama, J., Singh, S.J., Ogino, H., Srinivasu, V.V., :J. Supercond. Nov. Magn. **28**, 2927 (2015)
2. Srinivasu, V.V., Bhat, S.V., Muralidhar, G.K., Mohan Rao, G., Mohan, S.: Pramana **40**, 119 (1993)
3. Stalder, M., Stefanicki, G.,Warden, M., Portis, A.M., Waldner, F.: Physica C **153–155**, 659–660 (1988)
4. Panarina, N.Y., Talanov, Y.I., Shaposhnikova, T.S., Beysengulov, N.R., Vavilova, E.: Phys. Rev. B **81**, 224509 (2010)
5. Srivivasu V.V., Pinto, R., Sastry, M.D.: Appl. Supercond. **4**, 195 (1996)
6. Ji, L., Rzchowski, M.S., Anand, N., Tinkham, M.: Phys. Rev. B **47**, 470 (1993).
7. Deutscher, G., Muller, K.A.: Phys. Rev. Lett. **59**, 1745 (1987)
8. Srinivasu, V.V., Thomas, B., Hegde, M.S., Bhat, S.V.: J. Appl. Phys. **75**, 4131–4136 (1994)
9. Weides, M., Kemmler, M., Kohlstedt, H.,Waser, R., Koell, D., Kleiner, R., Goldobin, E.: PRL **97**, 247001(2006)
10. Knauf, N., Fischer, J., Schmidt, P., Roden, B., Borowski, R., Buchner, B., Micklitz, H., Freimuth, A., Kataev, V., Khomskii, D.I.: Europhys. Lett. **35**, 541 (1996)
11. Knauf, N., Fischer, J., Schmidt, P., Roden, B., Borowski, R.,Buchner, B., Micklitz, H., Freimuth, A., Khomskii, D.I.,Kataev, V.: Physica C **299**, 125 (1998)
12. Pradhan. A. K., Roy, S. B., Chaddah, P., Chen, C., Wanklyn, B. M.: Phys. Rev B **52**, 6215 (1995)
13. Pallecchi, I., Tropeano, M., Lamura, G., Pani, M., Palombo, M., Palenzona, A., Putti, M.: Physica C **482**, 68 (2012)
14. Senatore, C., Flukiger, R., Cantoni, M., Wu, G., Liu, R.H., Chen, X.H.: Phys. Rev. B **78**, 054514 (2008)
15. Fang, L., Jia, Y., Mishra, V., Chaparro, C., Vlasko-Vlasov, V.K., Koshelev, A.E., Welp, U., Crabtree, G.W., Zhu, S., Zhigadlo, N.D., Katrych, S., Karpinski, J., Kwok, W.K.: Nat. Commun. **4**, 2655 (2013)
16. Moll, P.J.W., Puzniak, R., Balakirev, F., Rogacki, K., Zarpinski, J., Zhigadlo, N.D., Batlogg, B.: Nat. Mat. **9**, 628 (2010)

17. Lida, K., Hanisch, J., Tarantini, C., Kurth, F., Jaroszynski, J., Ueda, S., Naito, M., Ichinose, A., Tsukada, I., Reich, E., Grinenko, V., Schultz, L., Holzapfel, B.: *Sci. Rep.* **3**, 2139 (2013)
18. Paglione, J., Greene, R.L., *Nat. Phys.* **6**, 645 (2010).
19. Johnston, D. C., *Advances in Physics* **59**, 803 (2010)
20. Hosono, H., Kuroki, K., *Physica C* **514**, 399 (2015)
21. Chen, X. H., Wu, T., Wu, G., Liu, R.H., Chen, H., Fang, D.F., *Nature* **453**, 761 (2008)
22. Singh, J.S., Shimoyama, J., Yamamoto, A., Ogino, H., Kishio, K.: *Supercond. Sci. Technol.* **26**, 065006 (2013)
23. Singh, S.J., Shimoyama, J., Yamamoto, A., Ogino, H., Kishio, K.: *IEEE Trans. Appl. Supercond.* **23**, 7300605 (2013)
24. Onyancha, R.B., Shimoyama, J., Singh, S.J., Hayashi, K., Ogino, H., Srinivasu, V. V.: *Physica C*: <http://dx.doi.org/10.1016/j.physc.2016.07.019> (2016)
25. Srinivasu, V.V., Itoh, K., Hashizume, A., Sreedevi, V., Kohmoto, H., Endo, T., Ricardo da Silva, R., Kopelevich, Y., Moehlecke, S., Masui, T., Hayashi, K.: *J. Supercond. Nov. Magn.* **14**, 41 (2001)
26. Bhat, S.V., Panguly, P., Rao, C.N.R.: *Pramana J. Phys.* **28**, L425 (1987)
27. Bhat, S.V., Ganguly, P., Ramakrishnan, T.V., Rao, C.N.R.: *Pramana J. Phys* **20**, L559 (1987)
28. Blazey, K.W., Muller, K.A., Bednorz, J.G., Berlinger, W., Amoretti, G., Buluggiu, E., Vera, A., Maticotta, F.C.: *Phys. Rev. B* **36**, 7241 (1987)
29. Dunny, R., Hautala, J., Ducharme, S., Lee, B., Symko, O.G., Taylor, P.C., Zheng, D.J., Xu, J.A.: *Phys. Rev. B* **36**, 2361 (1987)
30. Stankowski, J., Kahol, P.K., Dalal, N.S., Moodera, J.S.: *Phys. Rev. B* **36**, 7126 (1987)
31. Srinivasu, V.V.: *J. Supercond. Nov. Magn.* **23**, 305–308 (2010)
32. Talanov, Y., Beisengulov, N., Kornilov, G., Shaposhnikova, T., Vavilova, E., Nacke, C., Panarina, S., Hess, C., Kataev, V., Buchner, B.: *Supercond. Sci. Technol.* **26**, 045015 (2013)
33. Dulcic, A., Rakvin, B., Pozek, M.: *Europhys. Lett.* **10**, 593–598 (1989)
34. Portis, A.M., Blazey, K.W., Muller, K.A., Bednorz, J.G.: *Europhys. Lett.* **5**, 467 (1988)
35. Bhat, S.V., Srinivasu, V.V., Kumar, N.: *Phys. Rev. B* **44**, 10121 (1991)

36. Iga, F., Grover, A. K., Yamaguchi, Y., Nishihara, Y., Goyal, N., Bhat, S. V.: Phys. Rev. B **51**, 8521 (1995)
37. Felner, I., Galstyan, E., Lorenz, B., Cao, D., Wang, Y. S., Xue, Y., Chu, C. W.: Phys. Rev. B **67**, 134506 (2003)

Chapter 5

NRMA of $\text{SmFeAsO}_{0.80}\text{F}_{0.20}$ material

This section was published as “R. B. Onyancha ^{a*}, J. Shimoyama ^b, Jayashree Das^c, K. Hayashi^d, H. Ogino ^e and V. V. Srinivasu^a . *Non-resonant Microwave Absorption in $\text{SmFeAsO}_{0.80}\text{F}_{0.20}$: Lineshape and Structure Evolution with Temperature. J Supercond Nov Magn (2017) 30:2429–2434*”

Non-resonant Microwave Absorption in $\text{SmFeAsO}_{0.80}\text{F}_{0.20}$: Lineshape and Structure Evolution with Temperature.

I. Introduction

Discovered about decade ago, iron-based superconductors [3] have attracted enormous interests in the research field of condensed matter physics. This family provides a plethora of materials which forms an exciting playground in probing and understanding the exotic physics of superconductors hence shedding some light on debatable and contagious topics (like coexistence of superconductivity, nematicity, magnetism and pairing mechanisms). Furthermore, these materials possess unequivocal properties like robustness to impurity, high upper critical field (upper critical field is comparable to conventional superconductors and exceeds at high magnetic field) and well connected grain boundaries [4]. These properties coupled with the fact that it is absolutely possible to systematically manipulate the fundamental units i.e fluxons and Cooper pairs, makes iron based superconductors appealing in device applications like in the fabrication of microwave-related devices (SQUIDs and QuBits).

Similar to cuprates, the iron-based superconducting materials are granular in nature hence imperfectly screen out applied DC magnetic field. In fact they are 2D layered and possess very short coherence length which is responsible for weakening of the pair potential at surface. The formation of both intra-granular and inter-granular weak links traps magnetic fluxons. Therefore, a systematic application of microwave radiation can in principle detect the magnetic fluxons dynamics. One of the microwave absorption related technique which has been used effectively in the study of superconductors and other magnetic materials is Non-resonant microwave absorption (NRMA), also often known as Low field microwave absorption (LFMA) [5, 6].

Since then, many groups have successfully employed the same technique to explore magnetic dynamics in superconductors and magnetic materials [7-14]. The technique involves use of electron spin resonance (ESR) spectrometer where magnetic field dependent absorption is realised. The field modulation and phase sensitive detection are employed to enhance the signal of the power (P) absorbed and recorded as a field derivative (dP/dH). The

LFMA signal (line shape) depends on a number of factors that includes the nature of the sample, temperature, microwave power and DC magnetic field [15]. The LFMA as microwave detection technique is of utmost importance in the knowledge of microwave dissipative process in high- T_c superconductors, hence providing a guidance in passive device applications at either liquid nitrogen or helium temperatures.

In high- T_c superconductors, NRMA/LFMA technique has been indispensable in uniquely distinguishing absorptions arising from inter-granular and intra-granular regions. Moreover, exotic LFMA phenomena such as Wolleben effect (paramagnetic meissner effect), and 'anomalous' hysteresis have been realised [16-18]. In iron-based superconductors, thus far, LFMA studies have been rarely reported [1, 2, 19-21]. For instance, Panarima et al [19] and Talanov [20] have methodically showed co-existence of superconductivity and magnetism in Sm1111 and Ba122. Furthermore, they used the same approach to study the critical current density where they portrayed that Sm1111 has a strong pinning effect compared to YBCO.

Similarly, an observation of a structure with two peaks (broad peak and narrow peak) in Sm1111 have been reported [1]. Here the broad peak has been associated with microwave dissipation as result of damped motion whereas the narrow peak is a result of losses accrued to weak links. Again, Temperature dependence of LFMA in powder of Sm1111 has been presented [21]. The results revealed an anomalous hysteresis at all temperature measured. The anomaly was discussed on the framework of a two level critical state model (both intra-granular and inter-granular pinning). Finally, a microwave dependent LFMA where a cross over from 'normal' absorption to 'anomalous' behaviour has been witnessed. Here a system with both hysteretic and non-hysteretic Josephson junction has been invoked. So a change from hysteretic to non-hysteretic regime results to appearance of this phenomenon [2].

In this paper we report on LFMA studies of $\text{SmFeAsO}_{0.80}\text{F}_{0.20}$ superconducting sample. We confirm an existence of a structure (broad peak and narrow peak) similar to the one observed in Sm1111(0.12) which fundamentally imply that this structure is generic to this class of superconducting material. Again, we noted that the narrow peak persists up to a temperature 48 K which is close to the superconducting transition temperature of 49 K estimated by LFMA technique. The absence of crossover from 'normal' absorption to 'anomalous' absorption in this material depicts presence of only hysteretic-type of Josephson junction within the microwave power employed. This is dissimilar to the

microwave power variation studies reported on $\text{SmFeAsO}_{0.88}\text{F}_{0.12}$ where a ‘phase reversal’ at 2.247 mW was observed and discussed on the basis of Josephson junction changing from ‘hysteretic’ to ‘non-hysteretic’ nature.

II. Experiment

Non-resonant microwave absorption were carried out on polycrystalline sample of $\text{SmFeAsO}_{0.80}\text{F}_{0.20}$ using a Bruker EMX spectrometer operating at 9.45 GHz and equipped with an oxford ESR 910 continuous flow cryostat. The measurements were recorded at various temperatures in the range of 50 K – 10 K with modulation frequency of 100 KHz at zero field cooled sample. The static field H was scanned from -250 through 0 to + 250 K. The ESR signal was recorded as a derivative (dP/dH) and to check the phase, a resonance signal was used. Samples of polycrystalline sample of Sm1111 with nominal compositions of $\text{SmFeAsO}_{0.80}\text{F}_{0.20}$ were synthesized by solid-state reaction using SmAs, Fe, Fe_2O_3 and FeF_2 . The starting reagents were mixed and pressed into pellets under a pressure of 40 MPa and were sintered at 900 °C for 45 h in an evacuated quartz ampoules as discussed elsewhere [1, 2, 22, 23]. The critical superconducting temperature T_c was estimated by resistivity and DC magnetization measurements (figures 5.1 and 5.2 respectively). Resistivity measurement estimated $T_c = 53$ K while DC magnetization revealed $T_c = 49$ K, valued as half height of the superconducting transition and the superconducting onset transition temperature, $T_{c(\text{onset})} = 55$ K was obtained.

III. Results and Discussions

Figure 5.1 shows DC magnetization of $\text{SmFeAsO}_{0.80}\text{F}_{0.20}$ carried out at 10e. Kinks feature in superconducting transition region can be observed which clearly attests to granularity of a sample. Given the short coherence in superconducting materials ($\xi \sim 1.2\text{nm}$) [24], the superconducting grains are separated by non-superconducting matrix which practically forms Josephson-like junctions (JJs). At low temperatures, the grains and the non-superconducting matrix of molecular width contributes to superconductivity ensuring maximum Meissner shielding whereas on increasing temperature towards T_c the Josephson junction-like links are gradually broken. This is the scenario exhibited by ZFC susceptibility which results to both intra-granular and inter-granular superconductivity. From the resistivity in figure 5.2, a $T_c \sim 53$ K is obtained whereas DC magnetization measurement

indicates an onset superconducting transition temperature of 55 K and critical superconducting temperature, T_c of 49 K (which is estimated as half height of superconducting transition region)

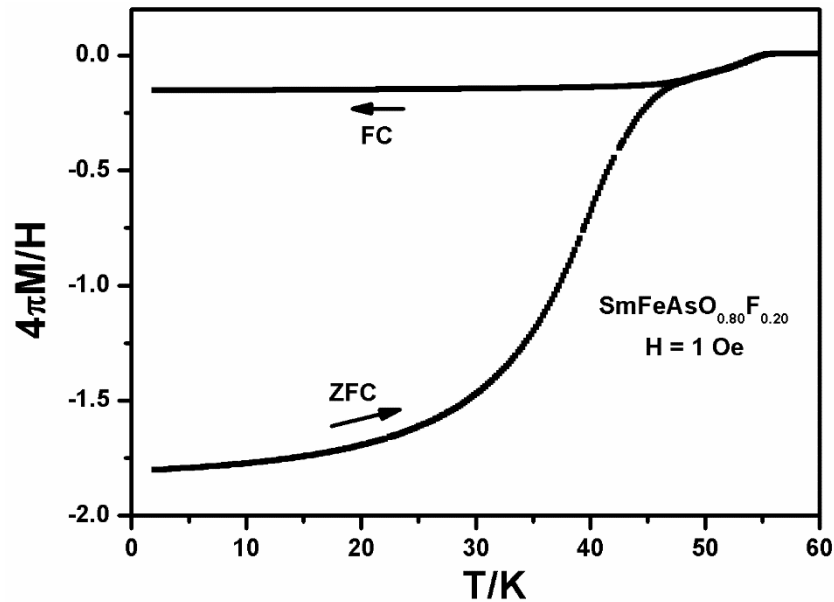


Figure 5.1: DC magnetic susceptibility of $\text{SmFeAsO}_{0.80}\text{F}_{0.20}$ measured at 1 Oe showing a $T_c = 49$ K and an onset superconducting transition 53 K.

A. Effect of temperature variation on LFMA line shape

Figure 5.3 shows NRMA derivative signal evolving as a function of temperature with all measurements recorded at microwave power of 0.710 mW and field modulation of 5 G. Two peaks namely; broad peak and narrow peak which are similar to work reported [1] are witnessed. Again, the signal intensity decreases with increase in temperature up to 49 K and vanishes at 50 K. Therefore, the NRMA has estimated T_c of this material to be 49 K which is similar to the value obtained from DC magnetic susceptibility measurements. The presence of the two peaks in this system is very interesting as it shows that these peaks are common feature in $\text{SmFeAsO}_{1-x}\text{F}_x$ material and they are F-doping independent. To begin with, NRMA signal intensity evolution with temperature can be explicated by considering two microwave loss mechanisms namely; loss through viscous motion of fluxons driven by microwave currents as a result of Lorentz force $(1/c)(j \times \phi_0)$ [25] and loss in JJs emanating from reduction of critical current when magnetic field penetrates the sample [26].

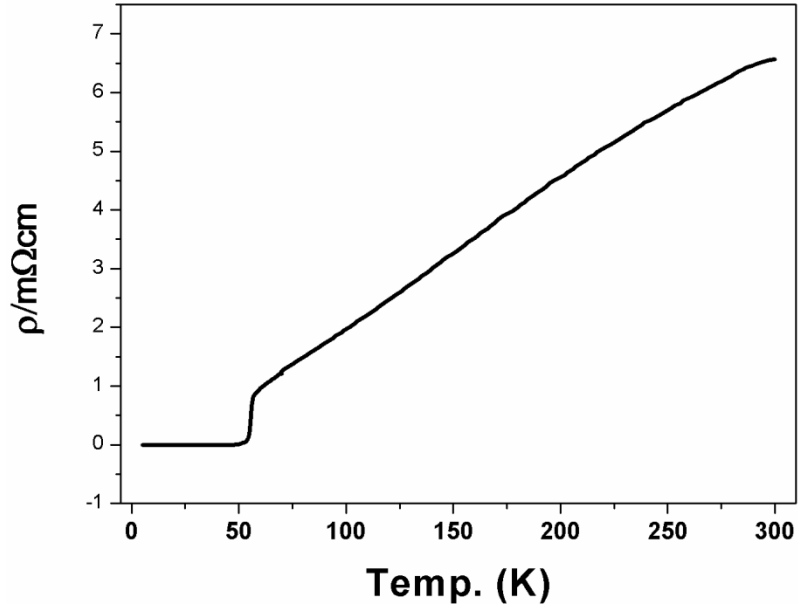


Figure 5.2: Resistivity measurements of $\text{SmFeAsO}_{0.80}\text{F}_{0.20}$ exhibiting a superconducting critical $T_c \sim 53$ K

Viscous motion of fluxons mechanism has been inferred when explicating the existence of the broad peak. It shows at glance the complex surface impedance ($Z = R_s - iX_s$) evolution to static DC magnetic field when subjected to microwave energy. According to the model, the surface impedance of sample has real and imaginary part defined by equation 5.1 and 5.2 respectively.

$$R_s = X_0 \left\{ \left[-1 + (1 + 4f^2 H^2 / B_0^2)^{1/2} \right] / 2 \right\}^{1/2} \quad 5.1$$

$$X_s = X_0 \left\{ \left[1 + (1 + 4f^2 H^2 / B_0^2)^{1/2} \right] / 2 \right\}^{1/2} \quad 5.2$$

here we define $X_0 = 4\pi\omega\lambda\mu^{3/2}/c^2$ and $B_0 = 8\pi\omega\mu\lambda^2\eta/\phi_0$ with λ , ω , η , μ , ϕ and f defined as London penetration depth, microwave frequency, viscosity coefficient of fluxons, magnetic permeability, flux and fraction of free fluxons respectively. In this experimental context, the real part represents the dissipative region and its derivative (dR_s/dH) needs to be computed since the NRMA signal is in a derivative form.

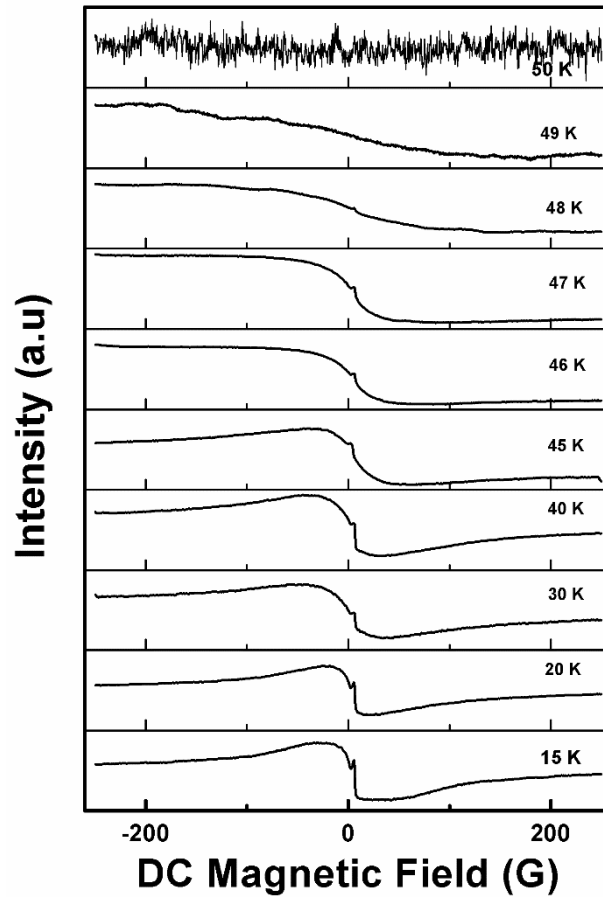


Figure 5.3: Non-resonant microwave absorption derivative of $\text{SmFeAsO}_{0.80}\text{F}_{0.20}$ recorded at different temperatures with microwave power of 0.710 mW.

If magnetic field applied is greater than lower Josephson junction field, H_{c1} , magnetic flux penetrates the sample and can move freely or get pinned in JJs. Then through Lorentz force, microwave currents drives fluxons causing dissipation. An increase in temperature fundamentally triggers the system to flux flow regime where energy dissipation is directly proportional to the number of fluxons and inversely proportional to the coefficient of viscous drag [27]. The resistivity at this regime can be expressed as in equation 5.3. It is paramount to state that viscous drag is dominant at flux flow regime where fluxons dissipates energy, consequently resulting to a gradual reduction of superconductivity with increase in temperature.

$$\rho_H = \frac{n\phi_0^2}{c^2\eta} = \frac{\phi_0 B}{c^2\eta} \quad 5.3$$

where, $\phi_0 = hc/2e$ is quantum flux unit and n is the number of fluxons (B/ϕ_0).

Moreover, weak links in the form of JJs are ubiquitously present in granular high-Tc superconductors. At low temperatures, these junctions are strongly coupled together and they have bulk superconductivity owing to large Josephson junction coupling energy, $(1/2\pi J_c \theta_0)$. This ensures an increased Meissner shielding effect in the system. The energy needed to decouple the junctions is large at these temperatures. However, an increase of temperature weakens the coupling energy and the junctions require less microwave energy to decouple. In trying to understand and explain the appearance of narrow peak, a model involving microwave loss in JJ has been invoked which defines microwave power loss as

$$P = \frac{1}{2} I_{mw}^2 \frac{R}{1+\eta} \quad 5.4$$

where η is a junction parameter defined by equation 5.5

$$\eta = \frac{I_c^2 (\cos\phi)^2}{\left(\frac{1}{R} \frac{h}{4\pi e} \omega_{mw}\right)^2} \quad 5.5$$

The microwave magnetic field induces a current I_{mw} and frequency ω_{mw} . R is the normal resistance and ϕ is the wave function phase between two grains. Finally, I_c is the critical current often represented as $I_c \sin\phi = I_0$, with I_0 being the current resulting from external magnetic field (H).

According to this model, the signal intensity varies as follows

$$S_I = \frac{(1/2)(I_{mw}^2 R)^{1/2}}{\left((1/2)(h/4e)\omega_{mw}\right)^2} \frac{1}{(1+N)^{3/2}} \times \left(\frac{dI_c}{dH} H_M + I_M \sin\phi_0\right) \cos(\omega_M t) \quad 5.6$$

From equation 5.6, it is clear that the intensity varies as a square root of microwave power. Given that less microwave power (energy) is needed to decouple Josephson junction as temperature is increased, the LFMA signal will decrease with increase of temperature.

Therefore the total microwave loss in this system which amounts to change in signal intensity is a combination of losses resulting from damped fluxons through Lorentz force and those arising from Josephson junctions.

$$T_{ml} = \frac{dR_s}{dH} + S_i \quad 5.7$$

Significant to this work is the narrow peak where in $\text{SmFeAsO}_{0.88}\text{F}_{0.12}$ the peak disappeared at $T_* = 38$ K which is 4K less the superconducting transition temperature of $T_c = 42$ K. However, in $\text{SmFeAsO}_{0.80}\text{F}_{0.20}$ sample, the peak disappears at $T_* = 48$ K which is 1 K less

the $T_c = 49$ K. To address this, we treat these two samples as systems comprising of arrays of JJs networks with statistically different coupling energy. At fixed microwave power, the sweeping of DC magnetic field and increasing of temperature leads to decoupling of JJ. By an assumption that JJs are mutually independent, the number of decoupled junctions varies with change in DC magnetic field $-dN/N = (H_d)^{-1}dH$. The microwave power absorbed is then defined as [28]

$$P_J = \Delta P_0(1 - e^{-(H/H_d)}) \quad 5.8$$

where H_d is the mean JJ decoupling field and ΔP_0 is the power absorbed when all junctions are decoupled at any given temperature. Fundamentally, it is clear that the power needed to decouple JJ in $\text{SmFeAsO}_{0.80}\text{F}_{0.20}$ is larger compared to $\text{SmFeAsO}_{0.88}\text{F}_{0.12}$ which clearly depicts stronger coupling energy of JJs present in $\text{SmFeAsO}_{0.80}\text{F}_{0.20}$. Imperatively, the weak links can be cracks, voids or material inclusions. Since the two materials are prepared by same technique in the same laboratory, the major contributing factor is likely to be fluorine concentration. In fact Panarina et al [18] has precisely showed that under-doped fluorine samples of SmFeAsO contain nanoscale mixing of non-superconducting phases. These inclusions reduce with increase in fluorine concentration towards optimal doping. Similar observations have been made in Co-doped BaFe_2As_2 where under-doped samples exhibit large non-superconducting phases [19].

B. Effect of microwave power variation on LFMA signal intensity

Figure 5.4 exhibits an influence of microwave power on NRMA derivative signal recorded at temperature of 8 K, field modulation of 5 G and the field were varied from -250 G through zero to + 250 G. Evidently, the peak-to-peak signal intensity increases with increase of microwave power as exhibited in the inset of figure 5.4. It is imperative to note that the NRMA line shape is actually a continuous spectral lines emanating from phase jumps in a superconducting loop. These micro-sized current loops in a granular sample are formed by Josephson-type links between superconducting islands (grains). Flux is quantized in these loops and as the DC magnetic field increases, phase jumps are witnessed and produce voltage pulses defined as $V(t) = -(h/2e)d\phi/dt$ (ϕ is the flux quantum). On the process, the superconducting critical current is exceeded and the resulting normal current flows which then absorbs microwave energy [29]. Now an increase of microwave power leads to an activation of a number of JJs in systems which in principle are capable of absorbing more

microwave energy and thus an increase of NRMA intensity with increase of microwave power.

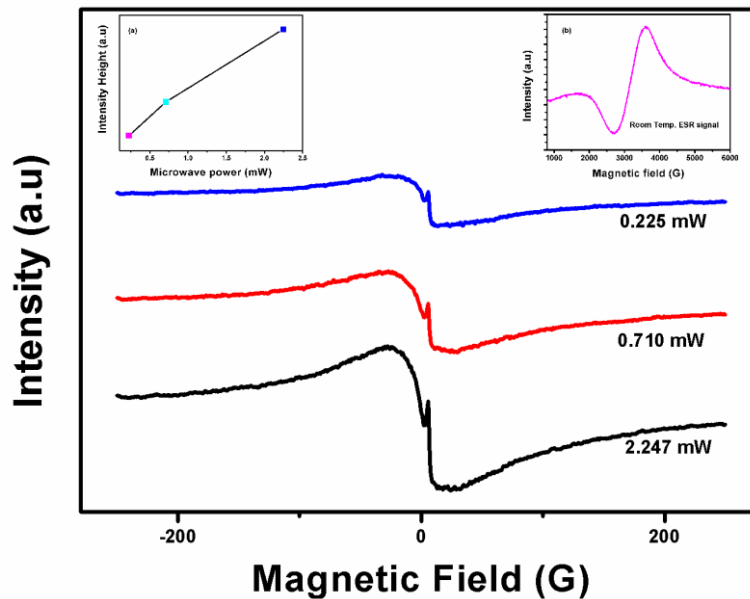


Figure 5.4: Non-resonant microwave absorption derivative of $\text{SmFeAsO}_{0.80}\text{F}_{0.20}$ evolution as a function of microwave power recorded at 8 K with field modulation of 5 G. inset; (a) represents peak to peak signal intensity height vs microwave power (b) Room temperature ESR signal used as phase reference signal.

An observation which is vital in this work is that the NRMA signal at all the microwave powers recorded here have the same phase as shown in figure 5. 4. The LFMA signal phase is opposite to ESR signal which is used as a reference signal (inset (b) of figure 5.4). This is dissimilar to work reported in $\text{SmFeAsO}_{0.88}\text{F}_{0.12}$, where there is a microwave power dependent ‘crossover’ from ‘normal’ absorption to ‘anomalous’ absorption at 2.247 mW [2]. The anomaly is well documented in HTSC and explicated based on the microwave power dependent change of JJs i.e from hysteretic to non-hysteretic regime [2]. Here a consideration of JJs with different coupling energy is taken into account and they will decouple at varied microwave power and DC magnetic fields. With an application of microwave power, the critical current of a fraction of JJ can be exceeded consequently changing the diffraction reduction of the critical current ($\sin \pi H_0 / \pi H_0$) (here H_0 is the saturation field). This renders some of the junctions non-hysteretic. Therefore a change from hysteretic to non-hysteretic is conceived which is the sole reason of the anomaly. Another possibility is that the presence of magnetic inclusions in superconducting system might

results to the formation of Pi junctions which can significantly influence the Fraunhofer pattern of critical current as a function of DC applied magnetic field [30].

The absence of the phase reversal clearly indicates an existence of only hysteretic JJs within the microwave power used. This can be attributed to an absence or significantly small traces of non-superconducting phase preferably magnetic nanoscale inclusions in $\text{SmFeAsO}_{0.80}\text{F}_{0.20}$. Therefore an application of DC magnetic field does not alter the Fraunhofer pattern of JJs critical current, hence no anomaly was observed.

IV. Conclusions

In conclusion, we have investigated the microwave dissipation process in $\text{SmFeAsO}_{0.80}\text{F}_{0.20}$ superconductor using NRMA technique. We have observed that NRMA evolves with both temperature and microwave power. The presence of structure consisting of two peaks (broad peak and narrow peak) analogous to one observed in $\text{SmFeAsO}_{0.88}\text{F}_{0.12}$ clearly indicates that it is a common feature in F-doped SmFeAsO system. The $T_c - T_* = 1\text{K}$ realised in this material is less compared to 4 K in $\text{SmFeAsO}_{0.88}\text{F}_{0.12}$ suggesting that fluorine doping has an important role. This observation has been discussed on view of the presence of strong JJs coupling energy accorded from few non-superconducting inclusions. Furthermore, NRMA signal as a function of microwave power does not show phase reversal i.e. 'normal' absorption to 'anomalous' absorption. This observation signifies that within the microwave power used; the system is in the hysteretic regime.

References

1. Onyancha, R.B., Shimoyama, J., Singh, S. J., Ogino, H., Srinivasu, V. V. :J Supercond Nov Magn 28, 2927–2934 (2015)
2. Onyancha, R.B., Shimoyama, J., Singh, S.J., Hayashi, K., Ogino, H., Srinivasu, V.V.: Physica C: Supercond. appl. 533 49–52 (2017)
3. Kamihara, Y., Watanabe T., Hirano, M., Hosono, H.: J. Am. Chem. Soc. 130 (2008) 3296
4. Hosono. H., Kuroki, K., phyica C. 514 (2015) 399-422
5. Bhat, S.V., Panguly, P., Rao, C.N.R.: Pramana J. Phys. 28, L425–L427 (1987)
6. Bhat, S.V., Ganguly, P., Ramakrishnan, T.V., Rao, C.N.R.: Pramana J. Phys 20, L559–L563 (1987)
7. Blazey, K.W., Muller, K.A., Bednorz, J.G., Berlinger, W.,Amoretti, G., Buluggiu, E., Vera, A., Maticotta, F.C.: Phys. Rev. B **36**, 7241 (1987)
8. Dunny, R., Hautala, J., Ducharme, S., Lee, B., Symko, O.G., Taylor, P.C., Zheng, D.J., Xu, J.A.: Phys. Rev. B **36**, 2361 (1987)
9. Stalder, M., Stefanicki, G.,Warden, M., Portis, A.M.,Waldner, F.: Physica C **153–155**, 659–660 (1988)
10. Veinger, A., Zabrodiskii, T., Tisnek, J., Alloys and Compounds 369, 751(2004)
11. Montiel, H., Alvarez, G., Betancourt I., Zamarano, R., Valenzuela, R.:Appl. Phys. Lett. 86 072503(2005)
12. Alvarez, G., Zamorano, R.: J. Alloys and Compounds **369**, 231(2004)
13. Rakhimov, R., Ries, H., Jones, D., Glebov, L.: Appl. Phys. Lett. 76, 751(2000)
14. Gavi, H., Ngom, B.D., Beye, A.C., Strydom, A.M., Srinivasu, V.V., Chaker, M., Manyala, N., J. Magnetism and Magnetic Materials 324, 1172 (2012)
15. Srinivasu V.V., Pinto, R., Sastry, M.D.: Appl. Supercond. **4**, 195– 201 (1996)
16. Knauf, N., Fischer, J., Schmidt, P., Roden, B., Borowski, R., Buchner, B., Micklitz, H., Freimuth, A., Kataev, V., Khomskii, D.I.: Europhys. Lett. **35**, 541–546 (1996)
17. Knauf, N., Fischer, J., Schmidt, P., Roden, B., Borowski, R., Buchner, B., Micklitz, H., Freimuth, A., Khomskii, D.I., Kataev, V.: Physica C **299**, 125–135 (1998)
18. Ji, L., Rzchowski, M.S., Anand, N., Tinkham, M.: Phys. Rev. B **47**, 470 (1993)

19. Panarina, N.Y., Talanov, Y.I., Shaposhnikova, T.S., Beysengulov, N.R., Vavilova, E.: Phys. Rev. B **81**, 224509 (2010)
20. Talanov, Y., Beisengulov, N., Kornilov, G., Shaposhnikova, T., Vavilova, E., Nacke, C., Panarina, S., Hess, C., Kataev, V., Buchner, B.: Supercond. Sci. Technol. **26**, 045015 (2013)
21. Onyancha, R.B., Shimoyama, J., Singh, S.J., Ogino, H., Srinivasu, V.V.: DOI 10.1007/s10948-016-3845-z
22. Singh, J.S., Shimoyama, J., Yamamoto, A., Ogino, H., Kishio, K.: Supercond. Sci. Technol. **26**, 065006 (2013)
23. Singh, S.J., Shimoyama, J., Yamamoto, A., Ogino, H., Kishio, K.: IEEE Trans. Appl. Supercond. **23**, 7300605 (2013)
24. Deutscher, G., Muller, K.A.: Phys. Rev. Lett. **59**, 1745 (1987)
25. Portis, A.M., Blazey, K.W., Muller, K.A., Bednorz, J.G.: Europhys. Lett. **5**, 467–472 (1988)
26. Dulcic, A., Rakvin, B., Pozek, M.: Europhys. Lett. **10**, 593–598 (1989)
27. Ji, L., Rzechowski, M. S., Tinkham, M.: Phys. Rev. B **42** 4838 (1990)
28. Silva, E., Giura, M., Marcon, R., Fastampa, R., Balestrino, G., Marinelli, M., Milani E.: Phys. Rev. B **45** 12566 (1992)
29. Owens, F.J.: Physica C **171** 25 (1990)
30. Weides, M., Kemmler, M., Kohlstedt, H. Waser, R., Koell, D., Kleiner, R., Goldobin, E.: PRL **97**, 247001 (2006)

Chapter 6

Novel normal-state LFMA of $\text{SmFeAsO}_{1-x}\text{F}_x$

This section will be submitted to Physical Review B Journal (2017) as “R. B. Onyancha ^{a*}, J. Shimoyama ^b, Jayashree Das^c, H. Ogino ^e and V. V. Srinivasu^a. *Novel normal-state Low Field Microwave Absorption in $\text{SmFeAsO}_{1-x}\text{F}_x$ Iron Pnictide Superconductors.*

Novel normal-state Low Field Microwave Absorption in $\text{SmFeAsO}_{1-x}\text{F}_x$ Iron Pnictide Superconductors.

I. Introduction

LFMA has become an excellent and unambiguous way of characterizing superconductors [1-13] and magnetic materials [14-18]. The LFMA in superconductors not only offers exotic physics but also provides crucial information on the suitability of a material-use in superconductivity related applications such as in filters, microwave devices, resonators and wave guides. Furthermore, room temperature LFMA magnetic materials have found possible applications as low field magnetic sensors, spin valves and magnetic tunnelling junctions [19]. Despite the fact that its mechanisms is far from being fully understood, this phenomenon has been reported in a number of magnetic materials like manganites [14], semi-conductors [15], silicate glass [16], soft magnetic materials [17] and in small band-gapped insulators [18]. To elucidate the subtle nature of this phenomenon, it will be interesting to identify and study the dynamics of a material that can exhibit this phenomenon both in the superconducting and normal state.

In that regards, iron pnictides superconductors which were discovered in 2008 [20] possibly provides excellent platform. Conversely, LFMA studies in the superconducting state of these materials are few and not completely understood so far. The studies on iron pnictides superconductors reported by Panarina et al [21] and Talanov et al [22] reveal that LFMA can be employed to uniquely reveal the critical current density dependence on temperature, obtain irreversibility field, adequately discriminate between inter-granular and intra-granular effects and ascertain a nanoscale co-existence of magnetism and superconductivity. Furthermore, LFMA in $\text{SmFeAsO}_{0.88}\text{F}_{0.12}$ [23] and $\text{SmFeAsO}_{0.80}\text{F}_{0.20}$ [24] has exhibited exciting features worth mentioning.

A generic structure with two peaks namely a broad peak and narrow peak have been reported in the two samples. Consequently, these peaks have been attributed to microwave loss as a result of damped motion [12] and in weak links in that order [13]. The $T_c - T_* = 1\text{ K}$ in $\text{SmFeAsO}_{0.80}\text{F}_{0.20}$ compared to 4 K in $\text{SmFeAsO}_{0.88}\text{F}_{0.12}$ (T_* is the characteristic temperature at which the narrow peak emerges the sample is cooled down from T_c) demonstrations that narrow peak is fluorine dependent. Yet again, 'anomalous' microwave

power dependent LFMA and ‘anomalous’ LFMA hysteresis features which connotes the presence of different kind of Josephson junctions [25] and a sample component with a two critical state [26] have been discussed. Nonetheless, all these aforementioned studies have been done in superconducting state. To the best of our knowledge, there is no report of LFMA study in the normal state of any iron-based superconductor.

In this paper, we present a methodical LFMA studies both in the normal and superconducting state of $\text{SmFeAsO}_{1-x}\text{F}_x$. We have established that the LFMA signal in the two states are distinctively different, in the normal state, two absorption modes are observed i.e. LFMA signal around zero magnetic field and a resonance signal at high fields whereas in the superconducting state only LFMA signal is observed. The signal intensity for LFMA signal in the normal state increases with decrease in temperature from room temperature up to 180K then decreases with decrease in temperature.

On the contrary, in the superconducting state the signal intensity decreases with increase in temperature. Moreover, the line width (ΔH_{pp}) in the normal state is $\sim 600\text{G}$ compared to $\sim 100\text{G}$ in the superconducting state. The observation of LFMA in the normal state which in essence reveals spin magnetization processes in the entire normal state is of fundamental importance. It adds a different way of exploring and unravelling magnetic dynamics in iron-based superconducting materials. Besides, it reveals that $\text{SmFeAsO}_{1-x}\text{F}_x$ can possibly be used in applications like in the area of spintronic, field-dependent microwave absorbers and low field magnetic sensors.

II. Experiment

Polycrystalline samples with nominal compositions of $\text{SmFeAsO}_{1-x}\text{F}_x$ ($x = 0.05, 0.12, 0.20$) were synthesized by solid-state reaction using pure SmAs, Fe, Fe_2O_3 and FeF_2 . The starting reagents were mixed and pressed into pellets under a pressure of 40 MPa and were sintered at 900 °C for 45 h in evacuated quartz ampoules. Detailed characterization of the samples under study in this chapter have been reported [23, 24]. The magnetization measurements were carried out in VSM-PPMS (Quantum design). Before, sweeping the magnetic field, the samples were zero-field cooled (ZFC) to the desired temperature. The ESR measurements were recorded using a Bruker EXM spectrometer operating in the X-band at 9.4 GHz frequency. The spectrometer was equipped with liquid helium flow from the Dewar to

access temperatures in 300- 20 K range. The ESR measurements records the power absorbed by the sample from the transverse magnetic microwave field as the static magnetic field H is scanned. The DC magnetic field in the range $-500 \text{ G} \leq H_{\text{DC}} \leq 9000 \text{ G}$ was applied for high magnetic field sweep and $-1000 \text{ G} \leq H_{\text{DC}} \leq 1000 \text{ G}$ for low field scan measurements. It should be pointed out that all the results presented hereafter are well reproducible.

III. Results and Discussion

Figure 6.1 (a) and 1(b) shows magnetic susceptibility and resistivity for $\text{SmFeAsO}_{0.95}\text{F}_{0.05}$ sample. similar measurements for samples $\text{SmFeAsO}_{0.88}\text{F}_{0.12}$ and $\text{SmFeAsO}_{0.80}\text{F}_{0.20}$. have been reported [23, 24] with T_c estimated to be 39 K and 53 K respectively. Precisely, $\text{SmFeAsO}_{0.95}\text{F}_{0.05}$ sample shows a kink at $\sim 140 \text{ K}$ in both resistivity and susceptibility which depicts a structural and magnetic transition.

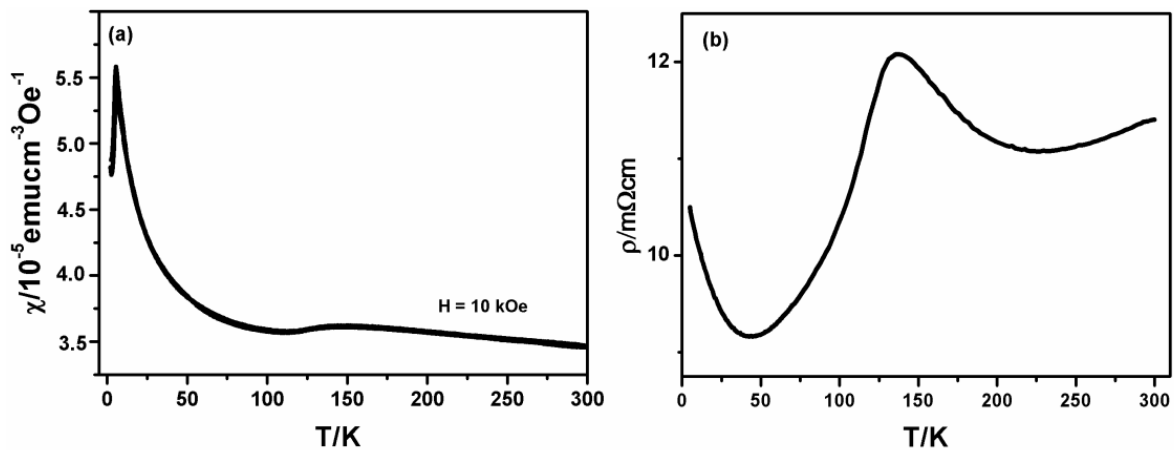


Figure 6.1: (a) Resistivity and (b) DC magnetizations of $\text{SmFeAsO}_{0.95}\text{F}_{0.05}$

Magnetization versus magnetic field (M - H) up to a field of 1 T were measured at several temperatures as shown in figure 6.2. The data for $\text{SmFeAsO}_{0.95}\text{F}_{0.05}$ in figure 6.2 (a) does not display any diamagnetic response at all temperatures thus affirming to the fact that the material is non superconducting. However, samples $\text{SmFeAsO}_{0.88}\text{F}_{0.12}$ and $\text{SmFeAsO}_{0.80}\text{F}_{0.20}$ in figure 6.2 (b) and figure 6.2 (c) exhibits this diamagnetic response. In the superconducting state of both samples, an increase in temperature results to a decrease in magnetization due to a reduction in diamagnetic shielding currents. Furthermore, in this state, the magnetization of $\text{SmFeAsO}_{0.80}\text{F}_{0.20}$ sample is always twice that of $\text{SmFeAsO}_{0.88}\text{F}_{0.12}$ at any given temperature thus attesting to the effect of fluorine doping as discussed in chapter five.

In addition, the magnetization loop of both samples is asymmetrical at $M=0$ indicating small bulk pinning (bulk pinning is response for symmetric behaviour) in these samples.

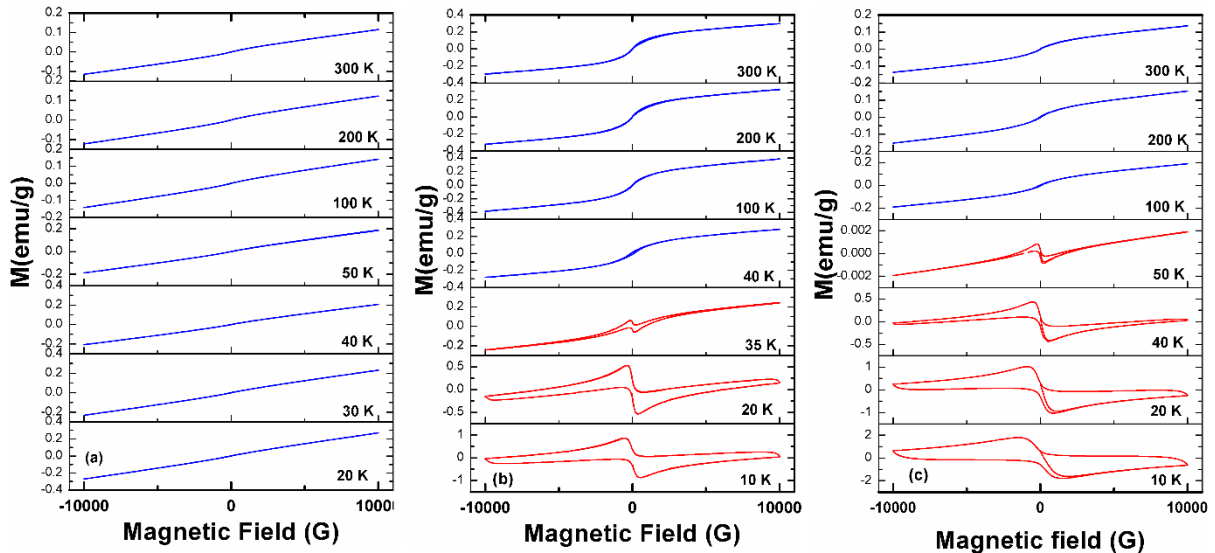


Figure 6.2: Magnetization curves at several temperatures for (a) $\text{SmFeAsO}_{0.95}\text{F}_{0.05}$ (b) $\text{SmFeAsO}_{0.88}\text{F}_{0.12}$ (c) $\text{SmFeAsO}_{0.80}\text{F}_{0.20}$.

Figure 6.3 represents an enlargement of magnetization curves extracted from Fig figure 6.2. Apparently, sample $\text{SmFeAsO}_{0.95}\text{F}_{0.05}$ exhibits a paramagnetic-like behaviour whereas $\text{SmFeAsO}_{0.88}\text{F}_{0.12}$ and $\text{SmFeAsO}_{0.80}\text{F}_{0.20}$ shows a ferromagnetic component. It is important to note that ferromagnetism can result in large negative moments as observed in the normal state of the two s superconducting samples. What remains unclear is the origin of this ferromagnetic behaviour. Possibly, it can be from impurity magnetic phases or an intrinsic property of the two samples that may have a connection to the high T_c observed.

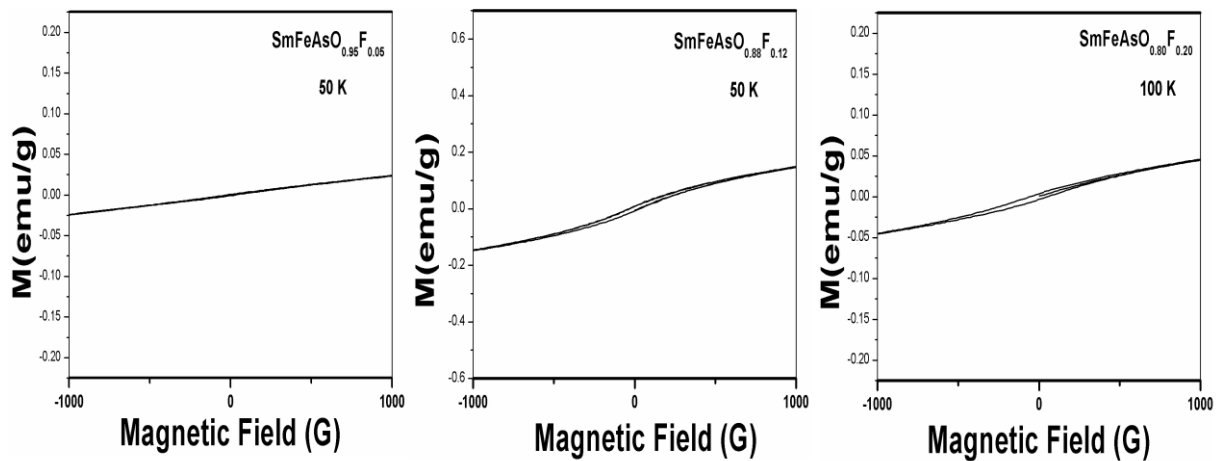


Figure 6.3: Magnetization hysteresis of $\text{SmFeAsO}_{1-x}\text{F}_x$

Figure 6.4 shows room temperature ESR derivative signal for both the pellet and powdered sample of $\text{SmFeAsO}_{0.88}\text{F}_{0.12}$ recorded by sweeping a DC magnetic field from -500 G through 0 to + 9000 G. At high fields, the signal displays a well-defined resonance spectrum. This spectrum corresponds to fully saturation state of a material and it gratifies Larmor condition ($\omega = \gamma H_{res}$). A similar absorption signal has been reported in $\text{LaFeAsO}_{1-x}\text{F}_x$ and attributed to local moments of Fe [27].

The powder sample signal appears larger and well defined. Similar observations have been made in various magnetic materials and accordingly associated to variations in particle sizes [14, 28, 29]. It has been argued that critical parameters such as the change from multi to single domain structure and the exchange correlation length which are related to the magnetic structure are found within range of 1-100 nm [30]. Therefore, owing to the fact that powder sample used here is in micro-meter range ($\sim 3 \mu\text{m}$) [26], the aforementioned parameters might have a significantly greater influence on powder sample signal compared to a pellet signal.

Prominently, room temperature microwave absorption signal centred around zero magnetic field is observed in both sample forms. The signal is often known as LFMA or NRMA clearly marked in figure 6. 4. The inset is an integrated LFMA signal showing a minimum microwave absorption at zero field and having a phase opposite to the resonance absorption signal. Quite strikingly, the LFMA phenomenon observed in the normal state of $\text{SmFeAsO}_{0.88}\text{F}_{0.12}$ is novel and is reported here for the first time.

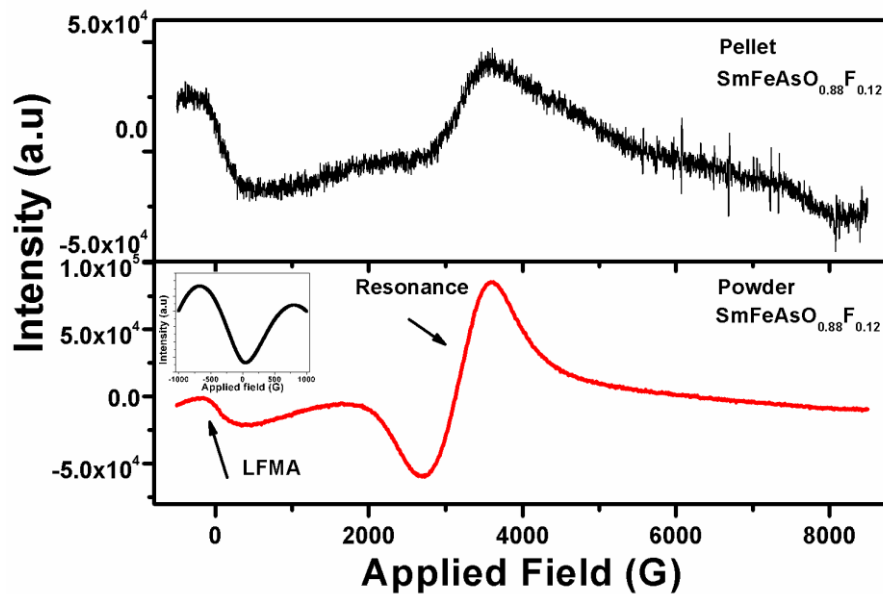


Figure 6.4: Derivative of microwave absorption as a function of the DC magnetic field of $\text{SmFeAsO}_{0.88}\text{F}_{0.12}$ (pellet and powder) at room temperature; inset shows integrated LFMA signal.

We have carried out room temperature measurements on the other two samples i.e. $\text{SmFeAsO}_{0.95}\text{F}_{0.05}$ and $\text{SmFeAsO}_{0.80}\text{F}_{0.20}$ as shown in figure 6.5. All the three samples exhibit the LFMA signal. Importantly, the phenomenon has been observed in various magnetic materials and can be ascribed to low field spin magnetization process in the unsaturated state [31]. Briefly, Valenzuela et al [32] elucidates this process as follows; that microwave absorption at zero fields is minimum as the magnetization is compensated by oppositely oriented domains. However, when the applied DC field is increased, domains get oriented in the field direction and the process leads to the a magnetic field dependent microwave absorption. The LFMA signal correlation with magneto-impedance (MI) in amorphous ribbons has been drawn and clearly divulges that the two have a general origin [17].

To account for LFMA in this material, it is worth mentioning the argument by Mahule et al [33] that this phenomenon can only be observed in magnetic materials that undergo spin polarization. In that effect, iron-based superconductors exhibit both spin polarization and orbital polarization enhanced at high energy and low energy respectively [34]. To be precise, the calculated spin polarizability in Fe is $\sim 45\%$ as reported [35]. Again, the presence of spin-orbit interaction in Fe 3d states results to band splitting [36 -40]. Fundamentally, this can cause spin asymmetry in the scattering of conduction electrons by impurities, hence the

charge imbalance results to Anomalous Hall effect (AHE) which is a well-recognized feature in spin polarized materials [41].

Resistivity can therefore be defined as, $\rho = \rho_0 H_z + \rho_s M_z$, where first component is resistivity due to ordinary Hall Effect (OHE) and second term is AHE. These resistivity components depend on the applied magnetic field. Consequently, an application of magnetic field can in principle induce microwave currents resulting to surface joule losses ($I_{rms}^2 R_s$ where I_{rms} is rms of the microwave current and R_s is the material surface resistance) which results to microwave loss in form of LFMA. Tentatively, we propose that the LFMA witnessed here is associated to microwave loss as result of joule surface loss emanating from AHE sample as discussed above. In fact, the magnetic characteristics of iron-based materials have close similarities with manganites; both are double-exchange materials [42] and exhibit magnetoresistance [43]. Significantly, manganites are spin polarized systems with AHE and have shown pronounced LFMA as well [14, 44, 45].

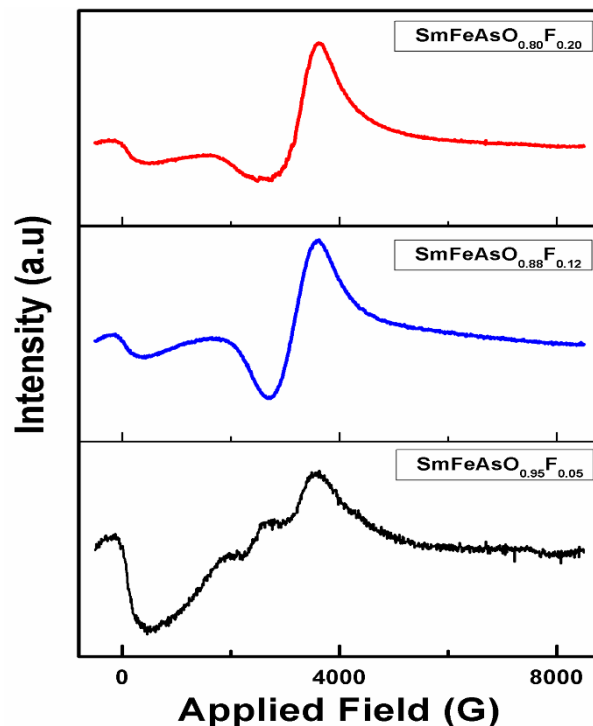


Figure 6.5: Derivative of microwave absorption as a function of the DC magnetic field for $\text{SmFeAsO}_{1-x}\text{F}_x$ at room temperature.

Figure 6. 6 shows LFMA derivative signal of the powder sample in the magnetic field range of -500 G to + 9000 G carried out for both forward and backward sweeps. A clear hysteresis is witnessed which can be associated to magnetization dynamics far from saturation state [46]. The hysteresis has been linked to a change in magnetic permeability at a given applied dc field which alters the ac field penetration depth thus changing the impedance response of the sample [47]. Inset (a) of figure 6.6 shows the enlarged normal state LFMA hysteresis which is distinctively different from the superconducting state LFMA hysteresis shown in the inset (b) of figure 6.6. Apparently, in the normal state the forward sweep curve is always lying above the backward sweep for the entire low field region (-450 G to + 650 G), whereas in the superconducting state, the forward only lies above the backward sweep curve at field range 200 G to 1750 G. This is a typical ‘anomalous’ hysteresis in high T_c superconductors and is well elucidated on the context of two-level critical state model [48].

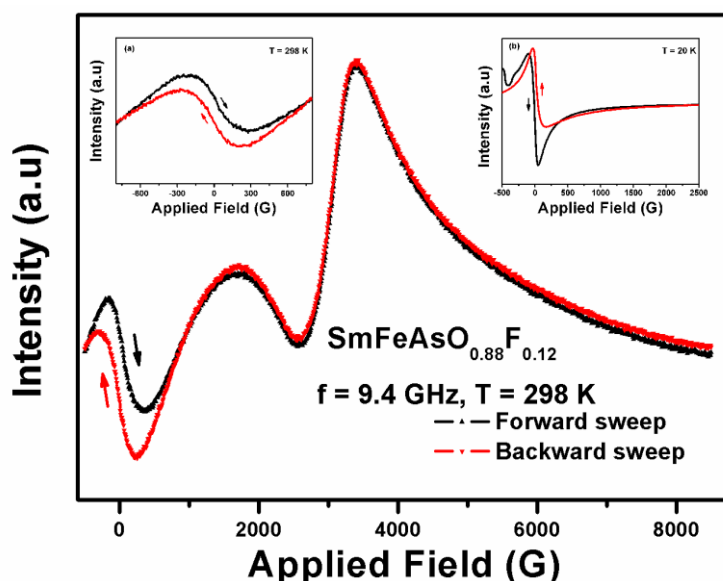


Figure 6.6: Derivative of microwave absorption as a function of the DC magnetic field of $\text{SmFeAsO}_{0.88}\text{F}_{0.12}$ at room temperature showing forward and backward sweep; insets: Left: LFMA hysteresis for $\text{SmFeAsO}_{0.88}\text{F}_{0.12}$ at room temperature; Right: Anomalous hysteresis for $\text{SmFeAsO}_{0.88}\text{F}_{0.12}$ at 20 K.

Figure 6.7 (a) represents an evolution of LFMA signal of $\text{SmFeAsO}_{0.88}\text{F}_{0.12}$ powder sample as a function of temperature in the range 260 K- 20 K. Here the resonance spectrum broadens and its intensity decreases on cooling the sample and eventually becomes an ‘ESR silent’ in the superconducting state. The broadening can be attributed to spin fluctuation

enhancement [49]. At low fields, LFMA spectrum is experienced in both the normal and superconducting states. Figure 6.7 (b) shows a plot of peak to peak intensity as function of temperature in the normal state whereas figure 6.7 (c) exhibits the peak to peak signal intensity evolution with temperature in the superconducting state. It is apparent that the two LFMA signals depicts different trends as a function temperature. In the normal state, the peak to peak intensity increases with increase in temperature in the range 20-180 K and decreases with increase in temperature thereafter.

Interestingly, according to our data, the largest intensity is at 180 K which is in the vicinity of a structural transition (symmetry breaking $C_4 \rightarrow C_2$) temperature (175 K) of this material [50, 51]. It is important to note that this transition which usher nematicity has been associated to spin and orbital ordering. Imperatively, the normal state electronic nematic fluctuations have been reported in the tetragonal phase at temperature ~ 200 K [52– 54] and the fluctuations tends to relatively decrease towards room temperature where it is considered negligible [46]. It will be interesting to carry out LFMA studies on other iron pnictide superconducting materials to ascertain whether there is any correlation between temperature corresponding to the highest peak to peak intensity and structural transition temperature.

On the contrary, the signal intensity in the superconducting state decreases with increase in temperature. Here the trend can be explained on the context of treating the sample as an effective medium where superconducting regions are separated by non-superconducting matrix. The system forms a Josephson type of junction where the non-superconducting layer between the superconducting grains acts as a barrier. Then as temperature is increased, the critical current of this Josephson-type weak links is gradually reduced consequently leading to reduction in Meissner shielding.

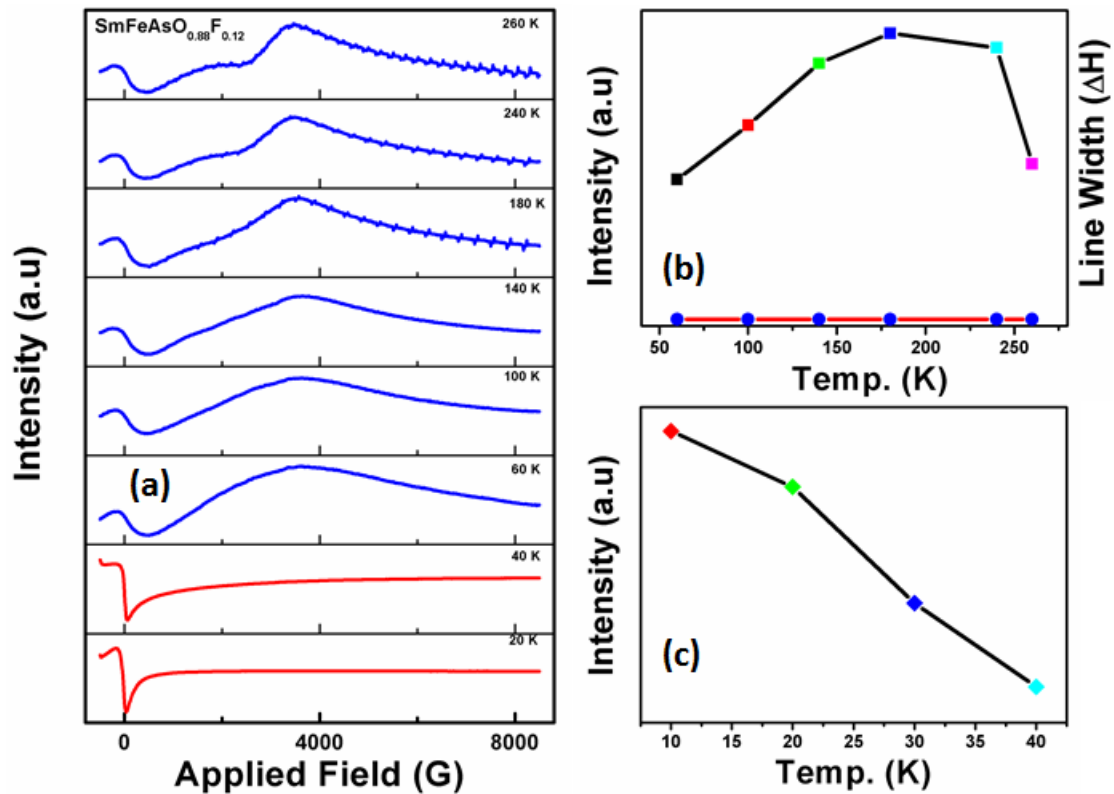


Figure 6.7: (a) Derivative of microwave absorption as a function of the DC magnetic field of $\text{SmFeAsO}_{0.88}\text{F}_{0.12}$ at various temperatures (20 – 260 K), (b) temperature dependence of peak to peak signal intensity in the normal state and line width (ΔH_{pp}) and (c) peak to peak signal intensity in superconducting state.

Accordingly, less microwave energy with increase in temperature is needed to decouple the junctions. Another distinctive way of differentiating the two forms of LFMA signals is through line width, ΔH_{pp} , (defined as the width between the highest point and the lowest point of the signal). In Fig. 4 (b), we have plotted a normal state line width (ΔH_{pp}) as a function of temperature. Clearly, $\Delta H_{pp} \sim 650$ G is independent of temperature. This value is six-fold larger in comparison to the linewidth obtained in the superconducting state (~ 100 G).

Figure 6.8 displays room temperature LFMA evolution as a function of microwave power measured with field scan of -1000 G through zero to 1000 G. From the inset of figure 6.8, it is clear that an increase of microwave power corresponds to an increase in signal intensity. In principle, an increase in microwave power in ESR measurements results to upsurge of microwave magnetic field in the cavity. Then the microwave magnetic field (H_m) induces microwave currents which as a consequences leads to ohmic microwave power loss in the sample.

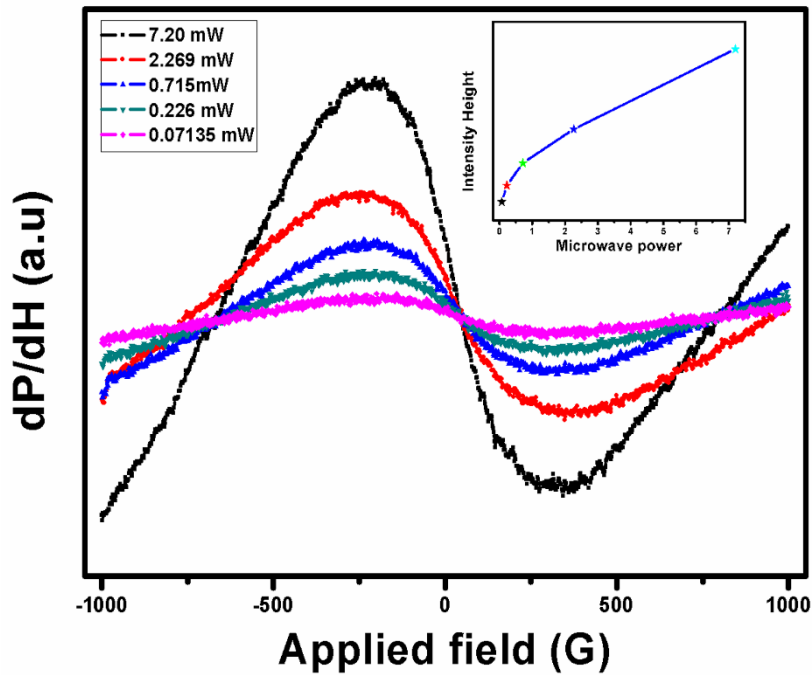


Figure 6.8: Microwave power dependence of LFMA measurements taken at room temperature and field modulation of 10 G. Inset show intensity height variation as a function of microwave power.

Finally, to examine the effects of modulation amplitude on the LFMA signal shape and intensity of the powdered sample, the incident microwave power was kept constant at 0.715 mW and the spectra recorded at room temperature as shown in figure 6.9. The modulation amplitude was varied between 2G – 10 G. The signal recorded is shown in figure 5 and the inset shows the peak to peak signal intensity. It is evident that there is a linear increase of intensity as function of modulation fields in the range 2G – 10 G. This can be understood on the framework that an increase in modulation amplitude H_M results to an increase of field penetration into the sample (as shown in equation 6.1.) which consequently changes the ac field penetration depth. Any variation of field penetration depth directly results to change in impedance $Re(Z)$ hence the signal increases as a function of modulation amplitude.

$$H(t) = H_0 + H_M \cos \omega t \quad 6.1$$

here H_0 is the static DC field, H_M is the modulation amplitude and ω is the modulation frequency which in this case is 100 kHz.

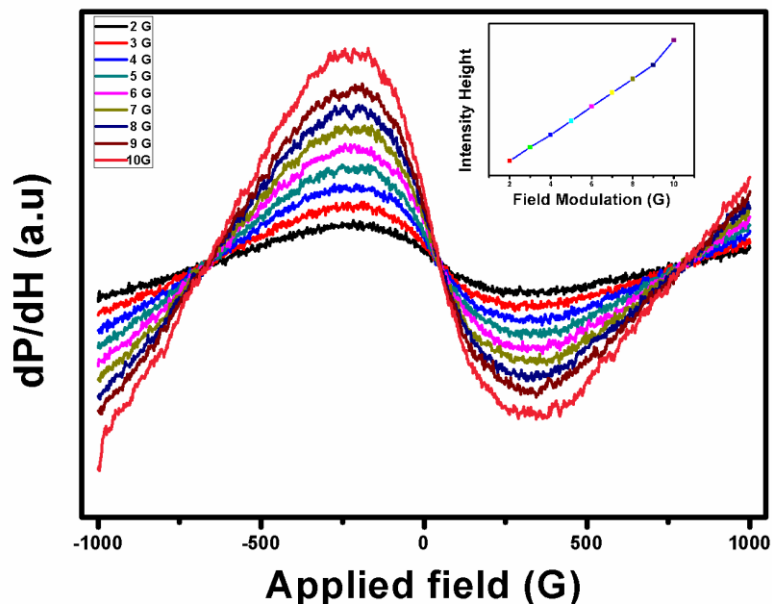


Figure 6.9: Field modulation amplitude dependence of LFMA measurements taken at room temperature and microwave power of 0.715 mW. The inset is a plot of peak to peak intensity vs field modulation.

IV. Conclusions

We have carried out LFMA measurements on $\text{SmFeAsO}_{1-x}\text{F}_x$ samples both in the normal and superconducting state. Interesting, the LFMA phenomenon has been observed at all the temperature measured. Of particular importance, the LFMA spectrum observed at the normal state of this material is novel in high T_c superconductors. In a methodical way, we have categorically distinguished the normal state LFMA signal with its counterpart in the superconducting state on these three scenarios: (1) in the normal state, the resonance spectrum persists in all the temperatures measured but reverts to ‘ESR silent’ in superconducting region (2) the peak to peak LFMA signal intensity height in the normal state increases with temperature up to 180 K and then decreases onwards whereas a decrease of intensity with increase in temperature is exhibited in superconducting state (3) the line width of LFMA spectrum in superconducting region is ~ 100 G compared to ~ 650 G in normal state. Moreover, it has established that the normal state LFMA evolves as a function of microwave power. The observation of this phenomenon in the normal state is crucial based on the view that it is associated to spin magnetization. Then it adds a different platform of studying and understanding debatable magnetic dynamics in superconducting materials. Furthermore, it opens a possible application of this material in the fields of

spintronic for example in room temperature low field magnetic sensor and as microwave absorbers.

References

1. Bhat, S.V., Panguly, P., Rao, C.N.R.: *Pramana J. Phys.* **28**, L425 (1987)
2. Bhat, S.V., Ganguly, P., Ramakrishnan, T.V., Rao C.N.R., *Pramana J. Phys* **20**, L559 (1987)
3. Stankowski, J., Kahol, P.K., Dalal, N.S., Moodera, J.S.: *Phys. Rev. B* **36**, 7126(1987)
4. Dunny, R., Hautala, J., Ducharme, S., Lee, Symko, O.G., Taylor, P.C., Zheng, D.J., Xu, J.A.: *Phys. Rev. B* **36**, 2361 (1987)
5. Blazey, K.W., Müller, K.A., Bednorz, J.G., Berlinger, W., Amoretti, G., Buluggiu, E., Vera, A., Maticotta, F.C.: *Phys. Rev. B* **36**, 7241 (1987)
6. Khachaturyan, K., Weber, E.R., Tejedor, P., Stacy, A.M., Portis, A.M.: *Phys. Rev. B* **36**, 8309 (1987)
7. Moorjani, K., Bohandy J., Adrian, F.J., Kim, B.F.: *Phys. Rev. B* **36**, 4036 (1987)
8. Bhat, S.V., Srinivasu, V.V., Kumar, N.: *Phys. Rev. B* **44**, 10121(1991)
9. Srinivasu, V. V., Pinto, R., Sastry, M. D.: *Appl. Supercond.* Vol. 4 no. 4 (1996) 195-201
10. Srinivasu, V.V., Thomas, B., Hegde, M.S., Bhat, S.V.: *J. Appl. Phys.* **75**, 4131–4136 (1994)
11. Srinivasu, V.V.: *J. Supercond. Nov. Magn.* **23**, 305–308 (2010)
12. Portis, A.M., Blazey, K.W., Muller, K.A., Bednorz, J.G.: *Europhys. Lett.* **5**, 467–472 (1988)
13. Dulcic, A., Rakvin, B., Pozek, M.: *Europhys. Lett.* **10**, 593(1989)
14. Srinivasu, V.V., Lofland, S.E. Bhagat, S.M., Ghosh, K., Tyagi, S.D.: *J. Physics Letters* **86**, 106 (1999)
15. Veinger. A., Zabrodiskii, A., Tisnek, T.: *J. Alloys Comp.* **369**, 751 (2004)
16. Rakhimov, R., Ries, H., Jones, D., Glebov, L.: *Appl. Phys. Lett.* **76**, 751(2000)
17. Alvarez, G., Montiel, H., Cos, D.D., Zamorano, R., Garcia-Arribas, A., Barandiaran, J.M., Valenzuela, R.: *J. Non-crystalline solids* **353**, 902-904 (2007)
18. Gavi, H., Ngom, B.D., Beye, A.C., Strydom, A.M., Srinivasu, V.V., Chaker, M., Manyala, N.: *J. Magn. Magn. Mat.* **324**, 1172 (2012)
19. Felix, J.F., Figueiredo, L.C., Mendes, J.B.S., Morais, P.C., de Araujo, C.I.L.: *J. Magn. Magn. Mat.* **395**, 130-133 (2015)

20. Kamihara, Y., Watabane, T., Hirano, M., Hosono, H.: J. Am. Chem. Soc. **130**, 3296 (2008)
21. Panarina, N.Y., Talanov, Y.I., Shaposhnikova, T.S., Beysengulov, N.R., Vavilova, E.: Phys. Rev. B **81**, 224509 (2010)
22. Talanov, Y., Beisengulov, N., Kornilov, G., Shaposhnikova, T., Vavilova, E., Nacke, C., Panarina, S., Hess, Kataev, C. V., Buchner, B.: Supercond. Sci. Technol. **26**, 045015 (2013)
23. Onyancha, R.B., Shimoyama, J., Singh, S.J., Ogino, H., Srinivasu, V.V.: J. Supercond. Nov. Magn. **28**, 2927–2934 (2015)
24. Onyancha, R.B., Shimoyama, J., Das, J., Hayashi, K., Ogino, H., Srinivasu, V.V.: J. Supercond. Nov. Magn. **30**, 2429–2434 (2017)
25. Onyancha, R.B., Shimoyama, J., Singh, S.J., Hayashi, K., Ogino, H., Srinivasu, V.V.: Physica C: Supercond. Appl. **533**, 49–52 (2017)
26. Onyancha, R.B., Shimoyama, J., Singh, S.J., Ogino, H., Srinivasu, V.V.: J Supercond Nov. Magn. **30**, 1097 (2017)
27. Wu, T., Ying, J.J., Wu, G., Liu, R.H., He, Y., Chen, H., Wang, X.F., Xie, Y.L., Yan, Y.J., Chen, X.H.: Phys. Rev. B **79**, 115121 (2009)
28. Srinivasu, V.V., Sreedevi, V., Pradhan, A.K., Roul, B.K.: J. Mat. Sci. Lett. **20**, (2001) 1193–1194
29. Montiel, H., Alvarez, G., Conde-Gallardo, A., Zamorano, R.J.: Alloys and Compounds **628**, 272–276 (2015)
30. Valenzuela, R., Ammar, S., Nowak, S., Vazquez, G.: J Supercond. Nov. Magn. **25**, 2389–2393 (2012)
31. Álvarez, G., Contreras, J., Conde-Gallardo, A., Montiel, H., Zamorano, R.: J. Magn. Mater. **348**, 13 (2013)
32. Valenzuela, R., Alvarez, G., Montiel, H., Gutierrez, M.P., Zamora, E.M., Barron, J. F., Sanchez, A.Y., Betancourt, I., Ulloa, R.Z.: J. Magn. Mater. **320**, 1961 (2008)
33. Tebogo, M., Srinivasu, V. V., Das, J.: Solid State Commun. **243** (2016) 60–64
34. Yin, Z.P., Haule, K., Kotliar, G.: Nat. Mat. **10**, 932 (2011)

35. Soulen, R.J., Jr, Byers, J.M., Osofsky, M.S., Nadgorny, B., Ambrose, T., Cheng, S.F., Broussard, P. R., Tanaka, C.T. Nowak, J., Moodera, J.S., Barry, A., Coey, J.M.D., *Science* **282**, 85 (1998)
36. Borisenko, S. V., Evtushinsky, D. V., Liu, Z. H., Morozov, I., Kappenberger, R., Wurmehl, S., Büchner, B., Yaresko, A. N., Kim, T. K., Hoesch, M., Wolf, T., Zhigadlo, N. D.: *Nat. Phys.* **12**, 311 (2016)
37. Borisenko, S., Evtushinsky, D., Liu, Z., Morozov, I., Kappenberger, R., Wurmeh, S., Buchner, B., Yaresko, A., Kim, T., Hoesch, M., Wolf, T., Zhigadlo, N.: *Phys. Status Solidi B* **254**, 1600550 (2017)
38. Fernandes, R. M., Vafeek, O.: *Phys. Rev. B* **90**, 214514 (2014)
39. Yin, Z. P., Haule, K., Kotliar, G.: *Nat. Phys.* **10**, 845(2014)
40. Korshunov, M.M., Togushova, Y.N., Eremin, I., Hirschfeld, P.J.: *J Supercond Nov. Magn.* **26**, 2873–2874 (2013)
41. Takahashi, S., Maekawa, S.: *Phy. Rev. Let.* **88**, 116601-1 (2001)
42. Yin, W.G., Lee, C.C., Ku, W.: *PRL* **105**, 107004(2010)
43. Yuan, H.Q., Jiao, L., Balakirev, F.F., Singleton, J., Setty, C., hu, J.P., Shang, T., Li, L.J., Cao, G.H., Xu, Z.A., Shen, B., Wen, H.H.: *ArXiv: 1102.5476*
44. Golosovsky, M., Monod, P., Muduli, P.K., Budhani, R.C., Mechin, L., Perna P.: *Phy. Rev. B* **76**, 184414 (2007)
45. O'Donnell, J., Onellion, M., Rzchowski, M.S., Eckstein, J.N., Bozovic, I., *Phy. Rev. B* **55**, 5873 (1997)
46. Kim, J., Kim, J., Kim, K. H.: *Current App. Phys.* **14**, 548 551 (2014)
47. Montiel, H., Alvarez, G., Betancourt, I., Valenzuela, R., Zamorano, R.: *Superficies Vacio* **19** (3) (2006) 27-29
48. Ji, L., Rzchowski, M.S., Anand, N., Tinkham, M.: *Phys. Rev. B* **47**, 470 (1993)
49. Li, L., Yang, Z. R., Zhang, Z. T., Tong, W., Zhang, C. J., Tan, S., Zhang, Y. H.: *Phys. Rev. B* **84**, 174501 (2011)
50. Martinelli, A., Palenzona, A., Tropeano, M., Putti, M., Ferdeghini, C., Profeta, G., Emerich, E.: *PRL* **106**, 227001(2011)

51. Martinelli, A., Palenzona, A., Putti, M., Ferdeghini, C.: Phys. Rev. B **85**, 224534 (2012)
52. Kruger, F., Kumar, S., Zaanen, J., Brink, J.: Phys. Rev. B **79**, 054504 (2009)
53. Mertelj, T., Stojchevska, L., Zhigadlo, N. D., Karpinski, J., Mihailovic, D.: Phys. Rev. B **87**, 174525 (2013)
54. Stojchevska, L., Mertelj, T., Chu, J. H., Fisher, I.R., Mihailovic, D.: Phys. Rev. B **86**, 024519 (2012)

Chapter 7

Summary and conclusions

In this piece of work, LFMA technique has been used to study $\text{SmFeAsO}_{1-x}\text{F}_x$ material from 1111 class of FeSc. The study was motivated by the fact that (1) few reports have been presented on LFMA in superconducting state of these materials (2) no normal state LFMA studies have been presented thus far in any superconducting material (3) incomplete understanding of LFMA phenomenon in general (4) possible normal state application of these materials in spintronics.

Based on the results and discussion from chapters 4, 5 and 6, conclusions have been drawn and presented at the end of each chapter. Here the highlights are provided and can be broken down into two broad parts namely: (1) LFMA in superconducting state (2) LFMA in normal state.

LFMA in Superconducting state

The LFMA studies in $\text{SmFeAsO}_{1-x}\text{F}_x$ ($x = 0.12, 0.20$) has been presented in chapters 4 and 5. The study in superconducting state was inspired by the fact that few work on LFMA has been reported on FeSc. More importantly, given that LFMA signal is sample-form dependent, the powder sample and pellet sample of $\text{SmFeAsO}_{1-x}\text{F}_x$ is expected to give exciting LFMA features with exotic physics. In that regard, chapter encompasses the LFMA in powder sample of $\text{SmFeAsO}_{1-x}\text{F}_x$. Interestingly, the results exhibit a line shape which evolves as a function of temperature.

This dependence of LFMA signal on temperature was explained based on the effective medium theory. Also, a structure (a broad peak and narrow peak) was observed and explicated based on losses accrued to damped motion and weak links in form of Josephson junctions. Finally, an anomalous hysteresis at all temperature below T_c is witnessed. The anomaly is demystified on the context of two-critical state model.

In chapter five, the LFMA in $\text{SmFeAsO}_{0.80}\text{F}_{0.20}$ evolves with both temperature and microwave power. The presence of structure consisting of two peaks (broad peak and narrow peak) which similar to one observed in $\text{SmFeAsO}_{0.88}\text{F}_{0.12}$ was revealed. The observation of this structure on powdered and pellet samples of different fluorine doping

clearly shows the structure is a common feature in F-doped SmFeAsO system. Furthermore, the $T_c - T_* = 1\text{K}$ for SmFeAsO_{0.80}F_{0.20} is smaller compared to 4 K in SmFeAsO_{0.88}F_{0.12} suggesting that fluorine doping plays an important role in the evolution of this structure and more specifically in the narrow peak (T_* is the characteristic temperature at which the narrow peak appears as we cool down the sample below T_c).

This observation has been discussed in view of the presence of strong JJs coupling energy accorded from few non-superconducting inclusions in SmFeAsO_{0.80}F_{0.20} as a result of higher fluorine concentration. Moreover, the signal as a function of microwave power does not show phase reversal i.e 'normal' absorption to 'anomalous' absorption. This is contrary to the results for SmFeAsO_{0.88}F_{0.12} (published elsewhere as 'anomalous non-resonant microwave absorption in SmFeAs(O,F) polycrystalline sample'). This observation signifies that within the microwave power used; the system is in the hysteretic regime.

LFMA in normal state

The study of LFMA in the normal state was prompted by the fact that no LFMA signal has been observed in the normal state of any superconducting material. Therefore we carried out LFMA measurements in SmFeAsO_{1-x}F_x ($x=0.05, 0.12, 0.20$). Interestingly, at room temperature, we observed the normal LFMA signal in all the fluorine doping which is novel in superconductors. Furthermore, at high magnetic fields, a resonance signal was detected as well. A comparison between LFMA signal in the normal and superconducting state of SmFeAsO_{0.88}F_{0.12} has been done.

The two signals differ on the following account: (1) at normal state, LFMA signal and resonance signal appear and evolve as a function of temperature whereas in the superconducting state only LFMA signal is observed (2) the peak to peak LFMA signal intensity in the normal state increases with temperature up to 180 K and then decreases onwards whereas a decrease of signal intensity with increase in temperature is exhibited in superconducting state (3) the line width of LFMA signal in superconducting region is ~ 100 G compared to ~ 650 G in normal state.

Significantly, an observation of this signal in the normal state is paramount given that it is detected for the first time in any superconducting material. Precisely, owing to the fact that LFMA signal in magnetic materials has been associated to spin magnetization, its observation

in $\text{SmFeAsO}_{1-x}\text{F}_x$ provides a good platform to study the magnetic properties thus shedding light on some unresolved topics in these materials. Moreover, it provides an avenue for possible application of this material in the spintronic areas such as room temperature low field magnetic sensors and microwave absorbers.

Future Investigations

The undertaking of this study has opened new frontiers of studying iron-based superconducting materials in the normal state. In that regard, the future work involves studying other sample forms such as single crystals and thin of $\text{SmFeAsO}_{1-x}\text{F}_x$ using LFMA technique. Furthermore, other FeSc materials from different groups like 122,111,11 and perovskite will be investigated. Moreover, given that the mechanisms of this phenomenon is still elusive, further investigations will conceivably provide vital information towards understanding its origin/mechanism.